

# LIBRARY Michigan State University

This is to certify that the

dissertation entitled

### OPTIMIZATION OF CRYSTALLIZATION PROCESSES USING VIBRATIONAL SPECTROSCOPIES

presented by

Fang Wang

has been accepted towards fulfillment of the requirements for

Ph.D. degree in Chemistry&Chemical Engin

Major professor

Date 8/3/2000

MSU is an Affirmative Action/Equal Opportunity Institution

0-12771

## PLACE IN RETURN BOX to remove this checkout from your record. TO AVOID FINES return on or before date due. MAY BE RECALLED with earlier due date if requested.

| DATE DUE | DATE DUE | DATE DUE |
|----------|----------|----------|
|          |          |          |
|          |          |          |
|          |          |          |
|          |          |          |
|          |          |          |
|          |          |          |
|          |          |          |
|          |          |          |
|          |          |          |
|          |          |          |

6/01 c:/CIRC/DateDue.p65-p.15

## OPTIMIZATION OF CRYSTALLIZATION PROCESSES USING VIBRATIONAL SPECTROSCOPIES

By

Fang Wang

#### A DISSERTATION

Submitted to
Michigan State University
in partial fulfillment of the requirements
for the degree of

Doctor of Philosophy

Department of Chemistry and Department of Chemical Engineering

2000

#### **ABSTRACT**

## OPTIMIZATION OF CRYSTALLIZATION PROCESSES USING VIBRATIONAL SPECTROSCOPIES

By Fang Wang

Control of crystallization directly affects the physical and chemical properties of the resulting crystals. Current studies demonstrate that optimal crystallization conditions can be determined using *in situ* vibrational spectroscopies.

The first study discusses optimization of pH swing crystallization of nicotinic acid(HNic). HNic is produced by adding hydrochloric acid (HCl) to a sodium nicotinate (NaNic) aqueous solution. In situ Attenuated Total Reflection-Fourier Transform Infrared (ATR-FTIR) spectroscopy allowed us to measure solubility and supersaturation including the metastable limit of HNic. The Partial Least Squares regression (PLS) method was employed for IR data analysis. The solubilities of HNic vary significantly with pH and the concentration of NaNic. Metastable zone width is dependent on the process parameters including the concentration of HCl, the addition rate of HCl and the agitation speed. A set of optimized parameters was obtained to produce crystals of HNic with larger mean size through spontaneous(primary) crystallization. The metastable zone defines the operation range for the controlled crystallization of HNic. We seeded HNic within the operation range to greatly increase mean crystal size of HNic. The degree of secondary nucleation is demonstrated to be dependent on the level of relative supersaturation at which seeding is performed. Throughout the post seeding acid addition, crystallization was controlled by keeping relative supersaturation at a constant

level, which was realized by feedback control of relative supersaturation. It was found that keeping the solution at low relative supersaturation throughout seeding and post seeding acid addition processes promotes crystal growth and suppresses secondary nucleation to the largest degree. Therefore, we are able to obtain HNic crystals with larger mean size with the optimized process parameters for both seeded and unseeded crystallization processes.

The second study covers an investigation of solvent-mediated polymorphic transformation of progesterone using in situ Raman spectroscopy. Many analytical techniques, such as Differential Scanning Calorimetry (DSC), X-Ray Diffraction (XRD). Infrared Spectroscopy (IR) and Raman spectroscopy can differentiate between crystalline polymorphs of the same chemical entity. While all of these techniques are routinely applied to off-line analysis of materials, only Raman instrumentation technology currently exists for in situ monitoring of solid phase behavior. We employed Raman spectroscopy to demonstrate the solvent-mediated polymorphic phase transformation of progesterone. In situ Raman analysis showed that the appearance of Form I progesterone is always preceded by the formation of Form II. Phase transformation rates increase monotonically as temperature increases, which indicates that the polymorphic system is monotropic. Form I is thermodynamically more stable than Form II, while Form II is kinetically favored over Form I. The results support Ostwald's law of stages and also lead to an in-depth understanding of the polymorphic transformation process. The in situ capabilities of Raman spectroscopy allowed us to define the processing parameters required to control the morphology of progesterone.

#### **ACKNOWLEDGMENTS**

First of all, I would like to thank my advisor, Dr. Kris A. Berglund, for all the opportunities he has created for me. Without his guidance and help, I would not have come to this point today. I am grateful for the unique opportunity to pursue the dual degree in Chemistry and Chemical Engineering. It helps me understand and solve problems from more than one perspective. I would like to thank all the other professors who are or have been my committee members, Dr. Blanchard, Dr. Briedis, Dr. Leroi and Dr. Crouch, for all their time, advice and support, especially Dr. Blanchard for his timely support.

I am thankful to Dr. John A. Wachter in Pharmacia Corp. for opening a new sight for me in the pharmaceutical industry. Last summer has been one of most important stages for me among these four years' endeavor. Without your valuable advice I would not have survived the last step in graduate school. I would like to acknowledge Dr. Tim C. Frank in Dow Chemical Company for helping me understand and solve problems from the real industrial point of view. I also appreciate the support from ASI Applied Systems and Kaiser Optical Inc. for their instrument donation, which has saved me so much time that I am able to finish timely.

I would like to say "thank you" to every member in Berglund group including Dilum, Jennifer, Lili, Hasan, Dale, Mike, Anna, Parminder, Sri, Charles, Carina, Sanjay and Adam. Each one of you has helped to made my time easier in many ways. I would also

like to thank all my friends for their encouragement and friendship, including Hongying, Liu Qiang, Chen Jing, Shi Yi and Liu Bangzhi. Graduate school in the U. S. would have seemed a lot longer without the pleasant time we had together.

I am indebted to my family for all their care, support and encouragement. Hearing my parents' voice has been the most comforting thing throughout my stay in this distant country. I am thankful to my husband, Yonggang, for all the sacrifice you made for me over these years. Thank you for all the endless discussions with me. It is your critisizm that helps me grow and your comfort that keeps me going.

#### **TABLE OF CONTENTS**

| List of Table                           | sx  |
|---|---|
| List of Figure                          | esxi  |
| Chapter 1                               |   |
| INTRODUC                                | TION1   |
| 1.1                                     | Background for pH Swing Crystallization Study2  |
|   | 1.1.1 Crystallization   |
|   | 1.1.1.1 Supersaturation   |
|   | 1.1.1.2 Nucleation  |
|   | 1.1.1.3 Crystal growth6   |
|   | 1.1.2 Attenuated Total Reflectance Fourier Transform Infrared Spectroscopy (ATR-FTIR)                         |
|   | 1.1.3 Partial Least Squares Regression Method (PLS)10   |
| 1.2                                     | Background for In Situ Monitoring of Polymorphic Transformation of Progesterone                               |
| Refer                                   | ences15   |
| Chapter 2                               |   |
| USE OF AT                               | NG pH SWING CRYSTALLIZATION OF NICOTINIC ACID BY THE FENUATED TOTAL REFLECTION FOURIER TRANSFORM SPECTROMETRY |
| • | 17  |
| 2.1                                     | Introduction17  |
| 2.2                                     | Experimental Section19  |
| 2.3                                     | Results and Discussion  |
|   | 2.3.1 The Structures of HNic and NaNic in Aqueous Solutions with Different pH and IR Peak Assignments21       |

|   | 2.3.2 Calibrations of NaNic and HNic + NaNic in Aqueous Solution                     |    |
|---|--|----|
|   | 2.3.3 Monitoring the Crystallization Process   | 29 |
| 2.                                      | Conclusions  | 33 |
| 2.                                      | Acknowledgments  | 33 |
| R                                       | rences   | 34 |
| Chapter 3                               |  |    |
| SWING                                   | TION OF THE PROCESS PARAMETERS FOR SPONTANEOUS pH<br>YSTALLIZATION OF NICOTINIC ACID |    |
| • |  | 35 |
| 3.                                      | Introduction   | 35 |
| 3.                                      | Experimental Section.  | 38 |
|   | 3.2.1 Apparatus  | 38 |
|   | 3.2.2 Procedures   | 39 |
| 3                                       | Results  | 41 |
| 3.                                      | Discussion   | 49 |
|   | 3.4.1 Effect of Acid Addition Rate – The Apparent Order of Nucleat                   |    |
|   | 3.4.2 Effect of Acid Concentration   | 52 |
|   | 3.4.3 Effect of Agitation Speed  | 53 |
| 3                                       | Conclusions  | 54 |
| 3                                       | Acknowledgments  | 55 |
| R                                       | rences   | 56 |

#### Chapter 4

| CRYSTAL                                 | CONTROL OF SEEDED SEMI-BATCH pH SWING IZATION OF NICOTINIC ACID             |
|---|---|
| • | 57  |
| 4.1                                     | Introduction57  |
| 4.2                                     | Experimental Section  |
|   | 4.2.1 Apparatus59   |
|   | 4.2.2 Interface between the LabMax® and the ReactIR 100060                  |
|   | 4.2.3 Procedures61  |
|   | 4.2.3.1 Seeding at Different Levels of Supersaturation61                    |
|   | 4.2.3.2 Seeding with Post Addition of HCl63                                 |
| 4.3                                     | Results and Discussion64  |
|   | 4.3.1 Seeding at Different Levels of Supersaturation64                      |
|   | 4.3.2 Seeding with Post-seeding Acid Addition Controlled by Supersaturation |
| 4.4                                     | Conclusions87   |
| Ref                                     | rences  |
| Chapter 5                               |   |
| TRANSFO SPECTRO                         |   |
| •••••                                   | 89  |
| 5.1                                     | Introduction90  |
| 5.2                                     | Experimental Section92  |
| 5.3                                     | Results and Discussion94  |
| 5.4                                     | Conclusions   |

| 5.5       | Acknowledgments | 107 |
|-----------|-----------------|-----|
| Refe      | rences          | 109 |
| Chapter 6 |                 |     |
| CONCLUSI  | IONS            | 111 |
| APPENDIX  |                 | 114 |

#### LIST OF TABLES

| Table 2.1 | The working range of the diamond ATR crystal19   |
|-----------|--|
| Table 2.2 | The IR peak assignments for nicotinic acid and sodium nicotinate in aqueous solutions.   |
| Table 3.1 | Metastable limit comparison for different addition rates of 2 M HCl.   |
| Table 3.2 | Metastable limit comparison for different acid concentrations45  |
| Table 3.3 | Metastable limit comparison for different agitation speeds.  |
| Table 3.4 | Metastable limit comparison for different addition rates of 0.5 M HCl.   |
| Table 3.5 | The rate of decrease of the concentration of sodium nicotinate at different acid addition rates and their corresponding metastable zone width.   |
| Table 4.1 | The number of crystals of each size and the mean crystal size of the product from 60% relative supersaturation seeding of nicotinic acid, the seed concentration is 1.5 g seeds/kg solution. |
| Table 4.2 | The number of crystals of each size and the mean crystal size of the product from 30% relative supersaturation seeding of nicotinic acid, the seed concentration is 1.5 g seeds/kg solution. |
| Table 4.3 | The mean crystal size from three experiments which are controlled by different levels of relative supersaturation.   |
|           |  |

#### **LIST OF FIGURES**

| Figure 1.1 | Types of nucleation4  |
|------------|---|
| Figure 1.2 | Degrees of supersaturation related to different nucleation processes.   |
| Figure 1.3 | Schematic showing total internal reflection.  |
| Figure 1.4 | ATR-IR probe immersed in a slurry with the number of reflection points, N = 6.  |
| Figure 1.5 | Factors of the data set in Principle Component Regression.  |
| Figure 2.1 | Schematic diagram of the crystallization experiment setup. A. water jacketed acid container, B. pump, C. water-jacketed crystallizer, D. diamond ATR probe, E. spectrometer, F. computer, M. Marine type impeller, P. pH meter, T. temperature control. |
| Figure 2.2 | IR spectrum of nicotinic acid in water. The concentration of nicotinic acid is $2.72 \times 10^{-3}$ mole fraction with pH of 3.22. The temperature is $30.0 \pm 0.1$ °C.   |
| Figure 2.3 | IR spectrum of sodium nicotinate in water. The concentration of sodium nicotinate is $6.04 \times 10^{-3}$ mole fraction with pH of 9.33. The temperature is $30.0 \pm 0.1$ °C.   |
| Figure 2.4 | IR spectrum of nicotinic acid after subtraction of the spectrum of water. The concentration of nicotinic acid is $2.72 \times 10^{-3}$ mole fraction with pH of 3.22. The temperature is $30.0 \pm 0.1$ °C.   |
| Figure 2.5 | IR spectrum of nicotinic acid in deuterated water ( $D_2O$ ). The concentration of nicotinic acid is $2.70 \times 10^{-3}$ mole fraction. The temperature is $30.0 \pm 0.1$ °C. $D_2O$ spectrum is not subtracted.                                      |

| rigure 2.6 | Solubility of nicotinic acid in sodium nicotinate solutions of various pH at $T = 30.0 \pm 0.1$ °C.  |
|------------|--|
| Figure 2.7 | Crystallization of nicotinic acid while 1 M HCl is being added at the rate of 1 mL/min to sodium nicotinate solution at $30.0 \pm 0.1$ °C with the starting concentration of sodium nicotinate of $8.14 \times 10^{-3}$ mole fraction. Region I: Undersaturated nicotinic acid in sodium nicotinate aqueous solution; Region II: Supersaturated solution with the degree of supersaturation increasing, no crystal forming; Region III: Rapid desupersaturation, nucleation and crystal growth occur; Region IV: Return to saturation, nucleation and crystal growth stop. |
| Figure 3.1 | The concentration of nicotinic acid vs. the concentration of sodium nicotinate during the metastable zone measurement of the spontaneous crystallization of nicotinic acid at $30 \pm 0.1$ °C, with agitation speed of 1.1 m/s and acid addition rate of 60 g/hr of 2 M HCl.   |
| Figure 3.2 | The metastable zone of the crystallization of nicotinic acid measured under the conditions that the solution is agitated at 1.1 m/s and 2 M HCl is added at the rate of 60 g/hr at 30°C.   |
| Figure 3.3 | Comparison of the first metastable limit measurement with different acid addition rates, 1 g/hr and 60 g/hr. The acid concentration is 2 M HCl and the agitation speed is 1.1 m/s. The temperature is $30 \pm 0.1$ °C.   |
| Figure 3.4 | Influence of the acid concentration on crystal size: (a): 2 M HCl, addition rate of 1 g/hr and 1.1 m/s agitation speed, The average size of the product is about 25 μm. (b) 0.5 M HCl, addition rate of 1 g/hr and 1.1 m/s agitation speed, (b.1), (b.2) and (b.3) are the crystals after sieving. The average size of (b.1) is 152 μm, that of (b.2) is 214 μm and that of (b.3) is 305 μm.   |
| Figure 3.5 | The crystal size distribution of the product from the experiment with the addition of 0.5 M HCl at the rate of 1 g/hr and agitation speed of 1.1 m/s.  |
| Figure 4.1 | Concentration profile of seeded crystallization of nicotinic acid at 60% relative supersaturation seeding and the seed concentration of 1.5 g  |

|            | seeds/kg of solution added at 30 mins after the relative supersaturation reached 60%. $T = 30 \pm 0.1$ °C.   |
|------------|--|
| Figure 4.2 | Relative supersaturation profile and HCl addition profile of seeded crystallization of nicotinic acid at 60% relative supersaturation seeding and the seed concentration of 1.5 g seeds/kg of solution added at 30 mins after the relative supersaturation reached 60%. $T = 30 \pm 0.1$ °C. |
| Figure 4.3 | The turbidity profile for 60% relative supersaturation seeding crystallization of nicotinic acid. The seed concentration is 1.5 g seeds/kg solution. $T = 30 \pm 0.1$ °C.  |
| Figure 4.4 | The crystal size distribution of the products from 60% relative supersaturation seeding crystallization of nicotinic acid. The seed concentration is 1.5 g seeds/kg solution. The average size of the seeds is 152 μm.   |
| Figure 4.5 | Relative supersaturation profiles comparison for 30% and 60% relative supersaturation seeding crystallization experiments of nicotinic acid. The seed concentration is 1.5 g seeds/kg solution.  |
| Figure 4.6 | The comparison of the crystal size distributions resulted from seedings at three levels of relative supersaturation, 30%, 45% and 60%. The seed concentration is 1.5 g seeds/kg solution.  |
| Figure 4.7 | The mean crystal size dependence on the level of the relative supersaturation at which seeding is performed. The seed concentration is 1.5 g seeds/kg of solution. The average size of the seeds is 152 µm. The line between the datum points is meant only to be a guide to the eye.        |
| Figure 4.8 | Concentration profiles of sodium nicotinate and nicotinic acid and the solubility and metastable limit of nicotinic acid for crystallization controlled at about 30% relative supersaturation with post seeding acid addition.   |
| Figure 4.9 | Relative supersaturation profile and HCl addition profile for crystallization controlled at about 30% relative supersaturation with post seeding acid  |

|             | addition. The seeds are added at 30% relative supersaturation. The seed concentration is 1.5 g seeds/kg solution.   |
|-------------|---|
| Figure 4.10 | Concentration profiles of sodium nicotinate and nicotinic acid and the solubility and metastable limit of nicotinic acid for the crystallization controlled at about 0% relative supersaturation with post seeding acid addition. The initial seeding is performed at just above saturation.  |
| Figure 4.11 | Relative supersaturation profile and HCl addition profile for crystallization controlled at about 0% relative supersaturation with post seeding acid addition. The seeds are added at just above 0% relative supersaturation. The seed concentration is 1.5 g seeds/kg solution.  |
| Figure 4.12 | Concentration profiles of sodium nicotinate and nicotinic acid and the solubility and metastable limit of nicotinic acid for the crystallization controlled about 0% relative supersaturation with post seeding acid addition. The initial seeding was performed at 30% relative supersaturation.   |
| Figure 4.13 | Relative supersaturation profile and HCl addition profile for crystallization controlled at about 0% relative supersaturation with post seeding acid addition. The seeds are added at 30% relative supersaturation. The seed concentration is 1.5 g seeds/kg solution.  |
| Figure 4.14 | The crystal size distribution from three controlled supersaturation experiments. The three cases are: I. Seeding at 0% relative supersaturation, and controlled about 0% relative supersaturation during post acid addition; II. Seeding at 30% relative supersaturation, and controlled about 0% relative supersaturation during post seeding acid addition; III. Seeding at 30% relative supersaturation, and controlled at about 30% relative supersaturation during post acid addition. |
| Figure 5.1  | The X-ray diffraction patterns of progesterone polymorphs: (A) Form I and (B) Form II.  |
| Figure 5.2  | The DSC thermodiagrams of progesterone: (A) Form I and (B) Form II.  The heating rate was 5 °C/min.   |

| Figure 5.3 | Raman spectra of solid state progesterone: (A) Form I and (B) Form II   |
|------------|---|
| Figure 5.4 | Molecular structure of progesterone.  |
| Figure 5.5 | Calibration curve for the relative concentration of Form I in the mixture of Form I and Form II of progesterone slurried in water.  |
| Figure 5.6 | Raman spectra showing peak shift during the phase transformation process at 45°C.   |
| Figure 5.7 | Concentration profiles of Form I and Form II of progesterone throughout the phase transformation process at 45°C. The lines are drawn through the data as a guide to the eye. |
| Figure 5.8 | The temperature dependence of phase transformation rate of progesterone. The line is drawn through the data as a guide to the eye.  |

#### Chapter 1

#### INTRODUCTION

Crystallization is one of the most widely used separation processes in the food, pharmaceutical, and chemical industries. Control of the crystallization processes will enable the production of a crystalline product with the desired physical and chemical properties. Crystal size distribution (CSD) is one of the most important targets for control. A controlled crystallization process yields crystals with a favorable CSD significantly reducing the cost of downstream processes such as filtration and drying. Crystals with uniform size improve the flow, handling and packaging in the later steps of the production processes. Polymorphism is another significant property that draws a lot of attention, particularly in the pharmaceutical crystallization processes. Polymorphs are different crystal forms of the same compound. Different polymorphs have different physical and chemical properties including dissolution rates and bioavailability. The polymorph with desired physical and chemical properties can be obtained through the optimization of the crystallization process parameters.

This work consists of two studies. The first study focuses on improvement of CSD through the optimization of pH swing crystallization. The second study aims at obtaining the desired polymorph by *in situ* monitoring of the polymorphic transformation process and subsequent optimization of the process parameters.

#### 1.1 Background for pH Swing Crystallization Study

In order to obtain crystals with desired CSD, it is necessary to understand the critical factor that controls the final CSD from a batch or semi-batch crystallization process. Supersaturation is the driving force for crystallization to occur. Once enough supersaturation is generated, the solute molecules aggregate to form nuclei, the aggregation process is called nucleation. Further integration of molecules to the nuclei is defined as crystal growth. The degree of supersaturation governs the rates of nucleation and crystal growth. The competition between nucleation and crystal growth determines the final CSD. Therefore, the *in situ* control of crystallization requires measurement and subsequent control of supersaturation.

A number of studies have been conducted to measure supersaturation in conventional crystallizations such as cooling (temperature control), evaporation of solvent (solvent control) and addition of antisolvent (solvent control). 1, 2, 3, 4, 5, 6 However, very little work has been focused on the measurement and control necessary for pH swing crystallization although it is a common practice in the chemical industry. In a pH swing crystallization, the solubility difference between a protonated and a deprotonated species is exploited to create supersaturation by the adjustment of pH. We performed *in situ* measurement and control of supersaturation during pH swing crystallization of nicotinic acid using Attenuated Total Reflectance-Fourier Transform Infrared Spectroscopy (ATR-FTIR) coupled with the Partial Least Squares regression (PLS) method.

#### 1.1.1 Crystallization

Crystallization proceeds by the formation of nuclei, followed by crystal growth. It is a complex process that is governed by both thermodynamics and kinetics of the interface between the crystalline phase and solution phase. The onset of crystallization is the result of the driving force caused by the thermodynamic equilibrium between a supersaturated solution and a saturated solution. The kinetics of mass transfer from the bulk solution phase to the solid surface determines the nucleation rate and crystal growth rate.

#### 1.1.1.1 Supersaturation

Supersaturation needs to be generated in order to achieve nucleation and crystal growth. Supersaturation is defined as the state of solution that has a concentration greater than the equilibrium saturation concentration at a given temperature. The fundamental driving force for crystallization is the difference between chemical potential of the given substance in the solution phase and in the crystalline state. Under a supersaturated condition, the chemical potential difference provides the driving force for the phase transition from solution to solid crystals. The following equation expresses the relationship between chemical potential and supersaturation.<sup>8</sup>

$$\Delta \mu = RT \ln(S) \tag{1.1}$$

where  $\Delta\mu$  is the chemical potential difference between a supersaturated solution and a saturated solution, R is the gas constant, and T is the absolute temperature.

Supersaturation, S, is defined as  $S = \frac{a}{a^*}$ , where a is the activity of the supersaturated solution and  $a^*$  is the activity of the saturated solution. Typically the ratio of activity

coefficients is assumed to be unity; therefore, we can replace activity with concentration.

Under the assumption, supersaturation can be approximated to the ratio of the concentration of the supersaturated solution to the concentration of the saturated solution.

#### 1.1.1.2 Nucleation

After supersaturation is generated, crystal formation from the solution takes place. There are two steps involved in the formation of a crystal. Nucleation first takes place, followed by crystal growth. If solid foreign particles are present in a supersaturated solution, nucleation can be facilitated by the so-called heteronuclei; the nucleation based on the heteronuclei is defined as *heterogeneous nucleation*. Otherwise, *homogeneous nucleation* will take place as a result of a large chemical potential driving force without the presence of foreign particles. It is generally accepted that true homogeneous nucleation is a not a common event. Both homogeneous and heterogeneous nucleation take place in the absence of crystals of its own type. *Secondary nucleation* occurs in the presence of growing crystals. Secondary nucleation takes place at a lower supersaturation than primary nucleation. This is summarized in Figures 1.1 and 1.2.9

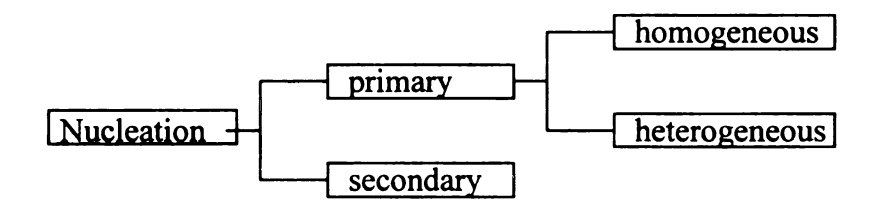


Figure 1.1. Types of nucleation

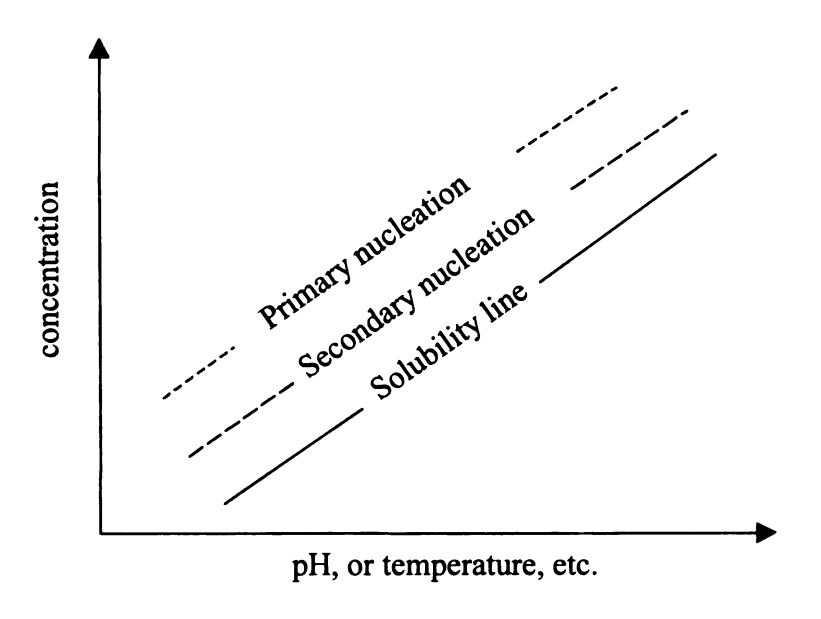


Figure 1.2. Degrees of supersaturation related to different nucleation processes.

Although no single nucleation theory is accepted for predicting nucleation rate, several correlations based on the power law model have satisfactorily explained the experimental data, <sup>10</sup>

$$B = k_N \Delta C_{MAX}^n \tag{1.2}$$

Where B is the nucleation rate,  $k_N$  is the nucleation rate constant and  $\Delta C_{MAX}$  is the metastable zone width. The exponent n is the apparent order of nucleation. During the process of nucleus formation, there is an equilibrium between the growth of nuclei and the dissolving of nuclei. Some of the nuclei reach a critical size, which is dependent on the change of the free energy of the particle, and they become stable nuclei. Post nucleation growth is made possible in the presence of stable nuclei.

#### 1.1.1.3 Crystal Growth

Various theories have been proposed to represent crystal growth, including the Two-Dimensional Growth, the BCF Model, and the Diffusion Layer Model. These models provide a theoretical basis to correlate the experimental data with the kinetic parameters. The basic expression relating crystal growth and supersaturation is 10

$$G = k_{\sigma} S^{g} \tag{1.3}$$

which employs a linear crystal growth velocity correlating the growth rate (G) with the supersaturation (S).  $k_g$  is defined as the growth rate constant and the exponent g is the order of crystal growth.

Comparing growth kinetics with nucleation kinetics helps us understand the effect of supersaturation on the final crystal size distribution. In most systems, the order of nucleation, n, is greater than g, the order of crystal growth. Consequently, higher supersaturation favors nucleation and lower supersaturation promotes crystal growth. Therefore, supersaturation becomes the critical parameter for controlling the kinetics of crystal growth and nucleation. The purpose of obtaining large mean crystal size in industrial crystallization processes requires maintaining the supersaturation at low levels, or close to the solubility, so as to suppress nucleation and promote crystal growth. This requires real time measurement and control of supersaturation. Attenuated Total Reflection Fourier Transform Infrared spectroscopy has been demonstrated to be a viable technique for this purpose.  $^{4,5}$ 

1.1.2 Attenuated Total Reflectance Fourier Transform Infrared Spectroscopy (ATR-FTIR)

Fourier Transform infrared (FTIR) spectroscopy is a widely used spectroscopic method for both quantitative and qualitative measurements. Infrared spectroscopy is classified as vibrational spectroscopy in that the absorption of infrared radiation is associated with the molecular vibrations. Therefore, FTIR is able to probe the molecular changes in the sample. The spectra recorded through FTIR spectroscopy require short collection times, e.g. on the order of seconds, which is a very important feature for the purpose of *in situ* control of supersaturation within the time frame of nucleation and crystal growth.

Total internal reflectance as a general-purpose sampling technique has paralleled the growth and development of FTIR. In total internal reflectance, also called attenuated total reflectance (ATR), the infrared radiation is directed into the interface between the reflectance element (ATR crystal), and the sample in such an angle that all the radiation is reflected. To achieve internal reflection, the reflectance element must be of higher optical density than the sample is, or the refractive index of the ATR crystal must be greater than that of the sample,  $\eta_c > \eta_s$ . Also, the incident angle of the radiation has to be greater than the critical angle, which is equal to  $sin^{-1}(\eta_s/\eta_c)$ . According to Cothup<sup>12</sup> and Mirabella<sup>13</sup>, despite the total reflection of radiation at the interface, radiation penetrates a small distance into the sample. This penetrating radiation is called the evanescent wave, as shown in Figure 1.3.

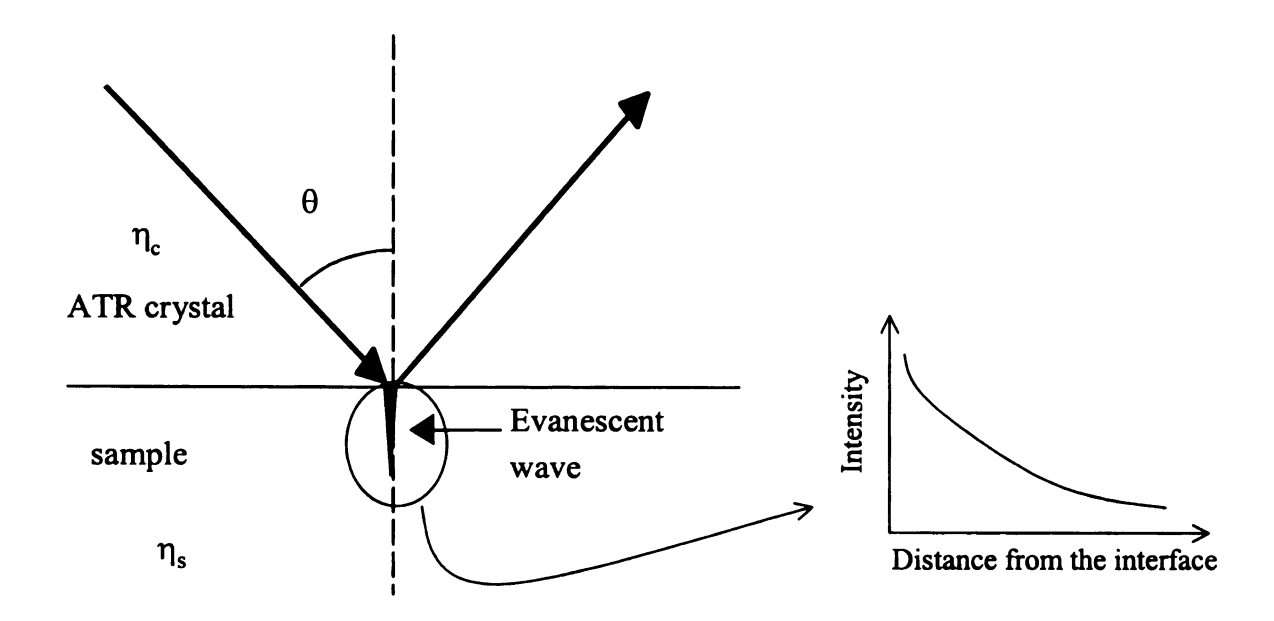


Figure 1.3. Schematic showing total internal reflection.

A sample is capable of absorbing the radiation from the evanescent wave at specific wavenumbers. Therefore, the reflected beam is attenuated at the characteristic wavenumbers corresponding to the absorption bands, which appear in the spectrum of the sample.

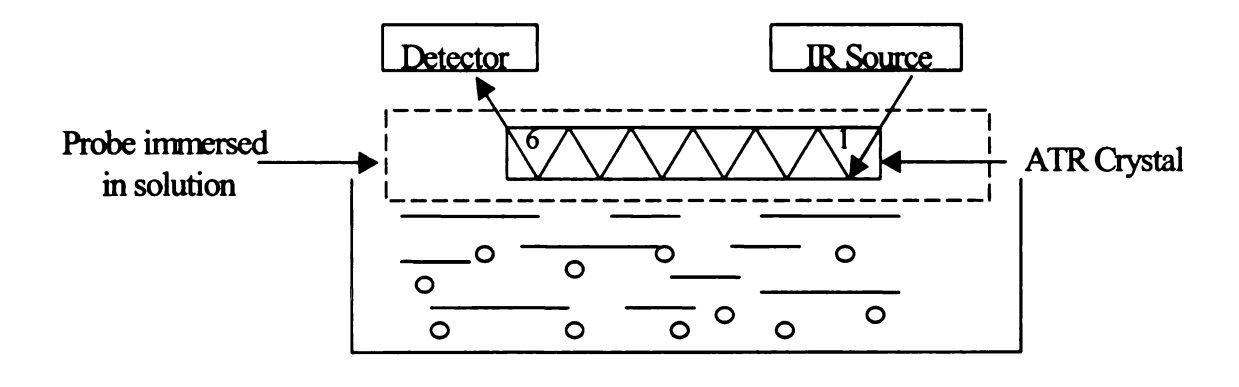
According to Beer's Law, A = abC, where A is absorbance, a is absorptivity, b is optical pathlength, and C is concentration, a calibration curve of A versus C can be constructed if the optical pathlength at a specific wavenumber is constant for samples of different concentrations and the absorptivity is constant. In an ATR-FTIR configuration, an effective optical pathlength is used. It is defined as the product of the number of reflection points in contact with the sample on the surface of reflection element, N, and

the depth of penetration,  $d_p$ , as shown in Figure 1.4.<sup>14</sup> The wavelength dependent penetration depth of the evanescent wave is given as <sup>15, 16</sup>

$$d_{P} = \frac{\lambda_{c}}{\left\{2\pi\left[\sin^{2}\theta - (\eta_{c}/\eta_{c})^{2}\right]\right\}^{1/2}}$$
(1.4)

where  $\lambda_c$  is the wavelength of the IR radiation in the ATR crystal, and  $\theta$  is the incident angle.

It was shown that  $d_p$  is nearly constant for species with different refractive index.<sup>17</sup> Also,  $Nd_p$  is so small, on the order of microns, that the sample thickness in current research always exceeds the effective optical pathlength. Therefore, variations in thickness do not affect the effective optical pathlength. The ATR absorption is proportional to concentration, thus useful quantitative measurements can be made with the ATR-FTIR technique.



Crystal in slurry; N=6

oe immersed in a slurry with the number of

Figure 1.4. ATR-IR probe immersed in a slurry with the number of reflection points, N = 6.

The combination of FTIR and ATR makes the instrument more efficient and more accessible to different samples. ATR extends the role of FTIR into new areas of application, and the improved performance of FTIR has helped attenuated total reflection to become one of the most flexible sampling techniques.

#### 1.1.3 Partial Least Squares Regression (PLS) Method

In this study, pH swing crystallization is carried out through a reaction which converts the salt to its corresponding acid form, in the presence of water. This situation presents a challenge to determine the concentrations of both the salt and the acid accurately because of the similarity in their structures. The conventional data analysis method such as univariate calibration based on peak area or a single point peak height can no longer predict the unknown concentration of a sample accurately.

More reliable data analysis techniques based on multivariate calibration, including Principle Component Regression (PCR) and Partial Least Squares Regression (PLS) methods, <sup>18, 19</sup> have been developed and are being widely utilized for quantitative analysis. Typically, we have two data matrices **X** and **Y** to be correlated with each other. In the current work, the elements in matrix **X** are the IR absorbances at all the wavenumbers within the specified peak region which correspond to certain vibrations of the sample. The concentrations of the standard samples form another matrix **Y**. The goal of the data treatment is to build a mathematical model, on the basis of the two matrices **X** and **Y**, to predict the concentrations in matrix **Y**. Both PCR and PLS are factor-based modeling techniques.

In PCR, a factor is defined as a vector that describes the maximum amount of variation in the sample. Mathematically, the first factor will be the eigenvector with the largest eigenvalue for the covariance matrix of the data set, X. If one factor cannot account for all of the variation, a second or even more eigenvectors need to be identified to describe the maximum amount of the residual variance. This can be explained graphically in Figure 1.5. The significance of the factors is that they best describe the variation within the sample with the minimum amount of data. Once the factors are determined, the original data set, X, will be re-expressed as a score matrix T, which is the projection of the original data set onto the eigenvectors, W. Then the regression coefficients matrix, Q, can be determined through multi-linear regression of Y matrix onto the score matrix. The prediction for the concentration of unknown samples can be performed using eigenvectors, W, and the regression coefficients matrix, Q.

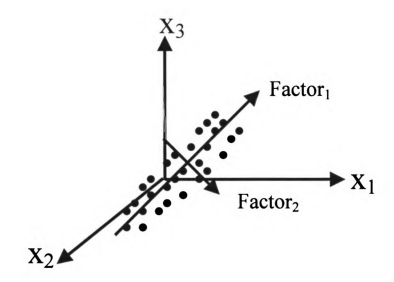


Figure 1.5. Factors of the data set in Principle Component Regression.

PLS differs from PCR in that it simultaneously estimates factors for both X and Y matrices. W, consisting of the factors of matrix X, describes the variation in Y better than the factors in PCR. This is achieved by starting with the columns of Y matrix to calculate the factors for X and using iterative substitution to determine all of the factors in both X and Y matrices. The factor matrix of X in PLS will deviate from the direction of the factors in PCR by being slightly rotated toward the Y vectors. It is this slight rotation that uses all the information available including both X and Y matrices to determine the inner relationship coefficient Y0 between Y1 and Y2, respectively. After the absorbance matrix, Y2, from an unknown sample is measured, the score matrix Y3 determined using Y4, the factor matrix of Y6. Utilizing the coefficient Y6, we can obtain the score matrix Y7 based on Y8 matrix. This new score matrix Y8 matrix Y9 matrix. This new score matrix Y9 matrix Y9 matrix of Y1.

$$\mathbf{X} = \mathbf{T} \cdot \mathbf{W} \tag{1.5}$$

$$\mathbf{Y} = \mathbf{U} \cdot \mathbf{Q} \tag{1.6}$$

$$X_{un} \xrightarrow{W} T_{un} \xrightarrow{b} U_{un} \xrightarrow{Q} Y$$

### 1.2 Background for *In Situ* Monitoring of Polymorphic Transformation of Progesterone

The pharmaceutical industry is frequently confronted with the different physiochemical properties of polymorphs of the same compound, particularly with solid, oral dosage drug products. The characteristics affected by polymorphism include solubility, dissolution rate, stability, hygroscopicity and solid state reactions. The effect of polymorphism on bioavailability is the most important consequence if the bioavailability is mediated via dissolution. In situ monitoring of the solvent mediated polymorphic transformation is therefore of great significance in understanding thermodynamics of the polymorphic systems and mechanisms of the polymorphic transformation, and consequently determining the optimized crystallization parameters to produce the desired polymorphs.

In polymorphic studies, Raman spectroscopy, coupled with an immersible fiber optic probe, has tremendous advantages over the traditional techniques, including X-ray powder diffraction (XRD), Differential Scanning Calorimetry (DSC), solid state NMR and Infrared spectroscopy (IR). The fiber optic probe in the Raman technique provides the capability of *in situ* or on-line monitoring of the formation of crystals and the transformation from one polymorph to another. DSC, XRD and NMR can perform offline analysis, which can distinguish the polymorph of the end product,<sup>24</sup> but cannot provide insight about transformation processes since the transformation may continue during drying and sampling.

Infrared Spectroscopy can be used to in situ monitor some processes. However aqueous solutions may cause problems in IR measurement. 12 If water is used as either a reagent or a byproduct or a solvent in a process, strong infrared absorption of water can mask some of the useful information from the interested species. In contrast, water is a poor Raman scatterer, which often makes Raman preferable to IR when water is present in the This can be explained by the different mechanisms of interaction of electromagnetic radiation with matter in the two spectroscopic techniques. Dipole moment changes during molecular vibrations cause IR absorption while changes in polarizability associated with molecular vibrations result in Raman scattering. Usually molecules with polar functional groups and asymmetric vibrational modes have stronger absorption in IR and weaker absorption in Raman.<sup>15</sup> Raman scatterring also favors solid phase in a slurry other than the solution phase as the ATR-FTIR technique. The higher density of the solid phase results in stronger Raman scattering than the solution phase does. This allows us to monitor the disappearance of one solid phase and the appearance of the other solid phase. In addition, we can use Raman spectroscopy to perform remote sensing since the fiber optic probe can be made as long as a couple of hundred meters.<sup>26</sup> By comparison, Attenuated Total Reflectance (ATR) probe in ATR-FTIR technique can only reach a couple of meters.<sup>27</sup> Remote sensing is especially useful in hazardous environments where operators can work safely by staying far from the reactor. This study employed Raman spectroscopy coupled with a fiber optic probe to study the polymorphic transformation of progesterone.

#### References

- 1. Garside, J.; Gibilara, L. B; Tavare, N. S. Chem. Eng. Sci. 1982, 37, 1625.
- 2. Tavare, N. S.; Garside, J. Chem. Eng. Res. Des. 1986, 64, 109.
- 3. Qiu, Y.; Rasmusson, A. C. AIChE J. 1990, 36, 665.
- 4. Dunuwila, D. D.; Berglund K. A. J. Cryst. Growth, 1997, 179, 185.
- 5. Uusi-Penttila, M. S.; Berglund, K. A. J. Cryst. Growth, 1996, 166, 967.
- 6. Schwartz, A. M.; Berglund, K. A.; J. Cryst. Growth, 1999, 203, 599.
- 7. Wang, F.; Berglund, K. A. Ind. Eng. Chem. Res. 2000, 39, 2101.
- 8. Mullin, J. W. Crystallization, 3rd ed.; Butterworth-Heinamann Ltd.: Oxford, 1993.
- 9. Mersmann, S. Crystallization Technology, 3rd ed., Butterworth-Heinamann Ltd.: Oxford, 1995.
- 10. Myerson, A. S. Handbook of Industrial Crystallization, Butterworth-Heinamann Ltd.: Boston, 1993.
- 11. Söhnel, O.; Gardise, J. *Precipitation: Basic Principles and Industrial Applications*, Butterworth-Heinamann Ltd.: Oxford, 1992.
- 12. Cothup, N. b.; Daly, L. H.; Wiberly, S. E. Introduction to Infrared and Raman Spectroscopy, 3rd ed., Academic Press: Boston, 1990.
- 13. Mirabella, F. M., Jr. Internal Reflection Spectroscopy, Theory and Applications, Mercel Dekker, Inc.: New York, 1993.
- 14. Coates, J. P. The Industrial Application of Infrared Internal Reflection Spectroscopy, In Internal Reflection Spectroscopy, Theory and Applications, Mercel Dekker, Inc.: New York, 1993.
- 15. Ingle, J. D., Jr.; Crouch, S. R. Spectrochemical Analysis, Prentice-Hall: New Jersey, 1988.
- 16. Muller, F. J.; Abraham-Fuchs, K. Matrix Dependence in Single and Multilayer IRS Spectra, In Internal Reflection Spectroscopy, Theory and Applications, Mercel Dekker, Inc.: New York, 1993.
- 17. Uusi-Penttila, S. M. Optimization of Batch Antisolvent Crystallization, PhD Dissertation, Michigan State University, East Lansing, Michigan, 1997.

- 18. Beebe, K. R.; Pell, R. J.; Seasholtz, M. B. Chemometrics, A Practical Guide, John Wiley & Sons, Inc.: New York, 1998.
- 19. Beebe, K. R.; Kowalski, B. R. Anal. Chem. 1987, 59, 1007A.
- 20. Esbensen, K.l Schönkopf, S.; Mictgaard, T. Multivariate analysis in practice; Computer-aided modelling AS: Trondheim, Norway, 1996.
- 21. Yu, L.; Reutzel, S. M.; Stephenson, G. Pharm. Sci. Technol. To. 1998, 1(3), 118.
- 22. Giron, D. Thermochim. Acta, 1995, 248, 1.
- 23. Byrn, S. R. Solid-State Chemistry of Drugs, Academic Press: New York. 1982.
- 24. Raghavan, K.; Dwivedi, A.; Campbell, G. C.; Nemeth, G.; Hussain, M. A. J. Pharm. Biomed. Anal. 1994, 12(6), 777.
- 25. Pelletier, M. J. Analytical Applications of Raman Spectroscopy, Blackwell Science Ltd: Oxford, 1999.
- 26. Kaiser Optical Systems, Inc. HoloLab Series 5000 Operations Manual, Kaiser Optical Systems, Inc.: Ann Arbor, Michigan, 1997.
- 27. ASI Applied Systems, *ReactIR 1000 User's Guide*; 3rd ed., ASI Applied Systems: Millersville, Maryland, 1997.

#### Chapter 2

## MONITORING pH SWING CRYSTALLIZATION OF NICOTINIC ACID BY THE USE OF ATTENUATED TOTAL REFLECTION FOURIER TRANSFORM INFRARED SPECTROMETRY\*

\*Industrial & Engineering Chemistry Research, 2000, 39, 2101-2104.

The crystallization of nicotinic acid is achieved by adding hydrochloric acid (HCl) to a sodium nicotinate aqueous solution. An Attenuated Total Reflection Fourier Transform Infrared (ATR-FTIR) spectrometer is used to monitor the crystallization process of nicotinic acid. The Partial Least Squares regression (PLS) method is employed for IR data analysis. The solubility of nicotinic acid varies with the pH and the concentration of sodium nicotinate. The ability to measure the concentration and solubility of nicotinic acid in situ in aqueous mixtures of nicotinic acid and sodium nicotinate provides the possibility of controlling the degree of supersaturation of the solution and in turn optimizing the crystallization conditions for nicotinic acid.

#### 2.1 Introduction

Crystallization is one of the most widely used separation processes in the food, pharmaceutical, and chemical industries. Control of the crystal size distribution (CSD) significantly impacts the cost of downstream processes such as filtration and drying.

Supersaturation is the driving force for both nucleation and crystal growth. It controls the rate of crystallization and the resulting CSD. Therefore, the control of a crystallization

process requires in situ measurement and subsequent control of supersaturation. Significant effort has been expended on the study of more conventional techniques of supersaturation generation, including temperature control or cooling of solutions, solvent control such as evaporation of solvents and the addition of anti-solvents. However, far less work has been directed at the measurement and control necessary for pH swing crystallization, which is a commonly encountered case in industrial separations.

In pH swing crystallization, solubility differences between protonated and deprotonated species are exploited to create supersaturation by the adjustment of pH. The chemical system for the current study is nicotinic acid (HNic)-sodium nicotinate (NaNic)-water (H<sub>2</sub>O). At 30 °C, NaNic has a solubility of about 60 g/100 g of H<sub>2</sub>O at pH = 9.53, while only 1.9 g of HNic can be dissolved in 100 g of  $H_2O$  at pH = 3.22 at the same temperature. The crystallization of HNic is achieved by the addition of hydrochloric acid to NaNic solution to decrease pH. It is proposed to monitor the crystallization process by the use of Attenuated Total Reflection Fourier Transform Infrared Spectroscopy (ATR-FTIR). IR spectra provide information about the molecular structure and chemical nature of the system under study. Any change in the system due to reaction will be reflected in the IR spectra. Differences in spectra are of two types, peak intensity changes and peak position shifts. Peak intensity changes are caused by concentration variation, and the peak position shifts are the result of the structural changes or intermolecular interactions. The multivariate data analysis technique of partial least squares regression (PLS) can be employed to analyze the spectral data obtained. This study demonstrates the feasibility of using ATR-FTIR combined with the PLS data analysis method to monitor the crystallization of HNic in situ.

## 2.2 Experimental Section

The experimental setup for monitoring the crystallization of nicotinic acid by ATR-FTIR is shown in Figure 2.1. A 500 ml, water-jacketed crystallizer was kept at a constant temperature (30.0  $\pm$  0.1 °C) with a Brinkmann RC6 LAUDA water circulator. The crystallizer was equipped with a marine type impeller. A Cole-Parmer Masterflex tubing pump was used to control the acid addition rates.

A dry air purged ASI-REACTIR 1000 Spectrometer was used for the ATR-FTIR measurements. An MCT detector cooled with liquid nitrogen was employed to detect the reflected light. A 0.25mm thick diamond wafer was used as a multiple reflection ATR element. The working range of this material is shown in Table 2.1. 98% Nicotinic acid, 98% sodium nicotinate and hydrochloric acid of volumetric standard were purchased from Aldrich Chemical Company. They were used without further purification. Distilled water was used in all experiments. In the solubility measurement, each datum point was extracted from the spectrum that was collected when both pH and the concentration of HNic had been stabilized.

**Table 2.1.** The working range of the diamond ATR crystal.<sup>3</sup>

| pН   | Temperature<br>Range, °C | Pressure         | Optical Range, cm <sup>-1</sup> |
|------|--------------------------|------------------|---------------------------------|
| 1-14 | -80-250                  | -10 torr-100 psi | 4400-2150 1950-650              |

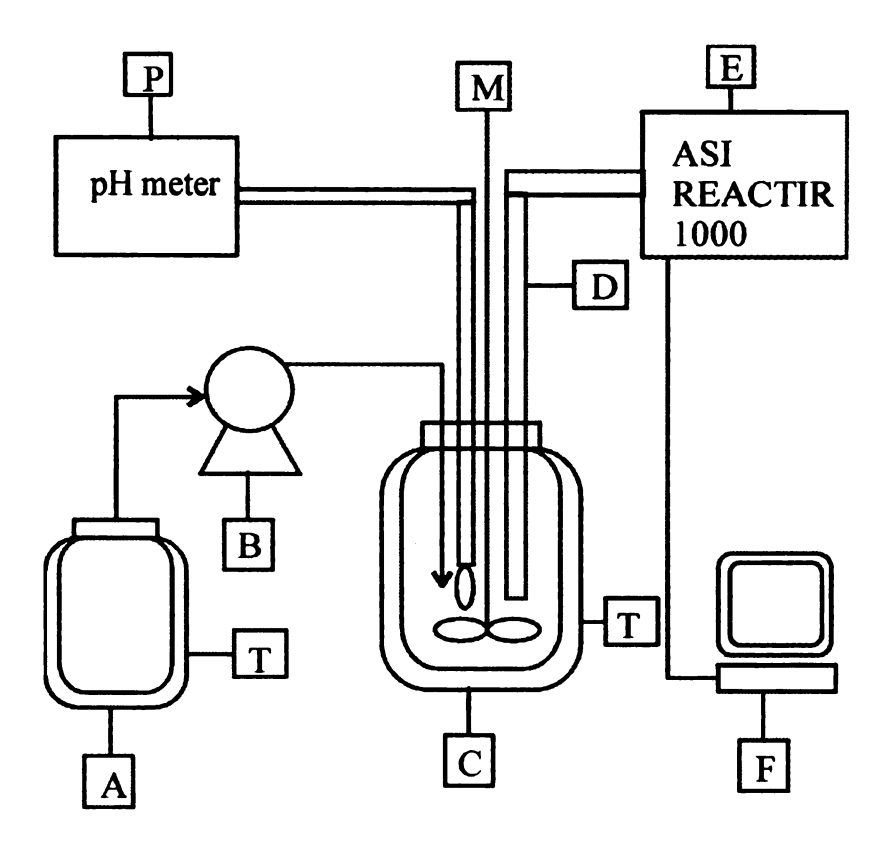


Figure 2.1. Schematic diagram of the crystallization experiment setup. A. water jacketed acid container, B. pump, C. water-jacketed crystallizer, D. diamond ATR probe, E. spectrometer, F. computer, M. Marine type impeller, P. pH meter, T. temperature control.

## 2.3 Results and Discussion

**2.3.1** The structures of HNic and NaNic in Aqueous Solutions with Different pH and IR Peak Assignments.

According to Nakomoto et al. <sup>4</sup> and Wojcik et al.,<sup>5</sup> the structure of HNic in aqueous solutions of different acidities changes according to several equilibria. HNic in the solid phase exists as the neutral molecule instead of the zwitterion. The equilibrium is shown as follows when HNic is dissolved in water,

$$\begin{array}{c}
N \longrightarrow C \\
OH
\end{array}$$

$$\begin{array}{c}
O \\
1:10
\end{array}$$

$$\begin{array}{c}
\bullet \\
N \\
\hline
O
\end{array}$$

$$\begin{array}{c}
O \\
\hline
C \\
O
\end{array}$$

The equilibria when HNic is dissolved in acidic aqueous solution are given below,

The equilibria are as follows when HNic is dissolved in a basic solution or NaNic is dissolved in a neutral aqueous solution.

HNic molecules form zwitterions when they dissolve in pure water. The quantity of zwitterions is almost 10 times as much as that of the nonionic molecules.<sup>4</sup> This explains the absence of strong absorbance around 1700 cm<sup>-1</sup> in Figure 2.2, which is characteristic of carbonyl (C=O) stretching and is a common peak for un-ionized carboxylic acids. Figures 2.2 and 2.3 present the IR spectra of HNic and NaNic dissolved in water, respectively. Similar to amino acids, HNic can be considered as a dibasic acid. The concentrations of the deprotonated nicotinate ions, zwitterions and protonated ions depend on the pH and the dissociation constants of the protonated ions and zwitterions.

The spectrum of HNic does not provide much information in the presence of  $H_2O$  except for one peak around 1390 cm<sup>-1</sup>. One reason is that the concentration of an aqueous HNic solution is low with its solubility only about 2%. The other reason is that some of the peaks expected such as the vibrations of the pyridine ring are overlapped with or masked by the strong peak at 1640 cm<sup>-1</sup> from water.

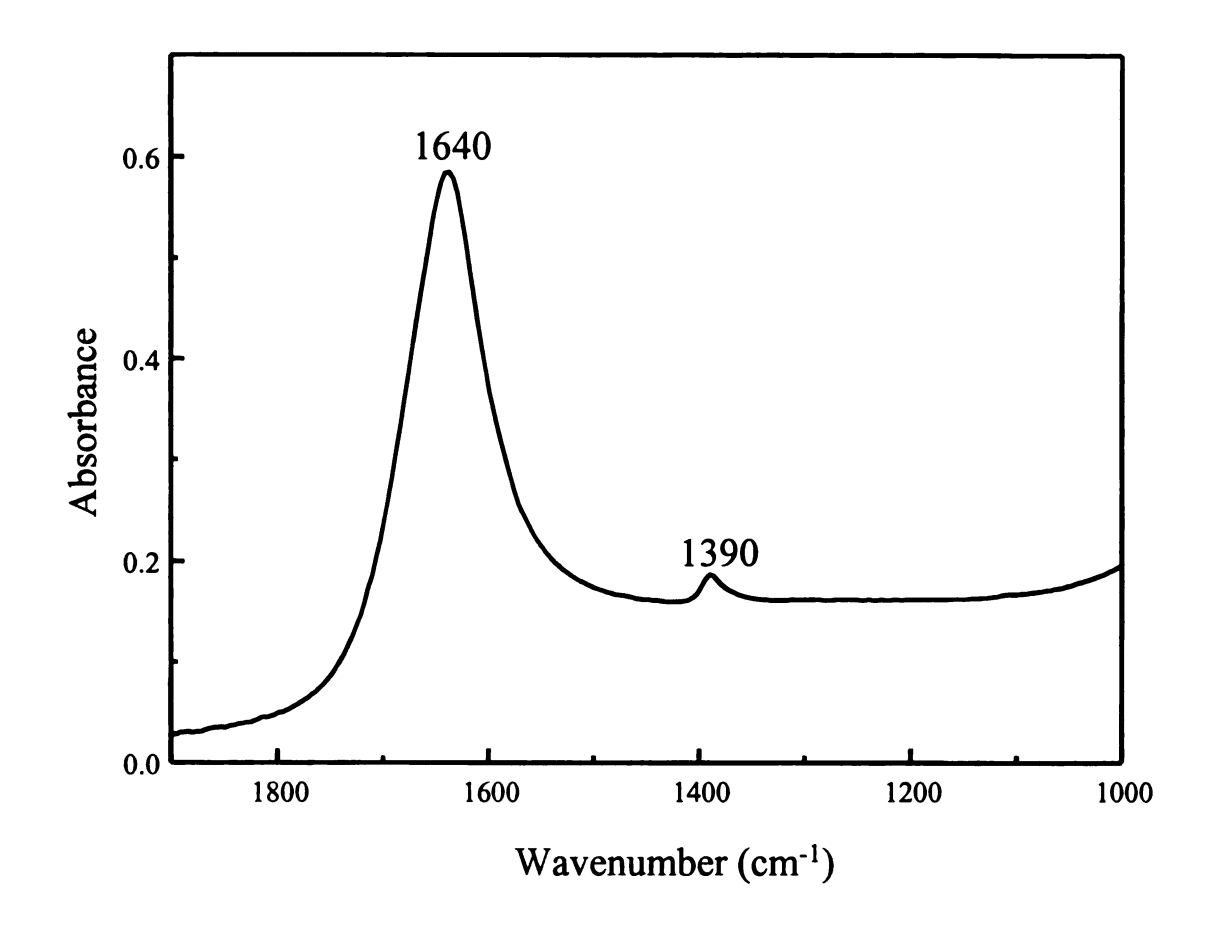


**Figure 2.2.** IR spectrum of nicotinic acid in water. The concentration of nicotinic acid is  $2.72 \times 10^{-3}$  mole fraction with pH of 3.22. The temperature is  $30.0 \pm 0.1$  °C.

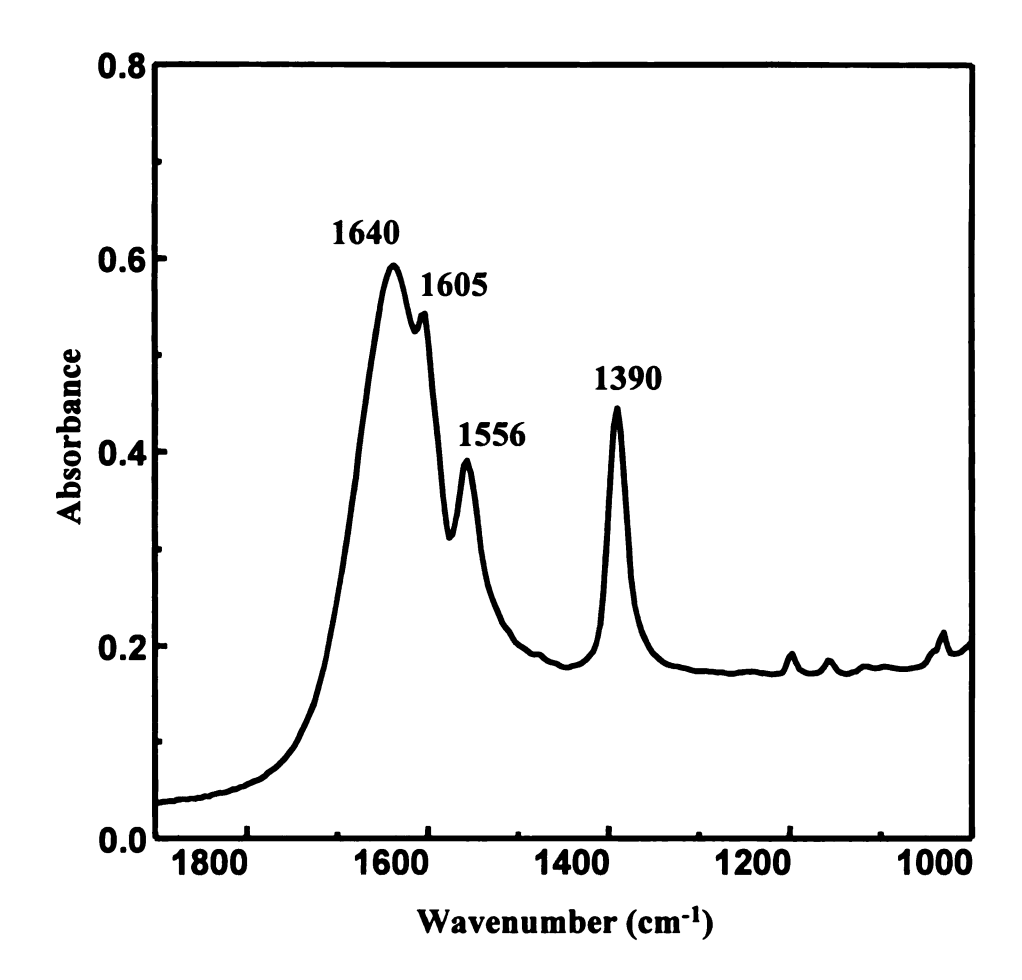


**Figure 2.3.** IR spectrum of sodium nicotinate in water. The concentration of sodium nicotinate is  $6.04 \times 10^{-3}$  mole fraction with pH of 9.33. The temperature is  $30.0 \pm 0.1$ °C.

This effect is verified by the subtraction of the water spectrum from the spectrum of HNic as shown in Figure 2.4 and it is also confirmed by the spectrum of HNic in a  $D_2O$  solution in Figure 2.5.

Because the solubility of NaNic is quite high, it is much easier to correlate the peak positions with the molecular vibrations. According to the structure transformation of HNic from un-ionized form in solid phase to ionized form in solution phase and comparison between the spectra of HNic zwitterion and NaNic in aqueous solution including H<sub>2</sub>O and D<sub>2</sub>O solutions,<sup>6,7</sup> the following peak assignments were made and shown in Table 2.2. The absorbance around 1390 cm<sup>-1</sup> is the characteristic frequency for ionized carboxyl group, which demonstrates that HNic molecules exist mainly as dipolar ions in aqueous solutions.

**Table 2.2.** The IR peak assignments for nicotinic acid and sodium nicotinate in aqueous solutions.

| Vibrational Mode              | HNic peak<br>position (cm <sup>-1</sup> ) | NaNic peak<br>position (cm <sup>-1</sup> ) |
|-------------------------------|---|--|
| Symmetric stretching of COO   | 1390                                      | 1390                                       |
| and pyridine ring deformation |   |  |
| Asymmetric                    | extremely weak                            | 1556                                       |
| stretching of COO             |   |  |
| Pyridine Ring deformation     | 1586                                      | 1605                                       |
|                               |   |  |
| N-H deformation               | 1640                                      |  |

## 2.3.2. Calibrations of NaNic and HNic + NaNic in Aqueous Solutions

Because the chemical system used is a mixture of NaNic and HNic in water, it is necessary to build calibrations for both NaNic and HNic in water in order to predict the



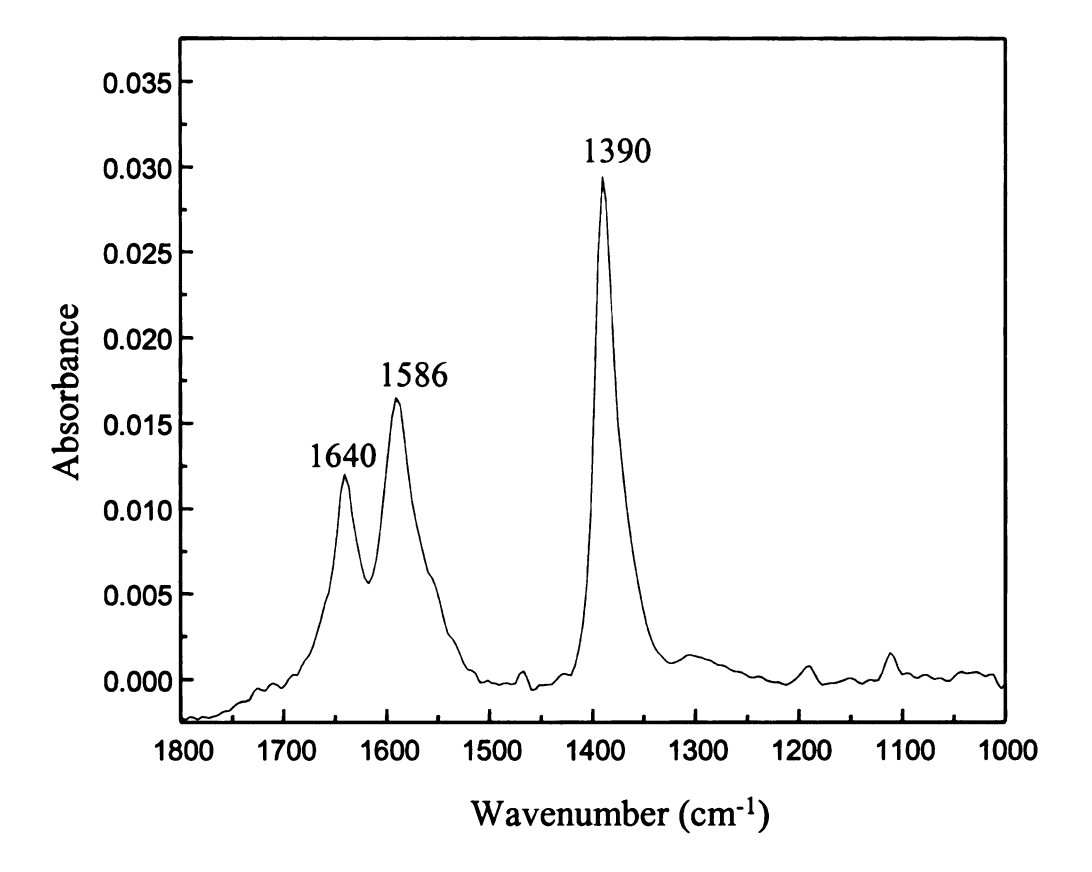


**Figure 2.4.** IR spectrum of nicotinic acid after subtraction of the spectrum of water. The concentration of nicotinic acid is  $2.72 \times 10^{-3}$  mole fraction with pH of 3.22. The temperature is  $30.0 \pm 0.1$ °C.

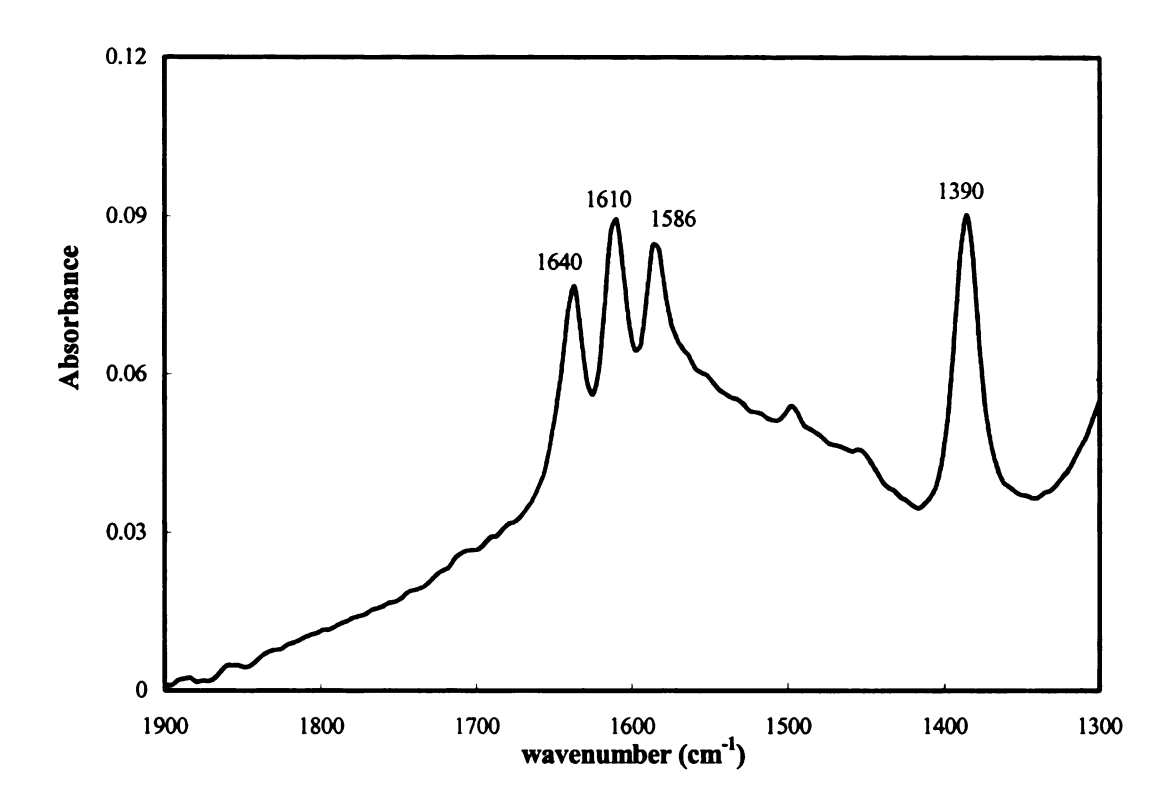


Figure 2.5. IR spectrum of nicotinic acid in deuterated water ( $D_2O$ ). The concentration of nicotinic acid is  $2.70 \times 10^{-3}$  mole fraction. The temperature is  $30.0 \pm 0.1$ °C.  $D_2O$  spectrum is not subtracted.

composition of the system at any point. However, from the information in Table 2.2, it is observed that HNic only exhibits three peaks, two of which are masked by the broad peak around 1640 cm<sup>-1</sup> from water. Subtraction of water from the spectra of HNic was attempted, however it did not give a good calibration since the subtraction of the H<sub>2</sub>O spectrum from the HNic spectrum cannot eliminate the interaction between these two compounds in solution. The only peak not obscured by water is around 1390 cm<sup>-1</sup>, but NaNic also has this peak at the same position, which implies that this peak cannot be used to calibrate either HNic or NaNic independently in the mixture. However, this peak region (1358 – 1416 cm<sup>-1</sup>) is very useful to calibrate the total amount of HNic and NaNic present in the solutions. The contributions from HNic and NaNic are counted in the PLS method and are validated by testing samples. For NaNic, there is a prominent peak centered about 1556 cm<sup>-1</sup>, which can be used to monitor the concentration of NaNic in the mixture. Now that both the concentrations of NaNic and HNic + NaNic can be determined, the concentration of HNic can be obtained through the mass balance. The calibrations of NaNic and HNic + NaNic were built using the peak regions 1510 - 1570  $cm^{-1}$  and 1358 – 1416  $cm^{-1}$ , respectively.

To extract precise information for both HNic and NaNic, the Partial Least Squares regression (PLS) technique is used to correlate the data from the IR spectra with the concentrations of solutions being analyzed. PLS starts with two matrices X and Y. In the current work, the elements in matrix X are the absorbances at all the wavenumbers within the specified peak region which correspond to certain vibrations of the molecules such as NaNic and HNic. The concentrations of the standard samples form another matrix Y.

The goal of the data treatment is to build a mathematical model, on the basis of the two matrices X and Y, to predict the concentrations in matrix Y. The process involves manipulating the two matrices to find the eigenvectors of matrix X which are in the directions of maximum covariance. 8,9 The number of eigenvectors which corresponds to the maximum covariance is also termed as the number of factors. The eigenvectors form a new set of mutually independent variables, which are combined with the regression coefficients to predict the concentrations of the samples in matrix Y. PLS calibrations for NaNic and NaNic + HNic are built by the cross validation called the "leave-one-out" method, in which one standard is left out and a calibration model is constructed using the remaining standards. The concentration of the sample that is left out is then predicted using this model. This process is repeated for every standard used in the calibration. The optimal number of factors is determined as the one that gives a minimum predicted residual error sum of squares (PRESS). The average percent errors for both of the "leave-one-out" calibrations of NaNic and NaNic + HNic are less than 1%.

#### 2.3.3 Monitoring the Crystallization Process

Once the calibrations are built, it is possible to monitor the crystallization process of HNic *in situ*. In order to better understand the crystallization of HNic, the solubility of HNic in NaNic solution was obtained first. It is found that the solubility of HNic varies with the concentration of NaNic or with the pH value of the solution, as shown in Figure 2.6. This result can be explained by the ionic strength effect<sup>10</sup> and the equilibrium between nicotinate anions, protons and zwitterions of HNic. The crystallization process of HNic was monitored and then compared with the solubility curve of HNic, which is

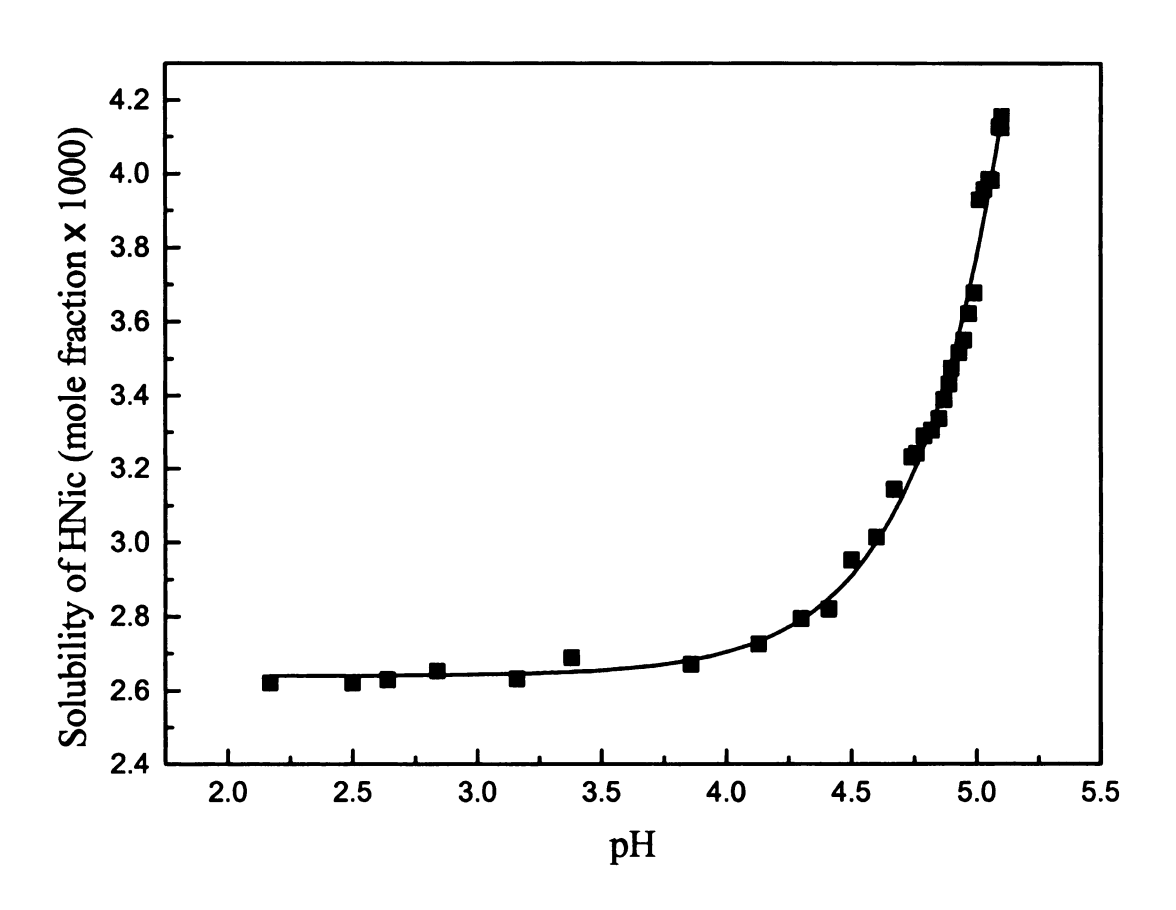


Figure 2.6. Solubility of nicotinic acid in sodium nicotinate solutions of various pH at T =  $30.0 \pm 0.1$  °C.

shown in Figure 2.7. As indicated in the figure, when a small amount of HCl is added into NaNic aqueous solution, the concentration of HNic is below its solubility, which corresponds to the stable undersaturated solution in region I. Once the concentration of HNic exceeds the solubility curve, the solution enters the metastable zone, in regions II and III, which is defined by the solubility and the highest supersaturation, called metastable limit. When the concentration reaches this limit, spontaneous crystallization occurs in region III and results in a large number of tiny nuclei. The concentration of HNic returns to the solubility limit when nucleation and crystal growth end, as shown in The ability to monitor the crystallization of HNic in situ is of great significance because it provides the possibility of controlling the degree of supersaturation. As can be seen from Figure 2.7, the degree of supersaturation is very high in region II, which is the favorable condition for nucleation to occur. Therefore, numerous nuclei were formed and the supersaturation was all consumed by nucleation, which is unfavorable for crystal growth. The undesired crystal size will lead to serious problems in the later stage operations such as filtration and drying. Ideally, the supersaturation should be relatively high at first so that enough nuclei can be produced. After the desired amount of nuclei are formed, the supersaturation should be kept as close to the solubility curve as possible so that the nuclei can grow further and form larger crystals. 11 Future work will be focused on controlling the crystallization process in order to obtain crystals with a desired crystal size distribution.

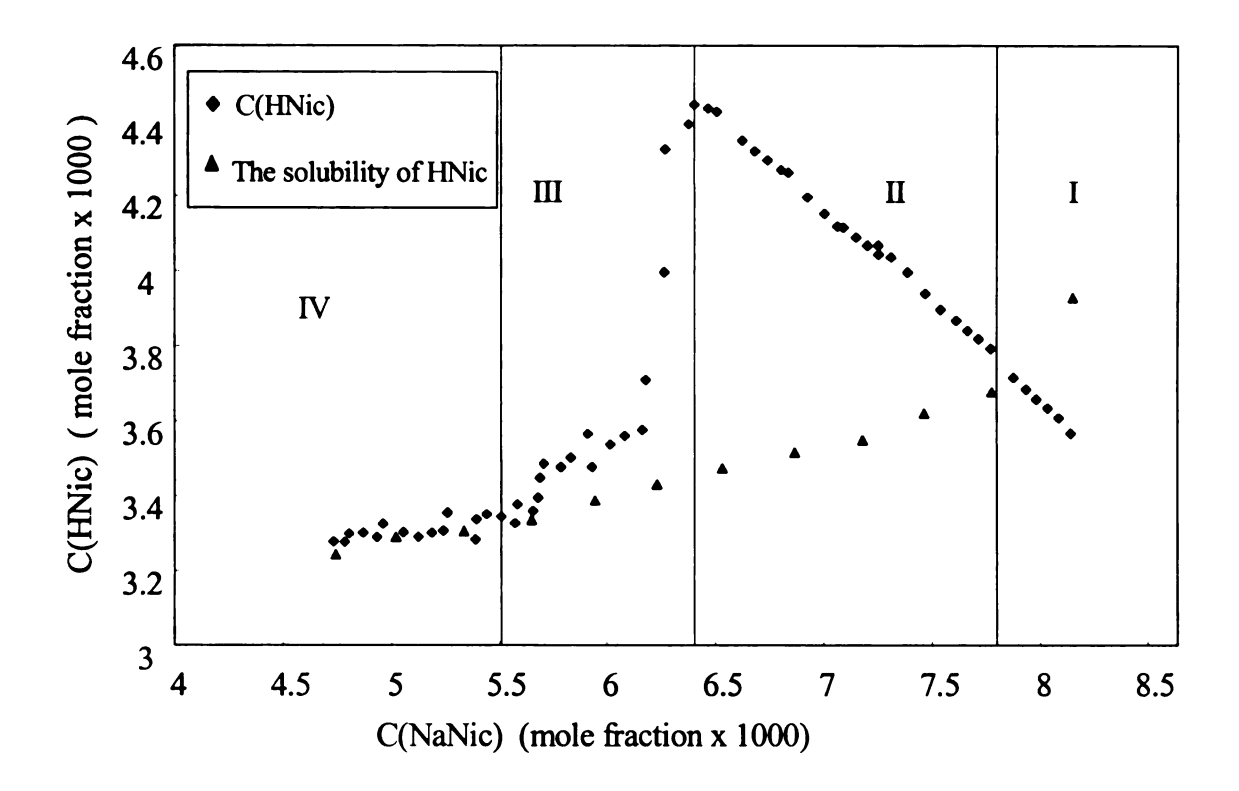


Figure 2.7. Crystallization of nicotinic acid while 1 M HCl is being added at the rate of 1 mL/min to sodium nicotinate solution at  $30.0 \pm 0.1$ °C with the starting concentration of sodium nicotinate of  $8.14 \times 10^{-3}$  mole fraction. Region I: Undersaturated nicotinic acid in sodium nicotinate aqueous solution; Region II: Supersaturated solution with the degree of supersaturation increasing, no crystal forming; Region III: Rapid desupersaturation, nucleation and crystal growth occur; Region IV: Return to saturation, nucleation and crystal growth stop.

## 2.4 Conclusions

It was demonstrated that pH swing crystallization of nicotinic acid can be monitored *in situ* with ATR-FTIR. The PLS method correlates the spectral information with the concentrations of samples. The solubility of nicotinic acid varies as the concentration of sodium nicotinate and pH of the solution change. The solubility curve of nicotinic acid and the measurement of supersaturation *in situ* make it possible to control and optimize the crystallization process of nicotinic acid.

# 2.5 Acknowledgments

The authors wish to express thanks to the Dow Chemical Company for the financial support of this project and also appreciate support provided by ASI Applied Systems.

#### References

- 1. Dunuwila, D. D. An investigation of the feasibility of using *in situ* ATR-FTIR spectroscopy in the measurement of crystallization phenomena for research and development of batch crystallization process; Ph.D. Dissertation, Michigan State University, 1996.
- 2. Uusi-Pentilä, S. M. Optimization of batch anti-solvent crystallization; Ph.D. dissertation, Michigan State University, 1997.
- 3. ASI Applied Systems, *ReactIR 1000 User's Guide*; 3rd Edition, ASI Applied Systems: Millersville, MD,1997.
- 4. Nakamoto, K.; Morimoto, Y.; Martell, A. E. Infrared Spectra of Aqueous Solutions. III. Ethylenediaminetetraacetic Acid, N-Hydroxyethylenediaminetriacetic Acid and Diethylenetriaminepentaacetic Acid. J. Amer. Chem. Soc. 1963, 85, 309.
- 5. Wojcik, J. F.; Stock, T. H. Aqueous Infrared Studies of the Pyridine Carboxylic Acids. J. Phys. Chem. 1969, 73, 7, 2153.
- 6. Colthup, N. B.; Daly, L. H.; Wiberley, S. E. *Introduction to infrared and raman spectroscopy*; 3<sup>rd</sup> Edition, Academic press: Boston, 1990.
- 7. Cohn, E. J. and Edsall, J. G. Proteins, amino acids and peptides as ions and dipolar ions; Waverly press: New York, 1943.
- 8. Beebe, K. R.; Kowalski, B. R. An Introduction to Multivariate Calibration and Analysis. *Anal. Chem.* 1987, 59, 17, 1017A.
- 9. Esbensen, K.; Schönkopf, S.; Mictgaard, T. Multivariate Analysis in Practice; Computer-aided modelling AS: Trondheim, Norway, 1996.
- 10. Green, R. W.; Tong, H. K. The Constitution of the Pyridine Monocarboxylic Acids in their Isoelectric Forms. J. Amer. Chem. Soc. 1956, 78, 4896.
- 11. Mullin, J. W. Crystallization; 3rd Edition, Butterworth-Heinemann Ltd: Oxford, 1993.

# Chapter 3

# OPTIMIZATION OF THE PROCESS PARAMETERS FOR SPONTANEOUS pH SWING CRYSTALLIZATION OF NICOTINIC ACID\*

\*Submitted to Crystal Growth & Design

Nicotinic acid (HNic) is crystallized by adding hydrochloric acid (HCl) to sodium nicotinate (NaNic) aqueous solution in a semi-batch crystallization process. The crystallization process is monitored *in situ* with an Attenuated Total Reflectance Fourier Transform Infrared Spectrometer (ATR-FTIR). The *in situ* measurement of the metastable limit and solubility enables us to define the metastable (operating) zone for the crystallization of nicotinic acid. The influence of the acid addition rate, acid concentration and agitation speed on the metastable zone width have been studied. The metastable zone width's dependence on the acid addition rate is used to obtain the apparent order of nucleation of HNic. The effectiveness of micromixing is correlated with and explained by the metastable zone width. The most favorable parameters that will facilitate the formation of larger crystals without seeding are determined to be slow addition (1 g/hr) of diluted HCl (0.5 M) with agitation at just complete suspension speed, N<sub>IS</sub>, which is equivalent to 1.1 m/s stirrer tip speed.

## 3.1 Introduction

pH swing crystallization is one of the most commonly used types of crystallization in the chemical industry. In a pH swing crystallization, a solution of the deprotonated form is mixed with an acid. The protonated species is formed by a neutralization reaction

resulting in the concentration of the acid exceeding its solubility. This requires that the deprotonated form have a higher solubility than the protonated form has. pH swing crystallization can also be carried out in the opposite direction if the protonated form has a higher solubility than the deprotonated form. However, this is less commonly encountered. pH swing crystallization exploits the generally large solubility difference between the deprotonated and protonated forms to crystallize the less soluble species. Crystallization through pH swing is more energy efficient than cooling crystallization, since heating and cooling are not necessary. It is also advantageous over antisolvent crystallization because there is no need to perform separation of the solvents in the post crystallization processes.

As in most industrial crystallization processes, the final crystal size distribution (CSD) is usually one of the most important properties of the product because the final CSD directly affects the cost of the post crystallization processes such as filtration, drying, and packaging. In order to improve the CSD, it is necessary to measure the level of supersaturation at which spontaneous(primary) crystallization takes place, which is also called the metastable limit. Mullin et al. determined the metastable zone for cooling crystallization of an ammonium sulphate aqueous solution using maximum allowable undercooling temperature to express the maximum allowable supersaturation. The use of temperature to represent the metastable limit avoids measurement of the real concentration. However, it is not possible to use any other parameters to replace the real concentration of the crystallizing species in pH swing crystallization because pH change is not sensitive enough for a buffered solution, which is true in pH swing crystallization.

Measurement of the concentration of the crystallizing species is more challenging in pH swing crystallization than in cooling and anti-solvent crystallization. Due to the nature of supersaturation generation in pH swing crystallization, the presence of reactants during the crystallization of the product makes it more difficult to extract accurate information about the crystallizing species. This problem does not exist in cooling crystallization, and is less serious in anti-solvent crystallization. This challenge has led to far less work directed toward the in situ monitoring of pH swing crystallization than that on the more traditional ways of crystallization. There is only some theoretical modeling work done by Lindberg and Rasmuson<sup>2</sup> that approximates absolute concentration as supersaturation neglecting the solubility change as reaction continues. Aslund and Rasmuson<sup>3</sup> presented some experimental results on the influence of process variables on the crystal size distribution in a semibatch reaction crystallization process of benzoic acid. However, they correlated the crystal size distribution with the processing parameters without measuring the changing supersaturation versus the changing concentration of the reactant, which is the real driving force of crystallization.

Based on the method we developed earlier,<sup>4</sup> this chapter presents the *in situ* experimental ATR-FTIR measurement of the supersaturation and solubility of HNic in aqueous nicotinate solutions with the presence of sodium and chloride ions, under the conditions of the actual crystallization process. With the knowledge of the metastable zone width, analysis is provided for the influence of the process parameters, including the acid concentration, acid addition rate and the agitation speed, on the final crystal size

distribution. Products with significantly improved crystal size distribution are obtained without tedious trial and error.

## 3.2 Experimental Section

#### 3.2.1 Apparatus

A LabMax<sup>®</sup> system manufactured by Mettler-Toledo was used to carry out the crystallization experiment. The LabMax's physical system consists of a 1-liter glass reactor, a propeller, an FTS thermostat and a computer. The LabMax has two electronic units, the thermostating unit and the controller unit. The thermostating unit measures and controls the stirrer and a temperature sensor inside the reactor. The controller unit measures and controls external sensors and devices including a pH electrode, a ProMinent<sup>®</sup> gamma G/4b metering pump by ProMinent Fluid Controls, Inc. and a turbidity probe by Dow Chemical Company. The ProMinent® pump is used to control the addition of HCl. The turbidity probe allows the determination of the onset of spontaneous crystallization. The gain of the turbidity probe was pre-determined to be 5.

The glass reactor has a 100 mm internal diameter. Agitation is performed by an upflow propeller which has a diameter of 50 mm and is positioned with a clearance of 25 mm from the bottom of the crystallizer as recommended in the literature.<sup>5, 6, 7</sup> During the experiment, an ATR-FTIR probe is immersed in the solution or slurry to *in situ* monitor C(HNic) and C(NaNic). With the presence of an ATR-FTIR probe, a turbidity probe, a pH electrode and a temperature sensor, it is not necessary to add any baffles to the crystallizer to enhance mixing.

#### 3.2.2 Procedures

First,  $N_{JS}$ , the just complete suspension stirrer speed was determined experimentally. When the slurry is completely suspended, all particles are in motion and no particles remain on the reactor bottom for more than 1-2 seconds.<sup>7</sup> Therefore, the entire surfaces of the particles are exposed to the fluid to ensure that maximum surface area is available for further nucleation and growth. A mixture of 3.6 grams of 455  $\mu$ m mean sized crystals and 600 mL saturated HNic aqueous solution was prepared, which has a similar density as the slurries in actual experiments. The reactor was well illuminated, and careful observation was made of the particles around the bottom of the reactor. No particles remained stationary on the base for more than 1-2 seconds when the agitation speed reached 420 rpm, which corresponds to a tip speed of 1.1 m/s. It is easier to correlate the tip speed with secondary nucleation than using the revolutions per minute, due to the different dimensions of different types of stirrers.

With the agitation speed at 1.1 m/s, the experiments were carried out at  $30 \pm 0.1$  °C by feeding HCl with the ProMinent pump to about 520 mL of 1M NaNic aqueous solution. One-half molar and 2 M HCl were made by dilution of the 32 wt% HCl, and were standardized with NaOH. NaOH was titrated against the primary standard, potassium hydrogen phthalate (KHP). NaNic was purchased from Aldrich Chemical Company and used as received. The ReactIR 1000 system was used to monitor C(HNic) and C(NaNic) in situ throughout the experiments. The first metastable limit was determined when the turbidity probe's signal reached 0.03 and then increased rapidly. The addition of HCl

was stopped once the relative intensity of the signal from the turbidity probe increased to 0.03. Enough time (about 2 hrs) was allowed for the spontaneous crystallization to take place so that C(HNic) could attain a constant value, which is the solubility of HNic at a specific conentration of NaNic. The slurry was filtered with the filtrate being kept about 30°C. The filtrate was put back to the LabMax® reactor, and the addition of HCl was restarted until the turbidity probe showed an increase in the signal again. The procedure was repeated to obtain multiple metastable limits and solubility data so that an apparent metastable zone can be defined. The apparent metastable zone is not a fundamental property of the chemical system, but depends on the process parameters employed.<sup>8, 9</sup> The experiment was repeated three times. The average values for metastable limits and solubility are reported, respectively, because three values of each would replicate. The metastable limit was also measured with another agitation speed of 750 rpm (a tip speed of 1.9 m/s). Different acid addition rates, 1 g/hr, 2 g/hr and 60 g/hr, were examined for their effect on the metastable limit.

The product from each experiment was filtered, dried and observed under an optical microscope at the magnification of 10. The product from the experiment with the addition rate of 1 g/hr of 0.5 M HCl and with agitation speed of 1.1 m/s was sieved for size distribution determination, but all the other combinations of the process parameters resulted in bulky solids that are aggregates of very small crystals that could not be sieved effectively. The crystal size distribution of the larger crystals was measured through sieving with a set of Scienceware Mini-Sieves from Fisher using a Tyler RX-86 sieve

shaker. Sieving was completed after about 1 hr or until the change of the weight above each sieve was less than 5%.

# 3.3 Results

Figure 3.1 shows the result of metastable zone measurement at 30°C with the addition of 2M HCl at the rate of 60 g/hr and with the agitation speed at 1.1 m/s.

The measurement starts with pure 1M NaNic solution. As 2M HCl is added, NaNic is converted to HNic. After about 80 grams of 2M HCl is added, the first spontaneous crystallization takes place. Averaging the three measurements, the best fit lines, which define the metastable zone, are plotted in Figure 3.2.

The solubility,  $C^*(HNic)$ , can be fitted into a linear equation as follows,

$$C^*(HNic) = 0.18C(NaNic) + 2.3$$
 (3.1)

The metastable limit, M(HNic), can be expressed with another linear equation below,

$$M(HNic) = 0.21C(NaNic) + 2.9$$
(3.2)

Similar measurements were performed varying the process parameters including the acid addition rate, acid concentration and agitation speed. Firstly, the acid addition rate is changed to 1 g/hr while the acid concentration is kept at 2M and agitation speed at 1.1 m/s.

Figure 3.3 shows the concentration profile of the spontaneous crystallization at different acid addition rates.

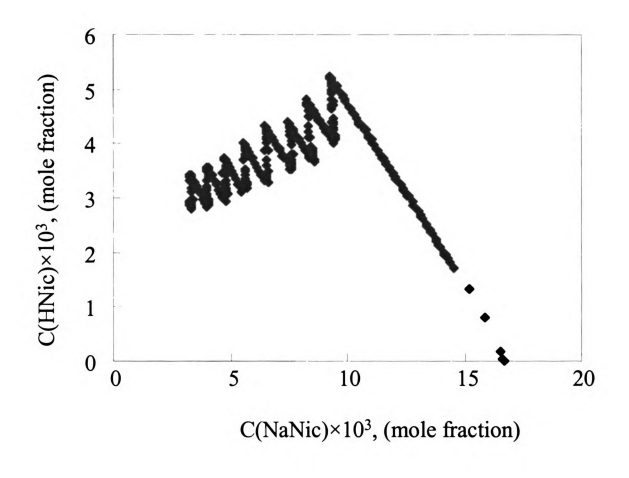


Figure 3.1. The concentration of nicotinic acid vs. the concentration of NaNic during the metastable zone measurement of the spontaneous crystallization of nicotinic acid at 30  $\pm$  0.1°C, with agitation speed of 1.1 m/s and acid addition rate of 60 g/hr of 2 M HCl.

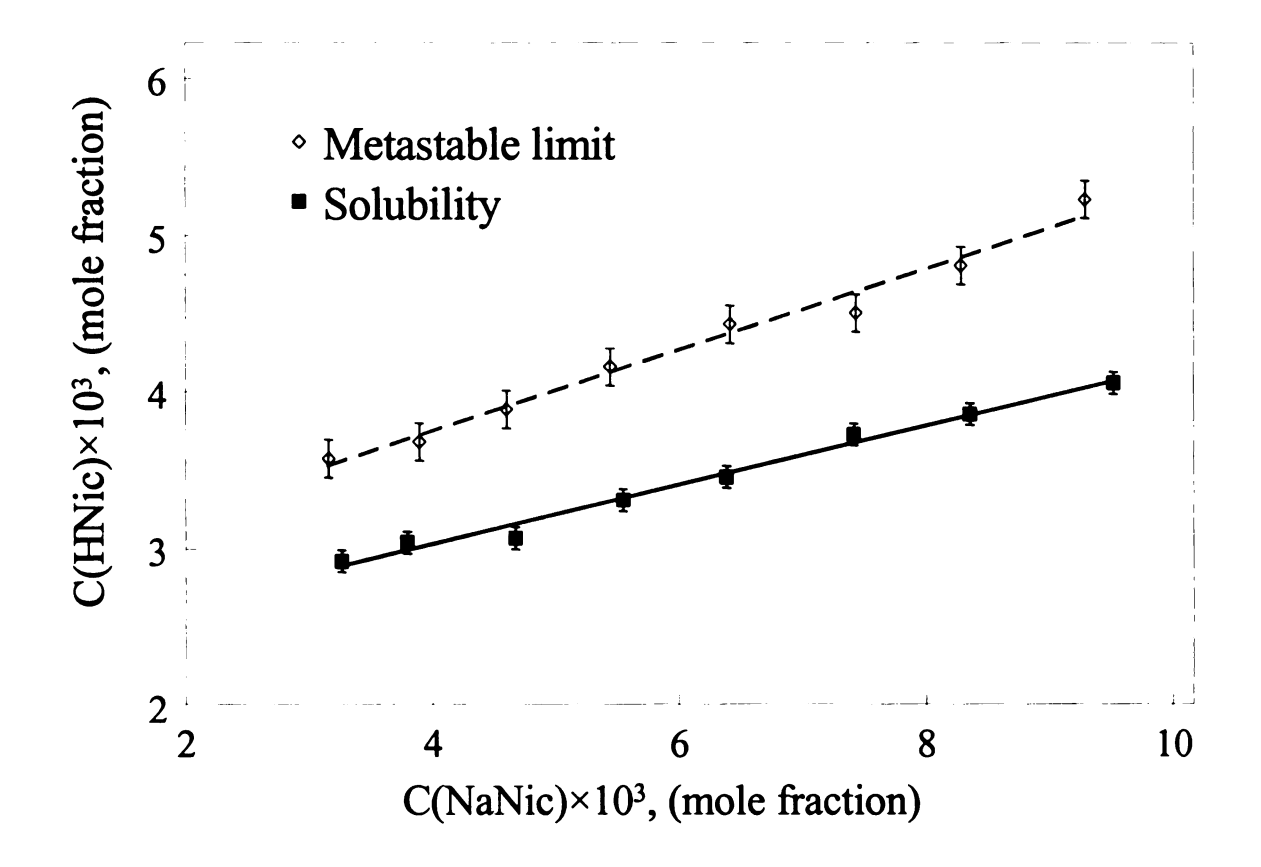


Figure 3.2. The metastable zone of the crystallization of nicotinic acid measured under the conditions that the solution is agitated at 1.1 m/s and 2 M HCl is added at the rate of 60 g/hr at 30°C.

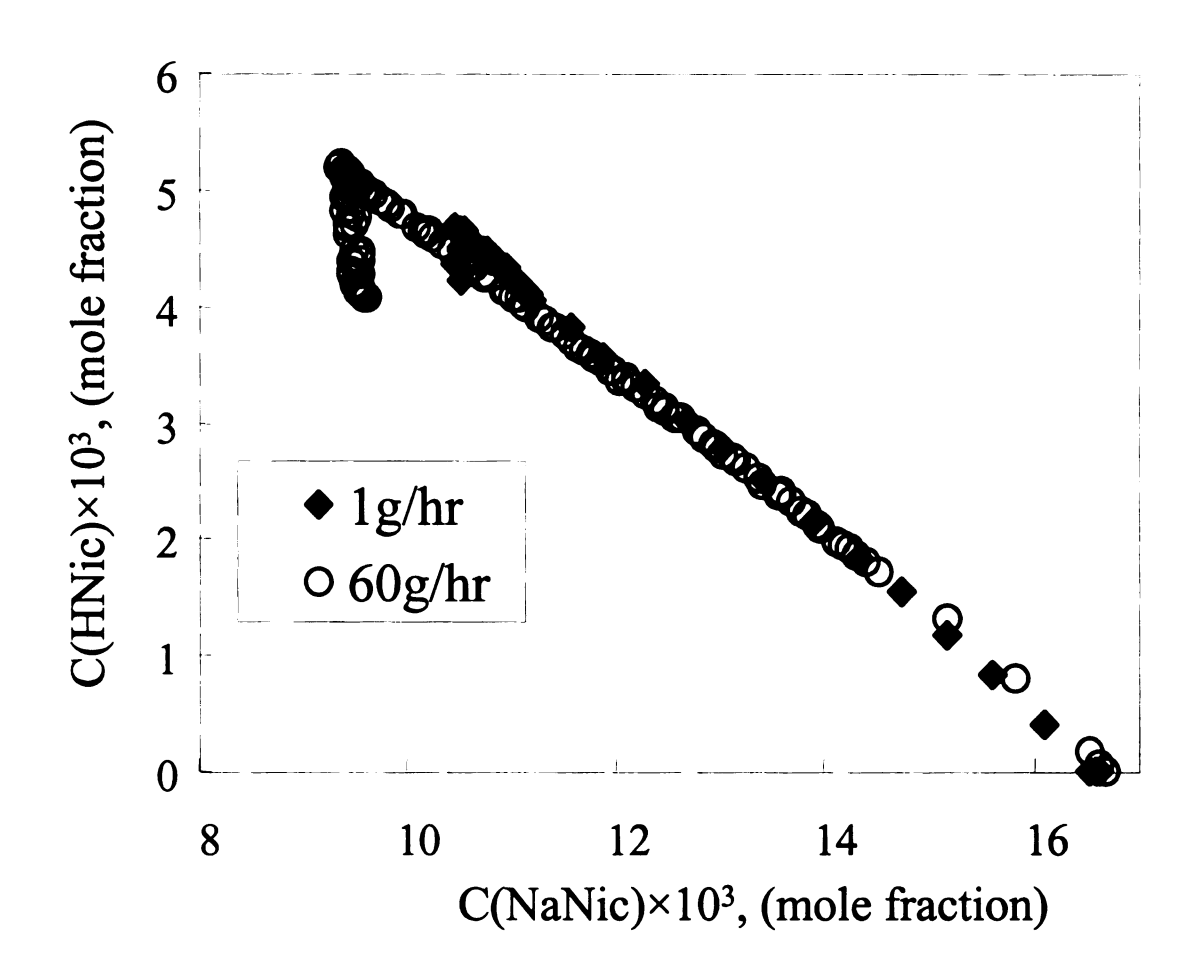


Figure 3.3. Comparison of the first metastable limit measurement with different acid addition rates, 1 g/hr and 60 g/hr. The acid concentration is 2 M HCl and the agitation speed is 1.1 m/s. The temperature is  $30 \pm 0.1$ °C.

If the width between the metastable limit and the solubility measured with the acid addition rate at 60 g/hr is taken as unity, the width between the metastable limit and solubility with the acid addition rate at 1 g/hr is equivalent to 0.51.

The result is summarized in Table 3.1 as follows.

**Table 3.1.** Metastable limit comparison with different addition rates of 2 M HCl.

| Acid addition | C(HCl)   | Agitation tip speed, | Metastable zone |
|---------------|----------|----------------------|-----------------|
| rate, (g/hr)  | (mole/l) | (m/s)                | width           |
| 1             | 2        | 1.1                  | 0.51            |
| 60            | 2        | 1.1                  | 1               |

The products from both of the two measurements are powder-like particles. There is no significant difference in size as observed under the optical microscope. The particles have similar size to those shown in Figure 3.4a.

In the second set of measurements, the acid concentration was varied with the addition rate at 1 g/hr and agitation speed at 1.1 m/s. Similar profiles are obtained to Figure 3.3. The results are summarized in Table 3.2, again with the metastable zone width normalized against that measured with the addition of 2 M HCl at the rate of 60 g/hr and agitation speed at 1.1 m/s.

**Table 3.2.** Metastable limit comparison with different acid concentration.

| C(HCl)   | Acid addition | Agitation tip speed, | Metastable zone |
|----------|---------------|----------------------|-----------------|
| (mole/l) | rate, (g/hr)  | (m/s)                | width           |
| 0.5      | 1             | 1.1                  | 0.50            |
| 2        | 1             | 1.1                  | 0.51            |

The products from the two experiments are significantly different. Figure 3.4 presents the photos of the two products taken with the optical microscope.

The experiment with the addition of 0.5 M HCl at the rate of 1 g/hr and agitation speed of 1.1 m/s produced crystalline materials of larger size as compared to the one with the addition of 2 M HCl at the same addition rate and agitation speed. The crystal size distribution for the case with addition of 0.5 M HCl is shown in Figure 3.5.

In the third set of measurements, the agitation speed was varied while the acid concentration was held constant at 0.5 M and the acid addition rate was kept at 1 g/hr. The metastable zone widths are compared in Table 3.3.

Table 3.3. Metastable limit comparison with different agitation speed.

| Agitation tip speed, (m/s) | C(HCl)<br>(mole/l) | Acid addition rate, (g/hr) | Metastable zone width |
|----------------------------|--------------------|----------------------------|-----------------------|
| 1.1                        | 0.5                | 1                          | 0.50                  |
| 1.9                        | 0.5                | 1                          | 0.29                  |

The products from both of the two measurements are powder-like particles. There is no significant difference in size between them as observed under the optical microscope. The particles have similar sizes to those shown in Figure 3.4a.

The results from the three sets of measurement suggest that the product with the following process parameters, 0.5 M HCl added at 1 g/hr and agitation speed of 1.1 m/s, results in the largest mean size crystal size distribution. However, the slow acid addition

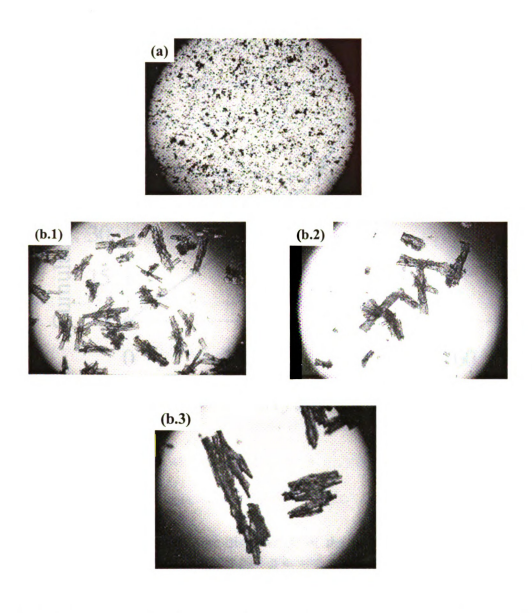


Figure 3.4. Influence of the acid concentration on crystal size: (a): 2 M HCl, addition rate of 1 g/hr and 1.1 m/s agitation speed, The average size of the product is about 25  $\mu$ m. (b) 0.5 M HCl, addition rate of 1 g/hr and 1.1 m/s agitation speed, (b.1), (b.2) and (b.3) are the crystals after sieving. The average size of (b.1) is 152  $\mu$ m, that of (b.2) is 214  $\mu$ m and that of (b.3) is 305  $\mu$ m.

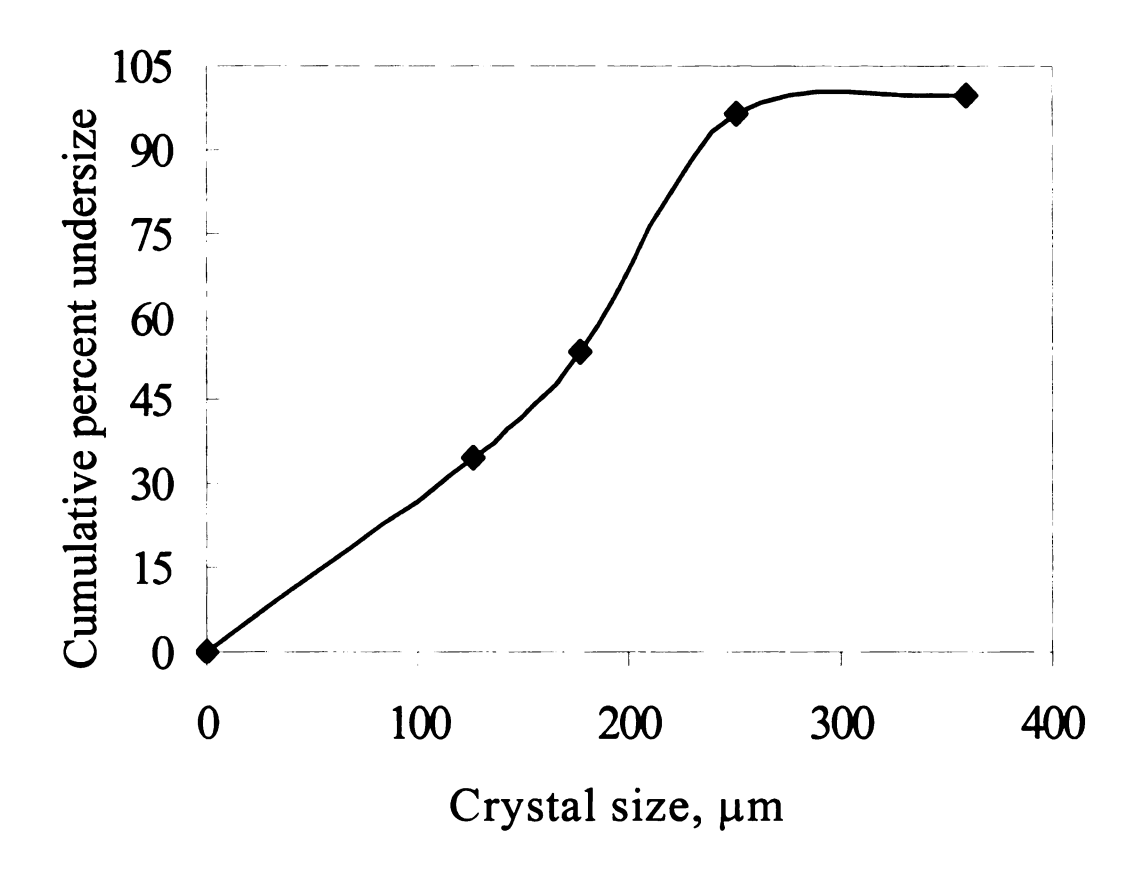


Figure 3.5. The crystal size distribution of the product from the experiment with the addition of 0.5 M HCl at the rate of 1 g/hr and agitation speed of 1.1 m/s.

rate made it very time consuming to conduct the crystallization. The next set of measurements was designed to study the possibility of increasing the acid addition rate without sacrificing the quality of the product. The other acid addition rates examined were 2 g/hr and 60 g/hr while C(HCl) and agitation speed were kept at 0.5 M and 1.1 m/s, respectively. The metastable zone width results are summarized in Table 3.4.

**Table 3.4.** Metastable limit comparison with different addition rates of 0.5 M HCl.

| Acid addition rate,<br>(g/hr) | Agitation speed, (m/s) | C(HCl)<br>(mole/l) | Metastable zone width |
|-------------------------------|------------------------|--------------------|-----------------------|
| 1                             | 1.1                    | 0.5                | 0.50                  |
| 2                             | 1.1                    | 0.5                | 0.66                  |
| 60                            | 1.1                    | 0.5                | 0.90                  |

Both of the acid addition rates at 2 g/hr and 60 g/hr resulted in powder-like particles. There was no significant difference in size between them under the optical microscope. The particles had similar sizes as those shown in Figure 3.4a. This result indicates that the acid addition rate of 1 g/hr is the only rate, with combination of 0.5 M C(HCl) and agitation speed of 1.1 m/s, with which the resultant crystals can grow into larger sizes.

#### 3.4 Discussion

As compared to other systems such as benzoic acid,<sup>3</sup> this particular crystallizing system, HNic, has a final crystal size distribution that cannot be directly correlated to the process parameters. Massive nucleation takes place once some nuclei are formed when micromixing is not effective or the intensity of agitation is too high. The metastable zone width helps us understand the interaction of the nucleation kinetics, micromixing and agitation intensity on the final CSD of the product.

# 3.4.1 Effect of Acid Addition Rate -- the Apparent Order of Nucleation

Utilizing the result shown in Table 3.1, we can estimate the nucleation kinetics with a similar method of those given in the literature.<sup>8,9</sup> The method developed by Nyvlt<sup>9</sup> is applied for cooling crystallization utilizing the approximation as follows,

$$B = \left(\frac{dC^*}{dT}\right)r_l = \frac{dC^*}{dt} \tag{3.3}$$

where B is the nucleation rate,  $\frac{dC^*}{dT}$  is the solubility's dependence on temperature,  $r_l$  is

 $\frac{dT}{dt}$ , the rate of cooling. This method is based on the assumption that, at least at the initial stage of nucleation (on attaining the metastable limit), the mass nucleation rate or the consumption rate of supersaturation equals the generation rate of supersaturation. We can derive a similar equation to express the nucleation rate for pH swing crystallization of HNic as follows,

$$B = \frac{dC_{MAX}}{dt} = \frac{dC(NaNic)}{dt} = r_{pH}$$
 (3.4)

where  $C_{MAX}$  is the concentration of HNic at the metastable limit.  $r_{pH}$  is the generation rate of supersaturation in the pH swing crystallization. The nucleation rate can also be expressed in the form of a power law when heterogeneous nucleation is considered to be the predominant form of primary nucleation,  $^{8,10}$ 

$$B = k_N \Delta C_{MAX}^n \tag{3.5}$$

where  $k_N$  is the nucleation rate constant and  $\Delta C_{MAX}$  is the metastable zone width. The exponent n is the apparent order of nucleation, which is not a fundamental property of a system.

Combining equations (3.4) and (3.5), we can calculate the apparent order of nucleation using the metastable zone width measured at different rates at which supersaturation is generated by the acid-base reaction.

$$n = \frac{\log_{10} \left( \frac{r_{pH}^1}{r_{pH}^2} \right)}{\log_{10} \left( \frac{\Delta C_{MAX}^1}{\Delta C_{MAX}^2} \right)}$$
(3.6)

From the data listed in Table 3.5, n is determined to be 6.3.

**Table 3.5.** The rate of decrease of concentration of sodium nicotinate at different acid addition rates and their corresponding metastable zone width.

| Addition rate of 2 M HCl<br>(g/hr) | $\frac{dC(NaNic)}{dt}$ (mole fraction/hr) | Metastable zone width |
|------------------------------------|---|-----------------------|
| 1                                  | $0.07 \times 10^{-3}$                     | 0.51                  |
| 60                                 | $4.82 \times 10^{-3}$                     | 1                     |

According to the apparent order of nucleation, 6.3, we can estimate that the nucleation rate for the case with the acid addition rate of 60 g/hr is 70 times as high as that for the case with the acid addition rate of 1 g/hr. A large nucleation rate results in very small particle size, which is observed experimentally. However, for the acid addition rate of 1 g/hr, the final crystal size should have been larger, which is contradictory to the experimental result. This can be due to the inadequate micromixing, which may cause high local supersaturation and consequently high nucleation rate, while the measured

bulk supersaturation is not a good indicator for the nucleation rate. This is further confirmed by the acid concentration's effect on the metastable limit and final product, as shown in Table 3.2 and Figure 3.4.

# 3.4.2 Effect of Acid Concentration

The results in Table 3.2 showed almost no difference in the metastable limit or metastable zone width between the additions of 0.5 M and 2 M HCl. However, their resultant products have very significant difference in terms of size. This further confirms that the addition of 2 M HCl generates highly supersaturated solutions in the reaction zone and micromixing is not effective in dispersing the high supersaturation before nucleation starts.<sup>3,11,12</sup> Micromixing is the mixing process by which two different liquids contact and mix at the molecular level so that the segregated areas of uniform, but mutually different composition disappear; in other words, the mixture attains complete homogeneity on the molecular level. 13 The time it takes for acid-base reactions to go to completion is generally considered to be shorter than the time of micromixing. The effectiveness of micromixing is determined by the micromixing time scale and the induction time scale.<sup>3, 12</sup> If the induction time is shorter than micromixing time, nucleation will take place in the reaction zone before the molecular diffusion facilitated micromixing dilutes the local concentrated solution. This is likely what happened in the experiment with the addition of 2 M HCl, which is so concentrated that it generates relatively high supersaturation in the reaction zone and results in a very short induction time. Conversely, the addition of 0.5 M HCl does not cause the generation of high local supersaturation and the induction time is longer than the micromixing time. Therefore,

nucleation happens in the bulk solution after the local supersaturation is dispersed into or diluted by the bulk environment.

# 3.4.3 Effect of Agitation Speed

Contradictions exist in the literature as to the effect of agitation speed on the mean size, as summarized by Rasmuson et al.<sup>3</sup> Some of the studies did not consider the necessity of employing agitation speed at least at the just complete suspension speed, N<sub>JS</sub>, which ensures the homogeneity of mixtures macroscopically. With agitation speed less than N<sub>JS</sub>, it is impossible to predict the mass transfer process for the unsuspended particles, which may cause some of the contradictions in the effect of agitation speed on the final particle size. In this study, the lowest agitation speed applied is N<sub>JS</sub>, 1.1 m/s. The higher speed of 1.9 m/s initiates crystallization when the relative metastable limit is 0.29, much lower than that at 1.1 m/s. This result indicates that the micromixing at 1.9 m/s results in faster redistribution of supersaturation. However, the final products are powder-like particles similar to that in Figure 3.4a. This appearance can be explained by attrition, breakage or fragmentation, which becomes significant for the needle-shaped crystals of HNic upon excessive intensive agitation.

The most favorable condition which yields the largest crystals is the addition of 0.5 M HCl at the rate of 1 g/hr with agitation speed at 1.1 m/s. Attempts were made to increase the acid addition rate to 2g/hr and 60g/hr to shorten the length of time needed with 1g/hr addition rate. The results show that neither of the two rates can compete with 1g/hr when the final products are compared. This is again due to the effect of micromixing on

nucleation as can be explained by the metastable zone width. Therefore, it can be concluded that 1 g/hr addition of 0.5 M HCl to 1 M NaNic aqueous solution stirred at 1.1 m/s is the best combination of the process parameters examined in current study to yield crystals through spontaneous crystallization with favorable CSD and filtration and drying properties. Further improvement can be made by seeding crystallization, which is the focus of the next chapter.<sup>14</sup>

## 3.5 Conclusions

The metastable zone for the semi-batch crystallization of HNic was measured using *in situ* ATR-FTIR spectroscopy when 2 M HCl was added to 1 M NaNic aqueous solution at the rate of 60 g/hr with agitation speed at 1.1 m/s. Process variables influence the metastable zone width and the product crystal size distribution significantly. With the knowledge of the metastable zone width from *in situ* measurement, the order of nucleation and the relative nucleation rate can be estimated. *In situ* results of metastable zone width also clarify our understanding of the effect of micromixing on the crystal size distribution. It is found that 2 M HCl can not be effectively mixed with NaNic at 1.1 m/s no matter whether the addition rate is 1 g/hr or 60 g/hr. When the acid concentration decreases to 0.5 M, the addition rate of 1 g/hr and agitation speed at 1.1 m/s will yield larger crystals with reduced times for filtration and drying. Excessive intensive agitation at 1.9 m/s causes fragmentation of particles and in turn unfavorable crystal size distribution.

# 3.6 Acknowledgment

The financial support from the Dow Chemical Company for this study is gratefully acknowledged. The authors would also like to express appreciation to ASI Applied Systems and Mettler-Toledo for the contribution of the LabMax<sup>®</sup> instrument.

#### References

- 1. Mullin, J. W.; Charkraborty, M.; Mehta, K. J. of Appl. Chem. 1970, 20, 367-371.
- 2. Lindberg, M.; Rasmuson, Å. C., Chemical Engineering Science 2000, 55, 1735-1746
- 3. Åslund, A. L.; Rasmuson, Å. C. AIChE J. 1992, 38(3), 328-342.
- 4. Wang, F.; Berglund, K. A. Ind. Eng. Chem. Res. 2000, 39, 2101-2104,
- 5. He. Y.; Takahashi. K. J. Chem. Eng. Japan 1995, 28(6), 786-789.
- 6. Shimizu, K.; Nomura, T.; Takahashi, K. J. Cryst. Growth 1998, 191, 178-184.
- 7. Harnby, N.; Edwards, M. F.; Nienow, A. W. Mixing in the Process Industries, 2nd Edition, Butterworth-Heinemann Ltd: Oxford, 1992.
- 8. Myerson, A. S. In *Handbook of Industrial Crystallization*; Myerson, A. S. Eds.; Butterworth-Heinemann Ltd: Oxford, 1992; Chapter 2, pp 43-52.
- 9. Nyvlt, J. J. Cryst. Growth 1968, 3/4, 377-383.
- 10. Mullin, J. W. Crystallization, 3rd Edition, Butterworth-Heinemann Ltd: Oxford, 1993.
- 11. Barata, P. A.; Serrano, M. L. J. Cryst. Growth 1996, 163, 426-43.
- 12. Phillips, R.; Rohani, S.; Baldyga, J. AIChE J. 1999, 45(1), 82-92.
- 13. Sohnel, O.; Garside, J. *Precipitation: Basic Principles and Industrial Applications*, Butterworth-Heinemann Ltd: Oxford, 1992.
- 14. Wang, F.; Berglund, K. A., submitted to Crystal Growth & Design

# Chapter 4

# FEEDBACK CONTROL OF SEEDED SEMI-BATCH pH SWING CRYSTALLIZAION OF NICOTINIC ACID\*

\*Submitted to Crystal Growth & Design.

Optimization of the process parameters for semi-batch pH swing crystallization was demonstrated in the preceding chapter. Due to the slow addition rate of diluted hydrochloric acid, it is extremely time-consuming to produce the large mean size crystals by spontaneous nucleation. The length of time needed to induce crystallization can be significantly reduced by external seeding. Seeding at different levels of supersaturation demonstrates increased supersaturation increases secondary nucleation. The level of supersaturation was *in situ* controlled at constant level through the automatic adjustment of post addition of HCl. It is found that keeping the solution at low supersaturation, or close to the equilibrium solubility promotes crystal growth and suppresses secondary nucleation to the largest degree.

#### 4.1 Introduction

As in most industrial crystallization processes, production of a specified crystal size distribution (CSD) is one of the primary goals in semi-batch pH swing crystallization. Significant cost reductions can be achieved by creating CSDs that have favorable filtration and drying properties. Supersaturation, as the driving force for crystallization, determines the relative rate of nucleation and crystal growth and, as such, controls the resulting CSD.<sup>1,2</sup> Therefore, control of crystallization processes requires *in situ* measurement and subsequent control of supersaturation. Compared to the numerous off-

line analytical techniques for the measurement of solubility and supersaturation,<sup>3</sup> ATR-FTIR provides a unique sampling configuration allowing *in situ* measurement of solution phase concentration in slurry without phase separation.<sup>4,5</sup> The ability of *in situ* measurement of supersaturation is critical for the *in situ* control of semi-batch pH swing crystallization. It has been demonstrated that maintenance of constant supersaturation during a crystallization process leads to improved crystal size distribution for batch cooling crystallization and semi-batch anti-solvent crystallization.<sup>6,7</sup> However, there have been few studies focused on the control of semi-batch pH swing crystallization. The primary reason may be due to the presence of multi-species in this type of crystallization. Based on the technique we developed earlier,<sup>5,8</sup> the study of *in situ* control of seeded pH swing crystallization of nicotinic acid (HNic) is presented in this chapter.

In the preceding chapter, we have demonstrated that production of crystals with favorable CSD through spontaneous crystallization is extremely difficult because of the high supersaturation and excessive nucleation that often occurs. Even though we have identified the process parameters which facilitate the production of favorable CSD, the productivity is extremely limited by the slow nucleation and crystal growth kinetics. One solution to overcome this difficulty is to use external seeding. Seeding the supersaturated solution not only avoids the time-consuming primary nucleation process, it also provides control over the product size and size distribution, and consequently consistency from batch to batch. In this chapter, we demonstrate the importance of the level of supersaturation's effect on secondary nucleation. The *in situ* supersaturation value is

used to control the rate of post-seeding acid addition so that secondary nucleation is continuously minimized, and thereafter the final crystal size distribution can be optimized.

#### 4.2 Experimental Section

#### 4.2.1 Apparatus

A LabMax<sup>®</sup> system manufactured by Mettler-Toledo was used to carry out the crystallization experiments. The LabMax<sup>®</sup> s physical system consists of a 1-liter glass reactor, a propeller, an FTS thermostat and a computer. The LabMax<sup>®</sup> has two electronic control units, the thermostat unit and the controller unit. The thermostat unit measures and controls the stirrer and the temperature sensor inside the reactor. The controller unit measures and controls external sensors and devices including a pH electrode, a ProMinent<sup>®</sup> gamma G/4b metering pump by ProMinent Fluid Controls, Inc. and a turbidity probe by Dow Chemical Company. The ProMinent<sup>®</sup> pump is used to control the addition of HCl. The gain of the turbidity was pre-determined to be 5.

The glass reactor has a 100 mm internal diameter. Agitation is performed by an upflow propeller which has a diameter of 50 mm and is positioned with a clearance of 25 mm from the bottom of the crystallizer. The ratio of the propeller diameter to the reactor diameter and the ratio of the clearance from the bottom to the reactor diameter are chosen as recommended in the literature to ensure the best macromixing.<sup>5, 6, 7</sup> During the experiments, an ATR-FTIR probe was immersed in the solution or slurry to monitor the concentrations of nicotinic acid (HNic) and sodium nicotinate (NaNic) *in situ*. With the

presence of an ATR-FTIR probe, a turbidity probe, a pH electrode and a temperature sensor, it is not necessary to add any baffles to enhance mixing.

## 4.2.2 Interface between the LabMax® and the ReactIR 1000

The LabMax®-ReactIR interface is a collection of programs and a serial cable which provides communications capabilities between the ASI Applied Systems ReactIR spectrometer and the Mettler LabMax<sup>®</sup> reactor. The interface transmits LabMax<sup>®</sup> status and values from the LabMax® to the ReactIR, and the ReactIR values from the ReactIR to the LabMax<sup>®</sup>. The interface also provides synchronization to allow a ReactIR experiment to start automatically when the LabMax® starts executing a recipe. The hardware requirement for the interface is a null modem serial cable that connects the LabMax® and the ReactIR computers through their RS-232-ports. The software required for the LabMax<sup>®</sup> is MaxSeril.exe written by Mettler Toledo. This program reads values from the LabMax® and sends them to the ReactIR system. It also accepts values from the serial port and uses DDE (Dynamic Data Exchange) to transmit them to the LabMax® program. The software required for the ReactIR is CommRW.exe written by ASI Applied Systems. The program reads data from the LabMax<sup>®</sup>, and also sends the ReactIR data to the LabMax® via the serial port. The interface automatically sends values for a specific set of variables to the LabMax<sup>®</sup>. These variables include: ReactIR Ready, Conc A, Conc B. Any ReactIR variables which are defined with the above names and profiled within the ReactIR software will be sent to the LabMax®. These variables may also be used to terminate a stage within the LabMax® recipe. We defined the relative supersaturation as ReactIR Ready, and employed this variable to terminate or start the addition of HCl when the supersaturation deviates from the set points. In doing so, supersaturation is controlled within the desired range to realize the control of final crystal size distribution.

#### 4.2.3 Procedures

With the agitation tip speed set to 1.1 m/s, as determined in the preceding chapter,<sup>8</sup> the experiments were carried out at  $30 \pm 0.1^{\circ}\text{C}$  by feeding HCl with the ProMinent pump to about 520 mL of 1M NaNic aqueous solution. One-half molar and 2M HCl were made by dilution of the 32wt% HCl, and were standardized with NaOH. NaOH was titrated against the primary standard potassium hydrogen phthalate (KHP). NaNic was purchased from Aldrich Chemical Company and used as received. The ReactIR 1000 system was used to monitor concentrations of HNic and NaNic *in situ* throughout the experiments.

#### 4.2.3.1 Seeding at Different Levels of Supersaturation

In this set of measurements, we adopt the same expression for supersaturation as in Chapter 3. The relative supersaturation is defined as a fraction of the unit metastable zone width, which is measured with addition of 2M HCl at the rate of 1g/min and agitation tip speed of 1.1 m/s. We have shown in the previous chapter that the equation for the solubility of HNic,  $C^{\bullet}(HNic)$ , as a function of C(NaNic) is,

$$C^{\bullet}(HNic) = 0.18C(NaNic) + 2.3$$
 (4.1)

And the metastable limit of HNic, M(HNic), as a function of C(NaNic) is

$$M(HNic) = 0.21C(NaNic) + 2.9$$
 (4.2)

The relative supersaturation compared to the metastable limit at any point of the reaction or crystallization is defined as,

$$S_R = \frac{C(HNic) - C^*(HNic)}{M(HNic) - C^*(HNic)} \tag{4.3}$$

For the seeding experiments, the seeds were prepared by dissolving HNic in ethanol at an elevated temperature. The solution is allowed to cool down at room temperature without being agitated, and the solvent was allowed to evaporate at room temperature and pressure. The recrystallized HNic was sieved with a set of Scienceware Mini-Sieves from Fisher using a Tyler RX-86 sieve shaker. Sieving was completed until the change of the weight above each sieve was less than 5%. The crystals with an average size of 152 μm, sieve cut between 127 μm and 177 μm, were used for seeding experiments. Five hundred and twenty milliliters of 1 M aqueous NaNic was prepared as the starting solution. Sixty grams of 2 M HCl were added to the NaNic solution at the rate of 6 g/min. Then the addition of 2 M HCl was slowed to 1 g/min until relative supersaturation reached the specified value, which is 30% or 45% or 60%. It is worth mentioning that the termination of acid addition is controlled by the value of the relative supersaturation transmitted from the ReactIR to the LabMax®. At least 30 minutes were allowed to ensure that no spontaneous crystallization occurred at the specified level of relative supersaturation before seeds were added to the supersaturated solution. C(HNic) measured by the ReactIR started to decrease until  $S_R$  approached 0%, which indicated that crystal growth of the added seeds and secondary nucleation had consumed all the supersaturation and crystallization was completed. At this point, the slurry was filtered and dried overnight. Sieve analysis was performed with a set of Scienceware Mini-Sieves from Fisher using a Tyler RX-86 sieve shaker. Sieving was completed until the change of the weight above each sieve was less than 5%.

### 4.2.3.2 Seeding with Post Addition of HCl

This set of experiments started with 520 mL of 1 M aqueous NaNic. The seed concentration was 1.5 g seeds/kg solution. The procedures up to the addition of seeds are the same as those mentioned in section 4.2.3.1. Once seeds were added into the crystallizer, HCl was changed from 2 M to 0.5 M. In the first experiment, relative supersaturation was controlled at about 30%  $\pm$  10%. In other words, the addition of 0.5 M was prompted automatically once  $S_R$  went below 20%, and the addition of the acid was terminated once  $S_R$  surpassed 40%. During the stages when 0.5 M HCl was added, the addition rate was at 6 g/hr. This rate was estimated from the previous data of seeding without post-seeding acid addition. The second experiment was to add the seeds at just above saturation or 0% relative supersaturation and then control the solution at 0% relative supersaturation during the post addition of 0.5 M HCl. The last experiment carried out was to introduce the seeds at 30% relative supersaturation and then control relative supersaturation at about 0%.

The products from each experiment were filtered and dried overnight. Then they were observed under an optical microscope at the magnification of 10. The crystal size distribution was measured by sieve analysis with the Scienceware Mini-Sieves from Fisher using a Tyler RX-86 sieve shaker. Sieving was completed until the change of the weight above each sieve was less than 5%.

#### 4.3 Results and Discussion

#### 4.3.1 Seeding at Different Levels of Supersaturation

The experiment started with pure 1 M NaNic aqueous solution. As 2 M HCl was added. NaNic was converted to HNic. The relative supersaturation reached 60% after about 73 g 2 M HCl was added. Upon addition of 1 g of the 152 µm HNic seed, C(HNic) started to decrease as crystal growth on the seeds took place. At the same time, secondary nucleation also consumed some of the supersaturation. Secondary nucleation and crystal growth stopped upon depletion of the supersaturation. Figure 4.1 presents the profiles of C(NaNic), C(HNic) and its relative position with respect to its solubility and metastable limit. The acid addition profile and the supersaturation profile for 60%- $S_R$  seeding are shown in Figure 4.2. The acid addition was set at a faster rate, 6 g/min, at the beginning of the experiment. After 60 g of 2 M HCl were added, the relative supersaturation value from the ReactIR indicated that the solution is close to saturation with respect to C(HNic) although it was still undersaturated. At this point, the acid addition rate was slowed to 1 g/min to ensure that no local supersaturated region was generated in the solution so that early nucleation could be avoided. As the acid was continuously added to convert NaNic to HNic, the relative supersaturation of HNic increased. The acid addition was terminated by the LabMax® once the value of the relative supersaturation transmitted from the ReactIR reached 60%. After this point, seeds were introduced to the solution and the relative supersaturation started to decrease. Finally the relative supersaturation was reduced to the value of 0%. Throughout the whole crystallization process, the solid phase was

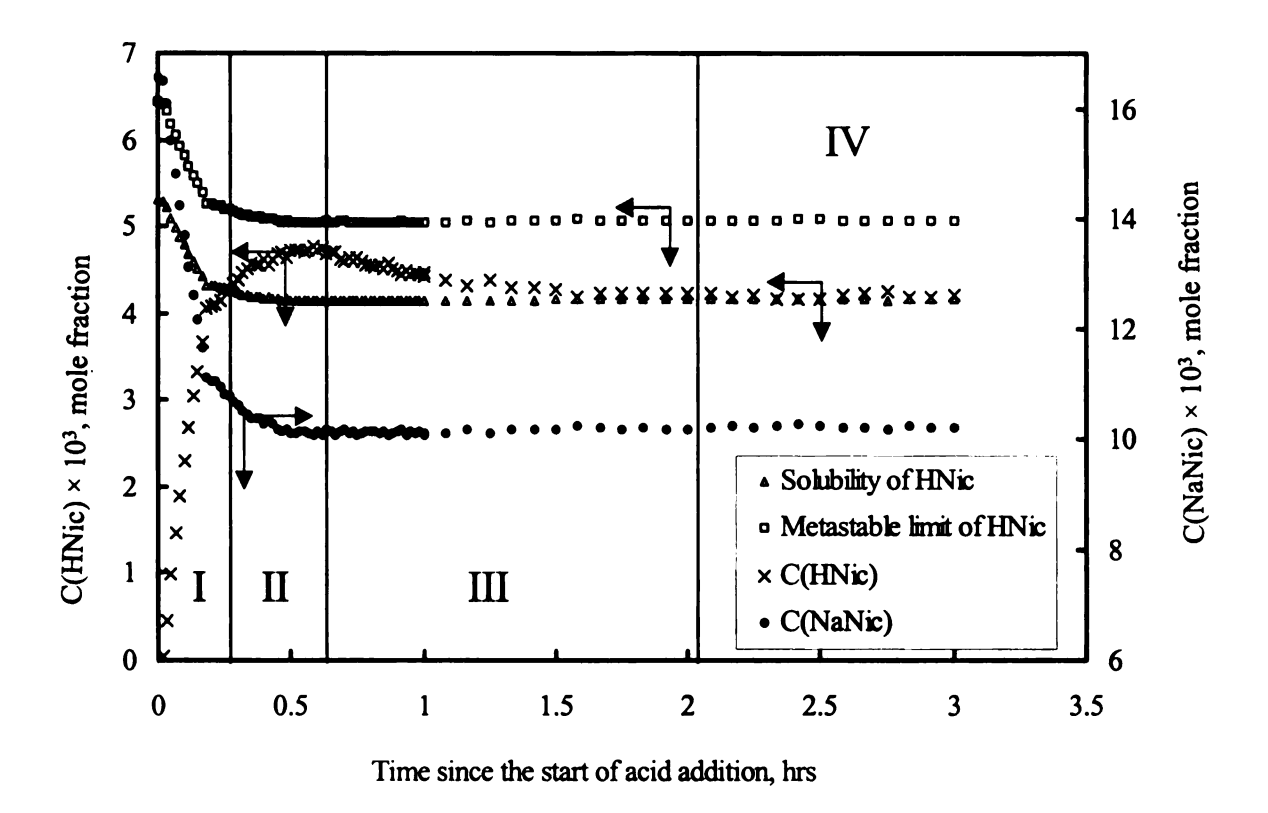


Figure 4.1. Concentration profile of seeded crystallization of nicotinic acid at 60% relative supersaturation seeding. The seeds were added at 30 mins after the relative supersaturation reached 60% with seed concentration of 1.5g seeds/kg of solution.  $T = 30 \pm 0.1$ °C. Region I: Starting with sodium nicotinate aqueous solution of 1 M, which is equivalent to  $16.5 \times 10^{-3}$  mole fraction, the concentration of nicotinic acid approaches its solubility as sodium nicotinate is converted to nicotinic acid by HCl. The solution is in the undersaturated state. Region II: Supersaturated solution with the degree of the relative supersaturation increasing until it reaches 60%, no nucleation or crystal growth takes place. Region III: Addition of 1 g of 152  $\mu$ m seeds of nicotinic acid. Supersaturation decreases as it is being consumed by crystal growth and secondary nucleation until it drops to saturation. Region IV: The solution equilibrates at saturation and crystal growth and secondary nucleation stop.

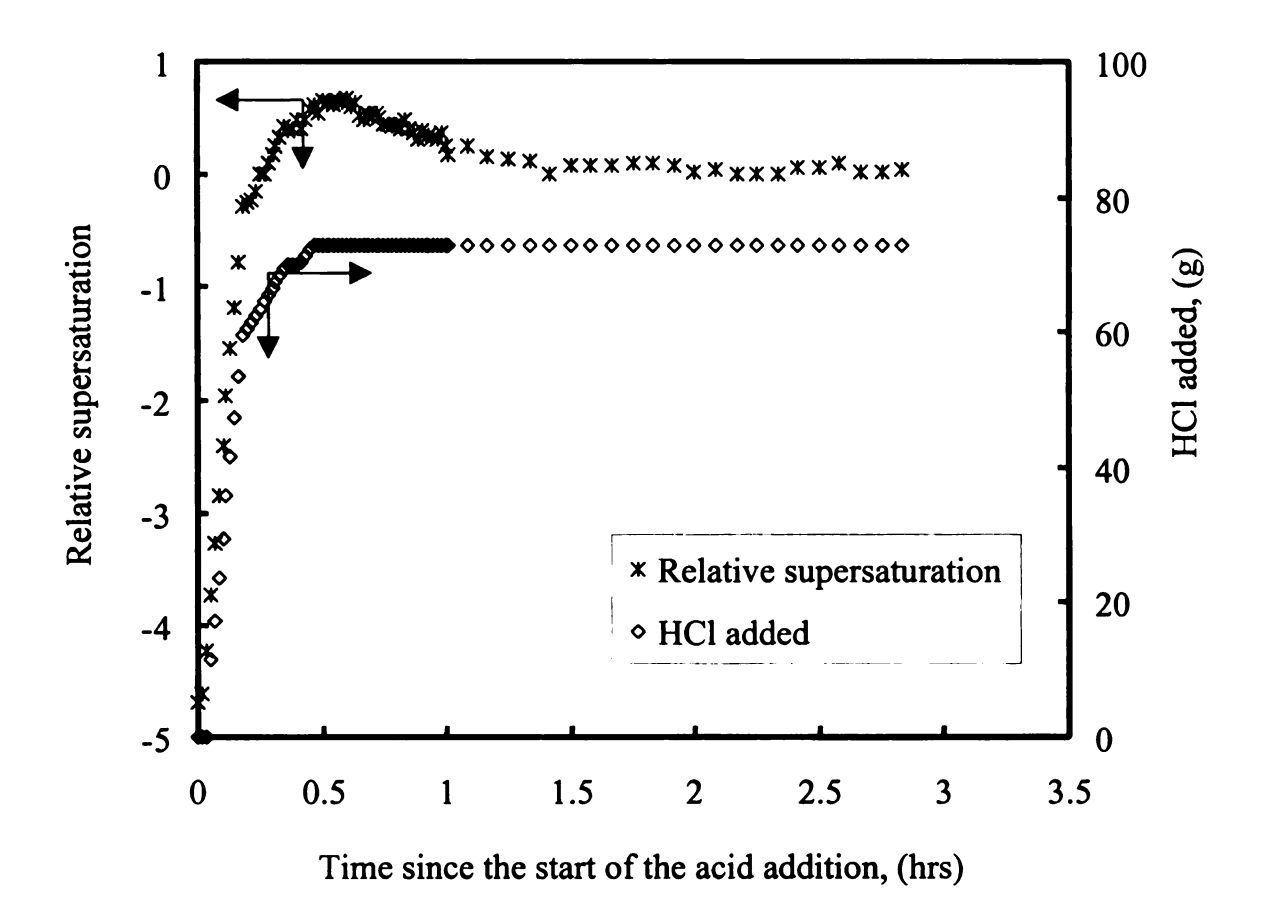


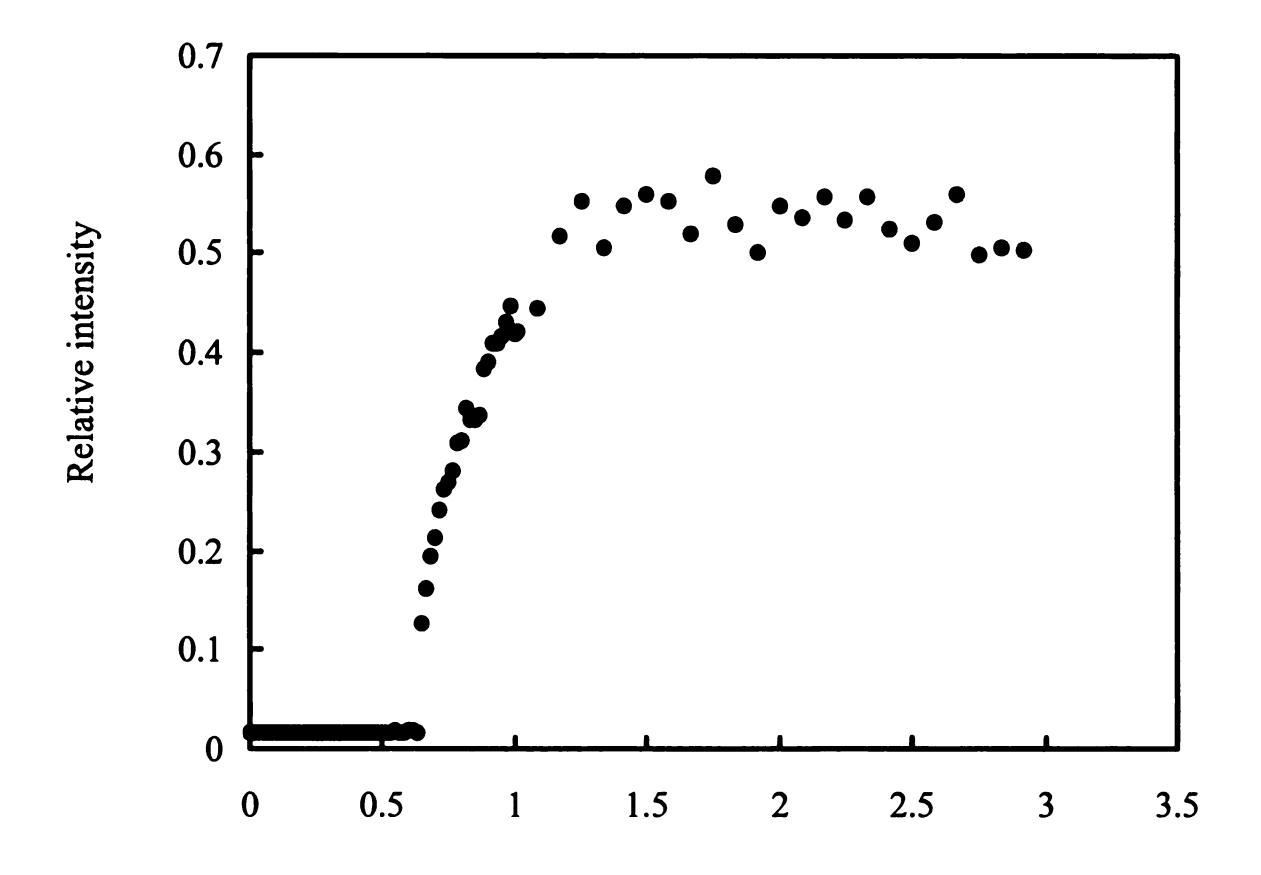
Figure 4.2. Relative supersaturation profile and HCl addition profile of seeded crystallization of nicotinic acid at 60% relative supersaturation seeding and the seed concentration of 1.5 g seeds/kg of solution added at 30 mins after the supersaturation reached 60%.  $T = 30 \pm 0.1$ °C.

monitored by a turbidity probe, which also facilitated the determination of the endpoint of the crystallization process. Figure 4.3 presents the turbidity profile as the crystallization was carried out. At the beginning of the experiment, there was no solid in the system so the turbidity intensity stayed constant. Upon introduction of the seeds to the supersaturated solution, the turbidity of the system increased rapidly at first, then continued to rise more slowly as the crystals grew. At the end of the crystallization, the signal reached a plateau, which indicates the solid phase does not change any more or the crystallization was complete. With the measurement of both the solution phase and solid phase, we were able to ensure the completion of the crystallization process.

The crystal size distribution of the final product from the 60%- $S_R$  seeding is shown in Figure 4.4. The results show that about 20 wt% of the particles are smaller than the seeds added. Fifity-three weight percent of them had the same average size as the seeds. Only 27 wt% of the overall particles were larger than the seeds added to the supersaturated solution. This result indicates that secondary nucleation is predominant over crystal growth for seeding at 60%- $S_R$ . This can be explained more explicitly by comparison of the number of particles of each size with the number of seeds added. We can calculate the number of crystals of each size using the equation given by Mullin, <sup>1</sup>

$$n = \frac{M}{m} = \frac{M}{f_{\nu} \rho d^3} \tag{4.4}$$

where n is the number of crystals of certain size; M is the mass of the crystals, m is the mass of each crystal;  $f_v$  is the volume shape factor which is 10 for needle shaped crystals as given in the literature;  $\rho$  is the density of HNic which has a



Time since the start of the acid addition, hrs

Figure 4.3. The turbidity profile for 60% relative supersaturation seeding crystallization of nicotinic acid. The seed concentration is 1.5 g seeds/kg solution.  $T = 30 \pm 0.1$ °C.

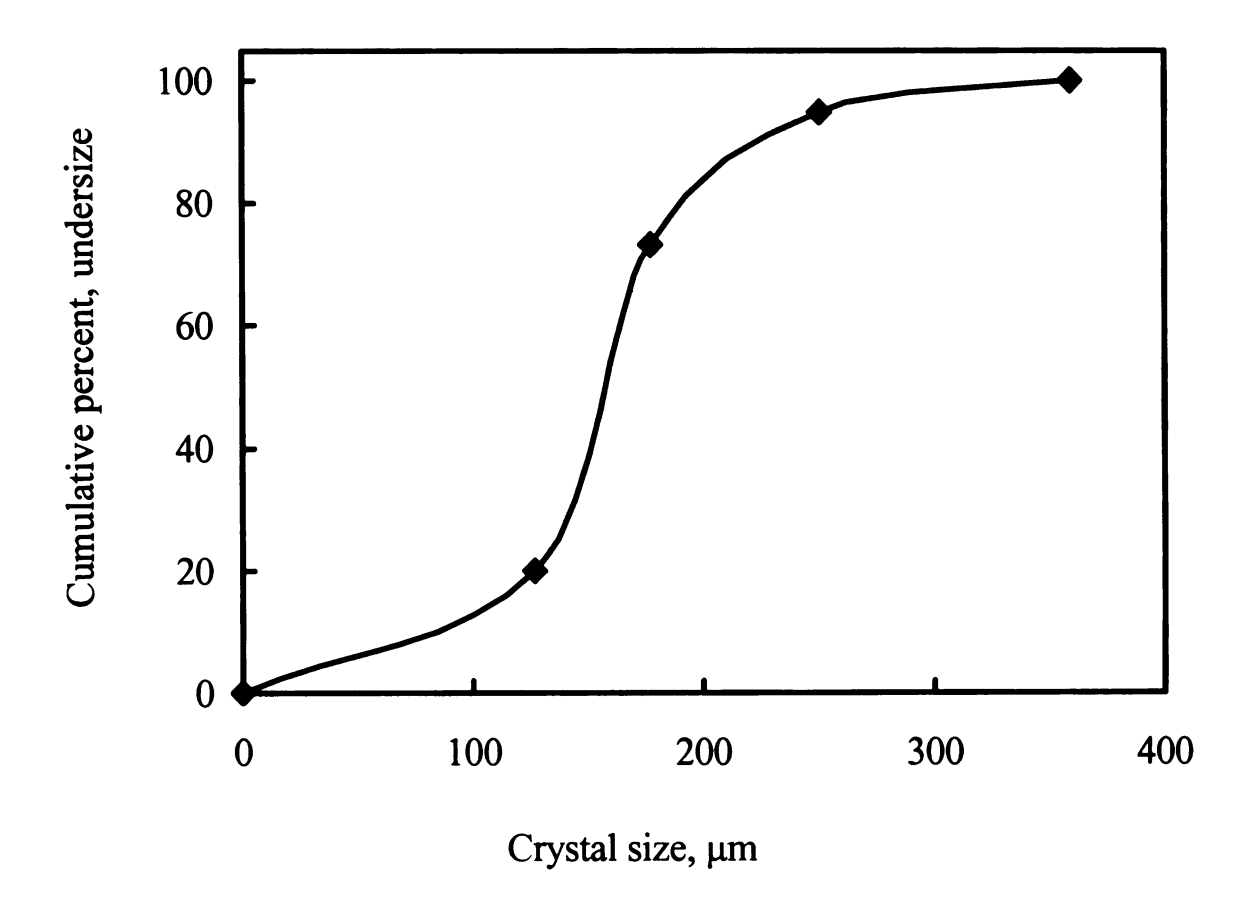


Figure 4.4. The crystal size distribution of the products from 60% relative supersaturation seeding crystallization of nicotinic acid. The seed concentration is 1.5 g seeds/kg solution. The average size of the seeds is  $152 \mu m$ .

value of 1.47 g/cm<sup>3</sup>, as given by J.T. Baker;<sup>10</sup> d is the equivalent diameter that is approximated as the average of the two sieves apertures between which the sieving has been carried out. Accordingly, the number of seeds added is determined to be about 19,400. Table 4.1 shows the number of crystals of each size at the end of the 60%- $S_R$  seeding crystallization.

**Table 4.1.** The number of crystals of each size and the mean crystal size of the product from 60% relative supersaturation seeding of HNic, the seed concentration is 1.5 g seeds/kg solution.

| Crystal Size (µm) | Number of Crystals | wt% of Total<br>Mass | Number of<br>Seeds Added | Mean Crystal<br>Size (μm) |
|-------------------|--------------------|----------------------|--------------------------|---------------------------|
| 64                | 90,300             | 20                   |                          |                           |
| 152               | 18,000             | 53                   | 19,400                   |                           |
| 214               | 2,600              | 22                   | •                        |                           |
| 305               | 200                | 5                    |                          |                           |
|                   |                    |                      |                          | 156                       |

Comparatively, there are 93,700 new crystals formed as a result of secondary nucleation. 96% of them are smaller than the added seeds, which made the mean crystal size (156  $\mu$ m) of the product only a little larger than the size of the seeds (152  $\mu$ m).

The result of 60%- $S_R$  seeding indicates that 60% relative supersaturation is too high for crystal growth to be predominant and consequently we are not able to suppress nucleation. For this reason, seeding was performed at lower levels of relative supersaturation, 45% and 30%. For illustration purposes, the supersaturation profiles are compared for only 60%- $S_R$  and 30%- $S_R$  seedings, as shown in Figure 4.5. It can be observed from Figure 4.5 that the desupersaturation rates for the two cases are significantly different. This is due to the

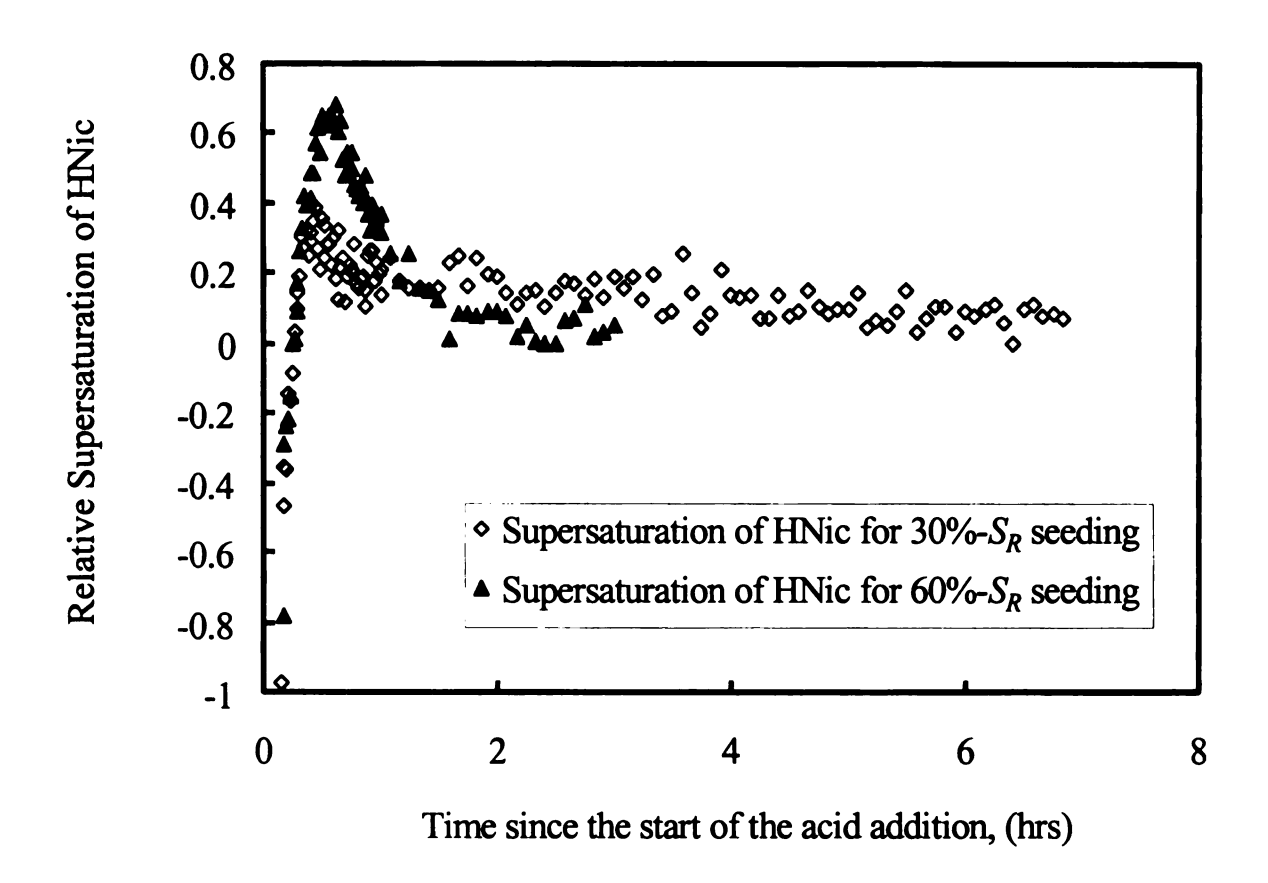


**Figure 4.5.** The relative supersaturation profile comparison for 30%- $S_R$  and 60%- $S_R$  seeding crystallization experiments of HNic. The seed concentration is 1.5 g seeds/kg solution.

kinetic difference in secondary nucleation and crystal growth caused by different level of supersaturation. Comparison of the crystal size distribution for the three measurements is shown in Figure 4.6. It is found that the weight percentage of the crystals larger than the added seeds increases from 27 wt% to 66 wt% as the level of relative supersaturation decreases from 60% to 30%. This can be more explicitly illustrated by Figure 4.7, which demonstrates the dependence of the mean crystal size on the level of relative supersaturation at which seeding is performed. As we decrease the level of relative supersaturation at which seeding is performed, the mean crystal size increases, which suggests that crystal growth has become more and more dominant over secondary nucleation as the relative supersaturation for seeding is lowered. Table 4.2 presents the number of crystals of each size for the 30%- $S_R$  seeding measurement. In comparison with the result in Table 4.1, there are only 13,000 new crystals formed as the result of secondary nucleation, seven times less than those formed in 60%- $S_R$  seeding experiment (93,700). The number of crystals that are larger than the seeds (6300) more than doubles those from 60%- $S_R$  seeding case (2800). Therefore we can conclude that seeding at 30% relative supersaturation produces crystals with significantly improved size distribution and mean size as compared to 60% relative supersaturation seeding.

**Table 4.2.** The number of crystals of each size and the mean crystal size of the product from 30% relative supersaturation seeding, the seed concentration is 1.5 g seeds/kg solution.

| Crystal Size (µm) | Number of Crystals | wt% of Total<br>Crystal Mass | Number of seeds added | Mean Crystal<br>Size (μm) |
|-------------------|--------------------|------------------------------|-----------------------|---------------------------|
| 64                | 16,700             | 4                            |                       |                           |
| 152               | 9,400              | 30                           | 19,400                |                           |
| 214               | 5,800              | 52                           |                       |                           |
| 305               | 500                | 12                           |                       |                           |
| 455               | 20                 | 2                            |                       |                           |
|                   |                    |                              |                       | 204                       |

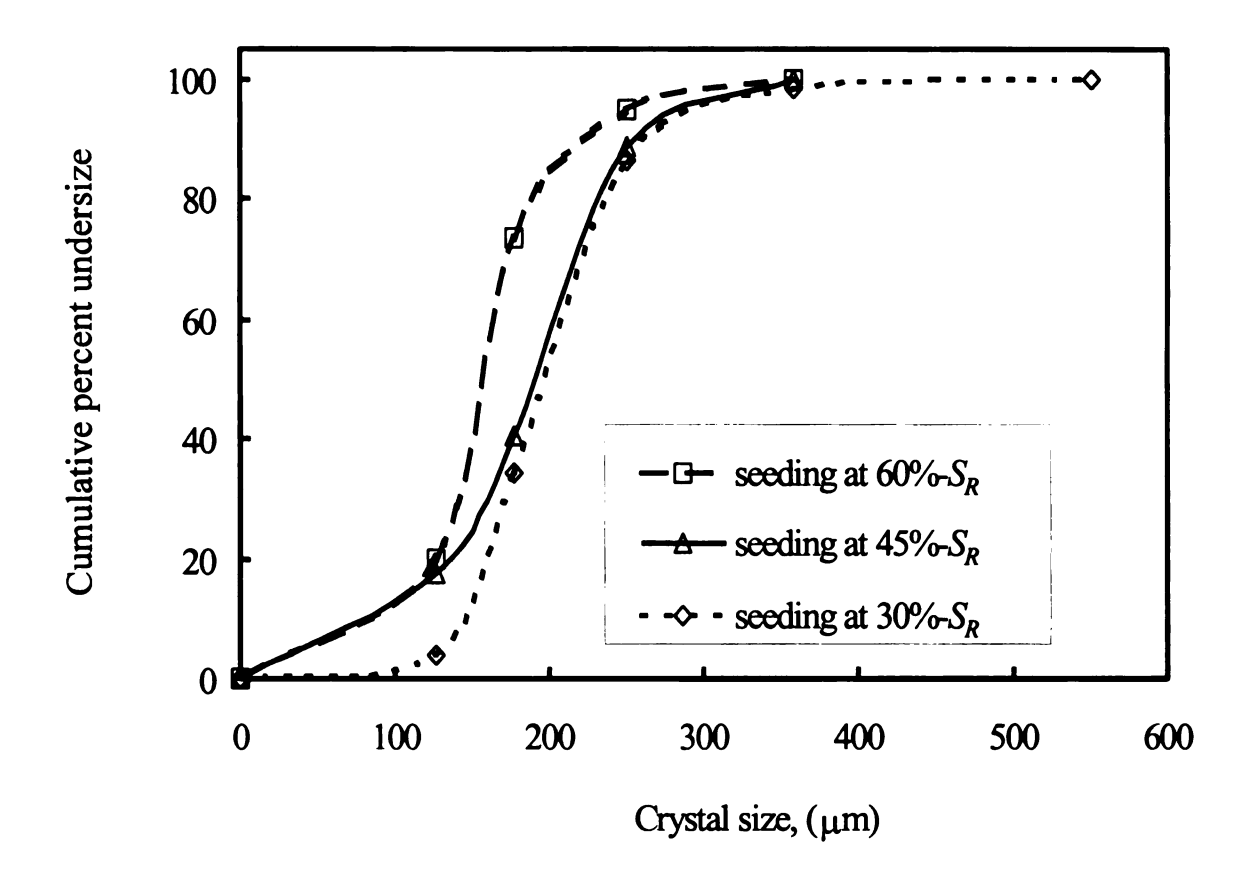


Figure 4.6. The comparison of the crystal size distributions resulted from seedings at three levels of relative supersaturation, 30%, 45% and 60%. The seed concentration is 1.5 g seeds/kg solution.

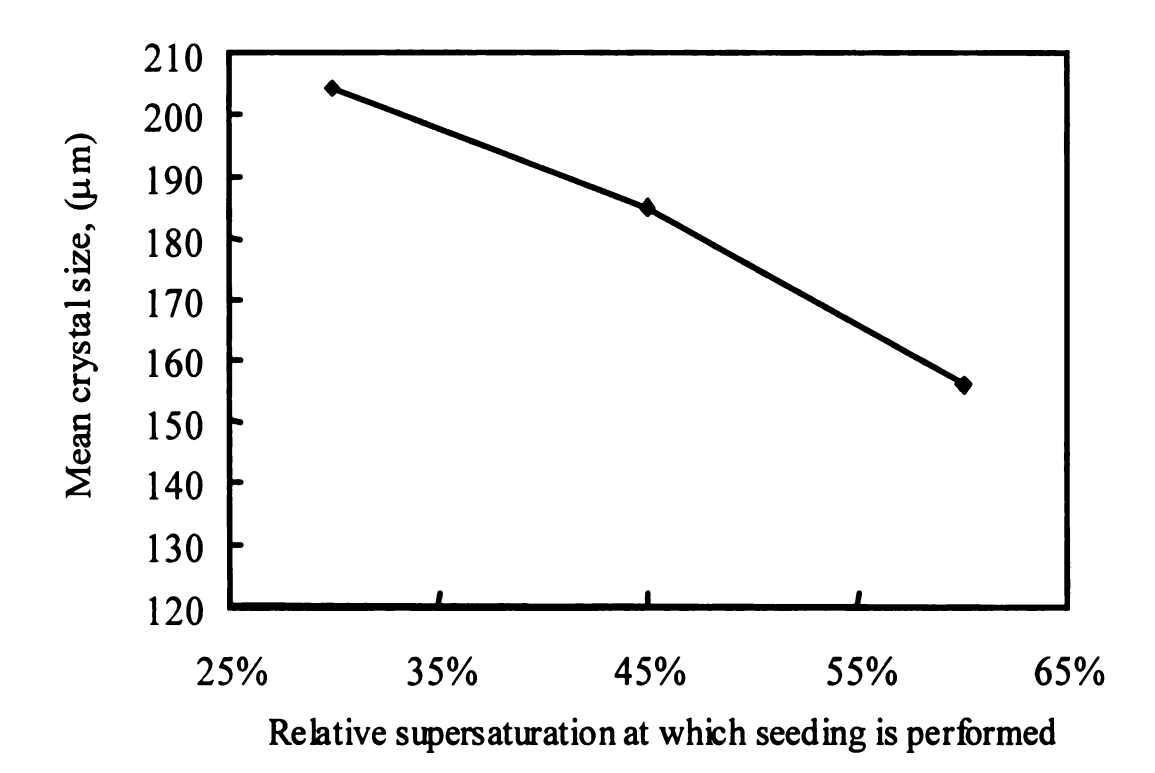
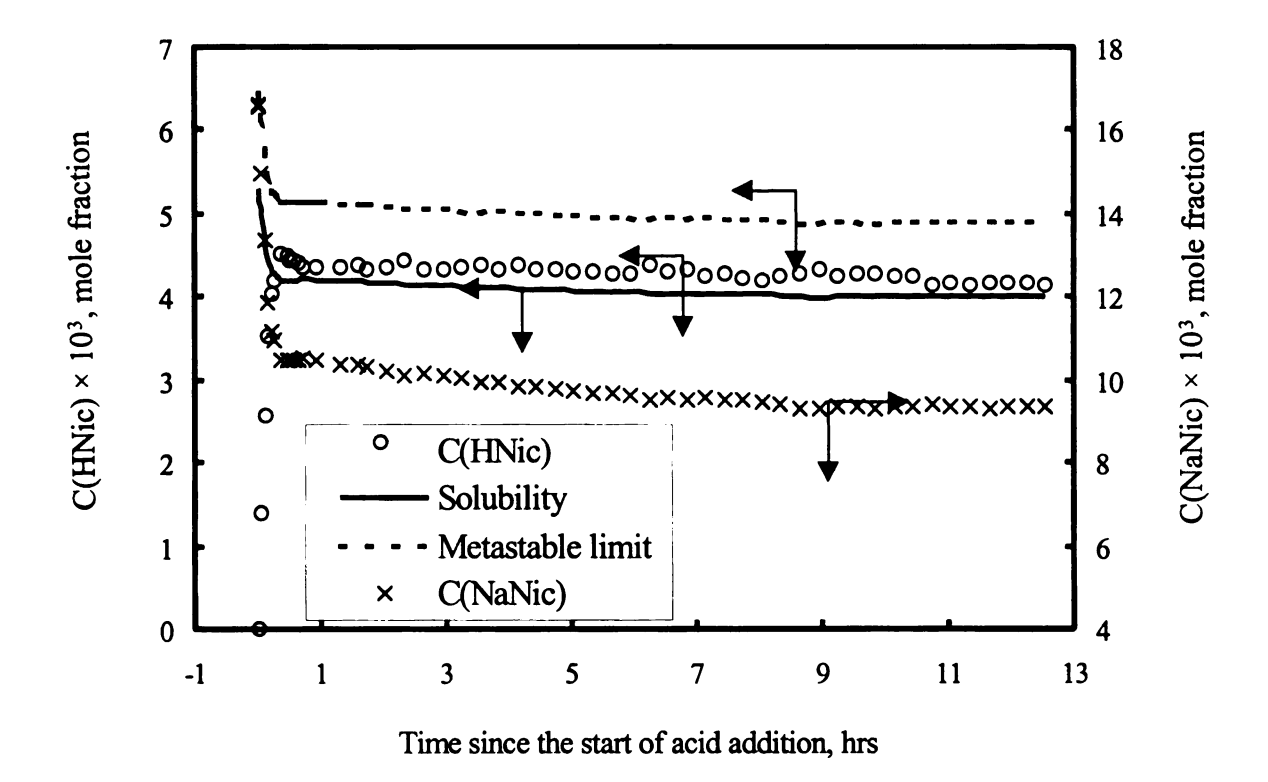


Figure 4.7. The mean crystal size dependence on the level of relative supersaturation at which seeding is performed. The seed concentration is 1.5 g seeds/kg of solution. The average size of the seeds is 152  $\mu m$ . The line between the datum points is meant only to be a guide to the eye.

4.3.2 Seeding with Post-seeding Acid Addition Controlled by Relative Supersaturation It has been frequently suggested <sup>7,11,12</sup> that constant supersaturation has to be maintained in order to suppress nucleation and maximize the product mean size. In this section, we demonstrate that relative supersaturation can be controlled at a constant level dynamically with the adjustment of acid addition after seeds are introduced. As it is found in the previous section, seeding at 30% relative supersaturation can produce crystals of larger mean size. We carried out the first experiment with seeding at 30%- $S_R$ and continued to control the relative supersaturation at about 30% during the post acid addition process. The concentration profiles are presented in Figure 4.8. The relative supersaturation profile and the acid addition profile are shown as Figure 4.9. As shown in the two figures, pure NaNic solution was used to start the experiment. During the first 10 min, 2 M HCl was added rapidly to bring the solution to saturation, then the addition rate was slowed until the specified relative supersaturation level, 30% was achieved. Upon the addition of seed crystals to the solution, the relative supersaturation started to decrease. One half molar HCl addition started when the level of relative supersaturation dropped below the lower limit 20%.

The addition rate of 0.5 M HCl was set at 6 g/hr, which was estimated from the desupersaturation profile of HNic in Figure 4.5. It can be estimated from the profile that it takes about 3 hrs for the relative supersaturation to drop from 30% to 10%, which corresponds to the supersaturation difference caused by about 4 g of 2 M HCl in the similar solution. Therefore, if we add the acid at a similar rate as it is consumed, 4 g



**Figure 4.8.** Concentration profiles of sodium nicotinate and nicotinic acid and the solubility and metastable limit of nicotinic acid for crystallization controlled at about 30% relative supersaturation with post seeding acid addition.

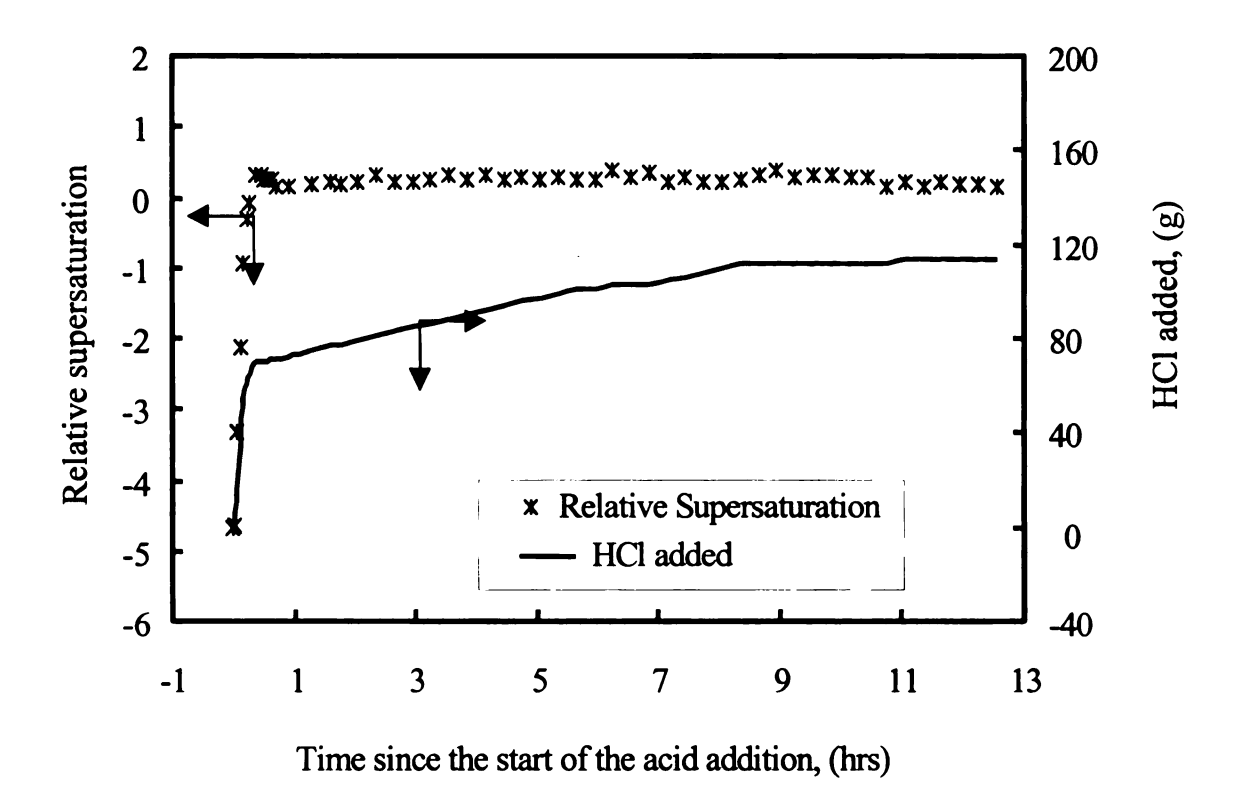


Figure 4.9. Relative supersaturation profile and HCl addition profile for crystallization controlled at about 30% relative supersaturation with post seeding acid addition. The seeds are added at 30% relative supersaturation. The seed concentration is 1.5 g seeds/kg solution.

HCl/3 hrs, there should not be accumulation of supersaturation and no significant nucleation as a result. As it has been demonstrated in Chapter 3, even when adding 2 M HCl at an extremely slow rate (1 g/hr), micromixing is still not effective in dispersing local high supersaturation to the bulk solution before nucleation occurs. Due to this concern, we chose to add 0.5 M HCl instead of 2 M HCl during the post seeding crystallization process. When we convert the addition rate for 2 M HCl (4 g/3 hr) to the rate for 0.5 M HCl, 6 g/hr is adopted considering the dilution effect of more solvent introduced when 0.5 M HCl is added.

As 0.5 M HCl was added to the slurry mixture, it can be seen from Figure 4.8 that C(NaNic) decreased; C(HNic) remained almost constant. The relative supersaturation in Figure 4.9 follows the same trend as C(HNic). This result indicates that there is no significant accumulation of supersaturation for the first 30 g HCl added. However, after the continuous addition of 30 g HCl, the overall addition rate was slowed down due to the unstable value of supersaturation. This suggests that there might be some accumulation of supersaturation after a significant amount of HCl was added. The final crystal size distribution in Figure 4.14 shows that the size of 85% of the particles are smaller or equal to that of the seeds, which indicates that secondary nucleation is predominant during the post addition of HCl. The mean crystal size (107  $\mu$ m) is much smaller than that from 30%- $S_R$  seeding without post addition of acid. It is implied that the generation of 30% relative supersaturation with the presence of crystals can no longer sustain crystal growth, but only enhance secondary nucleation. This is consistent with the suggestion that the so-

called "metastable limit for secondary nucleation" is much lower than the metastable limit for primary nucleation.<sup>1</sup>

In order to suppress secondary nucleation in the post acid addition process, an additional experiment was performed with minimized relative supersaturation, 0%- $S_R$ , or the solution kept about saturation throughout the crystallization process. The concentration profiles for HNic and NaNic are shown in Figure 4.10. The relative supersaturation and acid addition profiles are presented as Figure 4.11. Initially, 2 M HCl was added to 1 M NaNic aqueous solution to bring the solution to just above saturation with respect to HNic. One gram of 152 µm seeds was added when the relative supersaturation exceeds 0 It can be seen from Figure 4.11 that the relative supersaturation decreased a little which indicates that the added seeds consumed that little amount of supersaturation created earlier. Then 0.5 M HCl was added to facilitate post seeding growth. Initially 30 g of 0.5 M HCl were added continuously at the rate of 6 g/hr, and there was no accumulation of supersaturation. The addition of HCl was slowed due to the unstable value of relative supersaturation, which indicates that there might be some accumulation of supersaturation at this point. The final crystal size distribution in Figure 4.14 suggests that crystal growth is predominant for the 0% relative supersaturation controlled crystallization even though a small percentage of nucleation (17%) still occurs, which is almost impossible to overcome in a realistic seeding crystallization process.

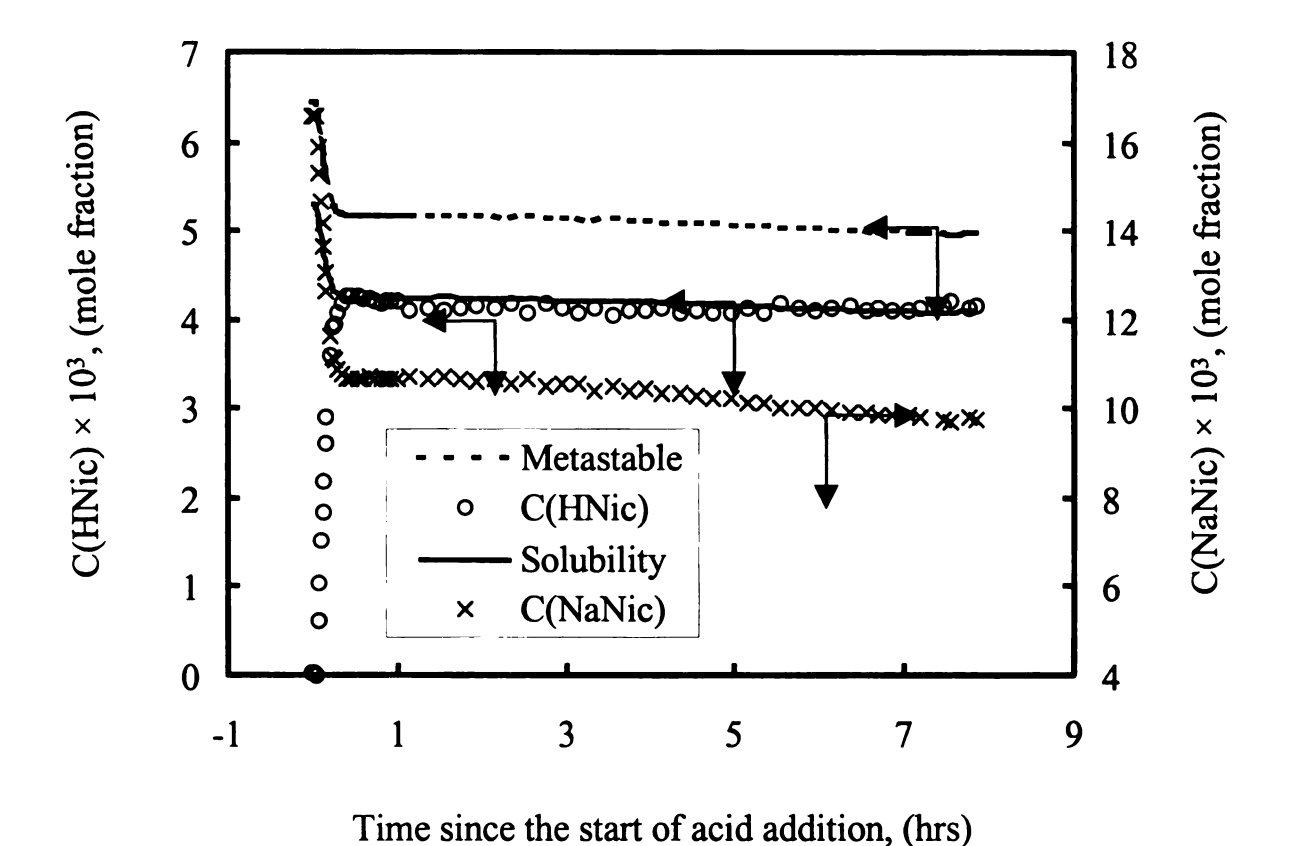


Figure 4.10. Concentration profiles of sodium nicotinate and nicotinic acid and the solubility and metastable limit of nicotinic acid for the crystallization controlled at about 0% relative supersaturation with post seeding acid addition. The initial seeding is performed at just above saturation.

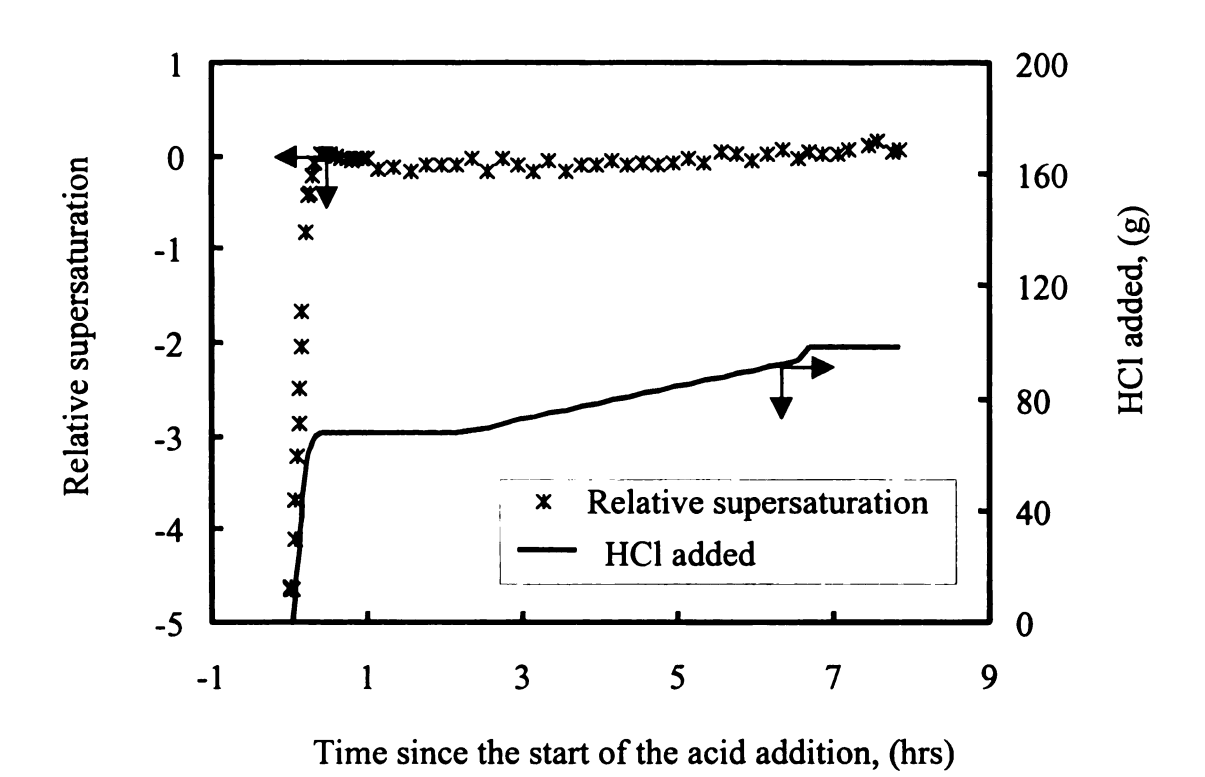
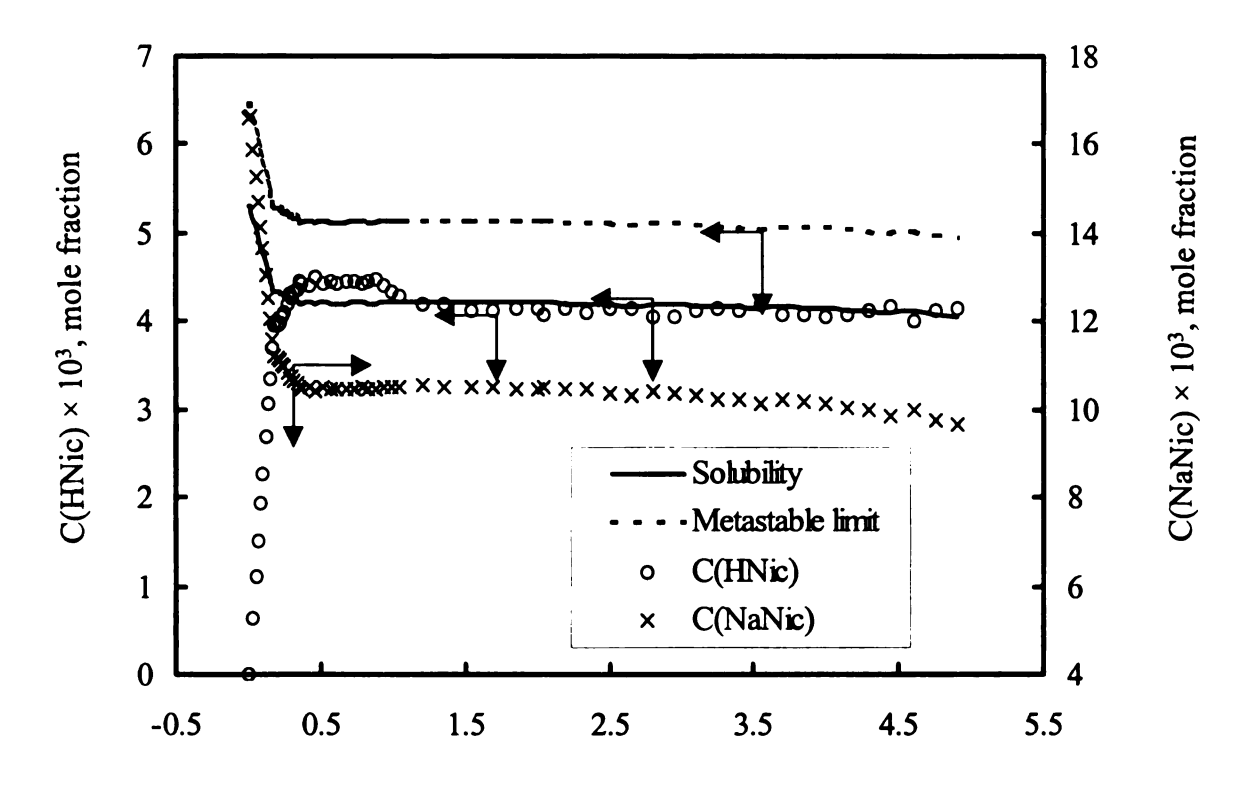


Figure 4.11. Relative supersaturation profile and HCl addition profile for crystallization controlled at about 0% relative supersaturation with post seeding acid addition. The seeds are added at just above 0% relative supersaturation. The seed concentration is 1.5 g seeds/kg solution.

The last controlled crystallization was conducted by seeding at 30% relative supersaturation and followed by control of relative supersaturation around 0% during the post addition of acid. The concentration profiles for HNic and NaNic are shown in Figure 4.12. The relative supersaturation and acid addition profiles are presented as Figure 4.13. Initially, 2 M HCl was added to 1 M NaNic aqueous solution to bring the solution to 30% supersaturation with respect to HNic. One gram of 152 µm seeds was added once the relative supersaturation exceeded 30%. The seeds were allowed an hour to grow until the supersaturation dropped to 0%. It can be seen from Figure 4.12 that the relative supersaturation decreased after the addition of seeds, which indicates that the seeds consumed the supersaturation created earlier. One half molar HCl was added to facilitate post seeding growth once the relative supersaturation dropped to saturation  $(S_R)$ = 0). The same acid addition rate, 6 g/hr of 0.5 M HCl was applied for the first 10 g of acid. There was no accumulation of supersaturation. The addition of HCl was increased to 12 g/hr for the next 10 g of acid, and then further increased to 24 g/hr for the last 10 g of acid added. There was no significant accumulation of supersaturation in the postseeding acid addition process. The final crystal size distribution shown in Figure 4.14 suggests that crystal growth is still predominant for the 30% relative supersaturation seeding and 0% relative supersaturation controlled crystallization. However, secondary nucleation seems more pronounced in this case than the 0% relative supersaturation seeding and 0% relative supersaturation controlled crystallization. This can be explained by two facts, the first is that 30% relative supersaturation initial seeding results in higher degree of secondary nucleation than the 0% relative supersaturation seeding. The second reason is that faster addition of acid during the later stage of the crystallization may also



Time since the start of acid addition, hrs

Figure 4.12. Concentration profiles of sodium nicotinate and nicotinic acid and the solubility and metastable limit of nicotinic acid for the crystallization controlled about 0% relative supersaturation with post seeding acid addition. The initial seeding was performed at 30% relative supersaturation.

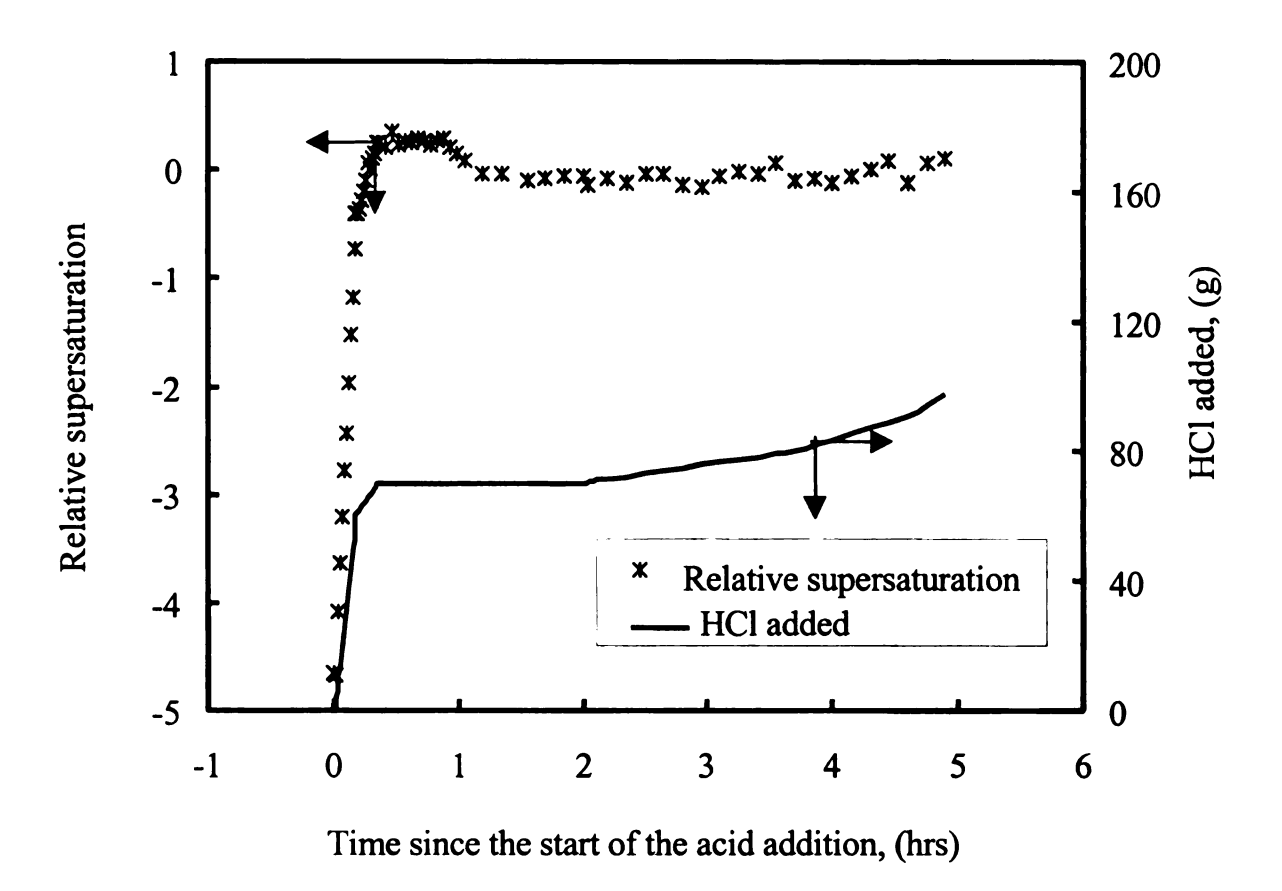


**Figure 4.13**. Relative supersaturation profile and HCl addition profile for crystallization controlled at about 0% relative supersaturation with post seeding acid addition. The seeds are added at 30% relative supersaturation. The seed concentration is 1.5 g seeds/kg solution.

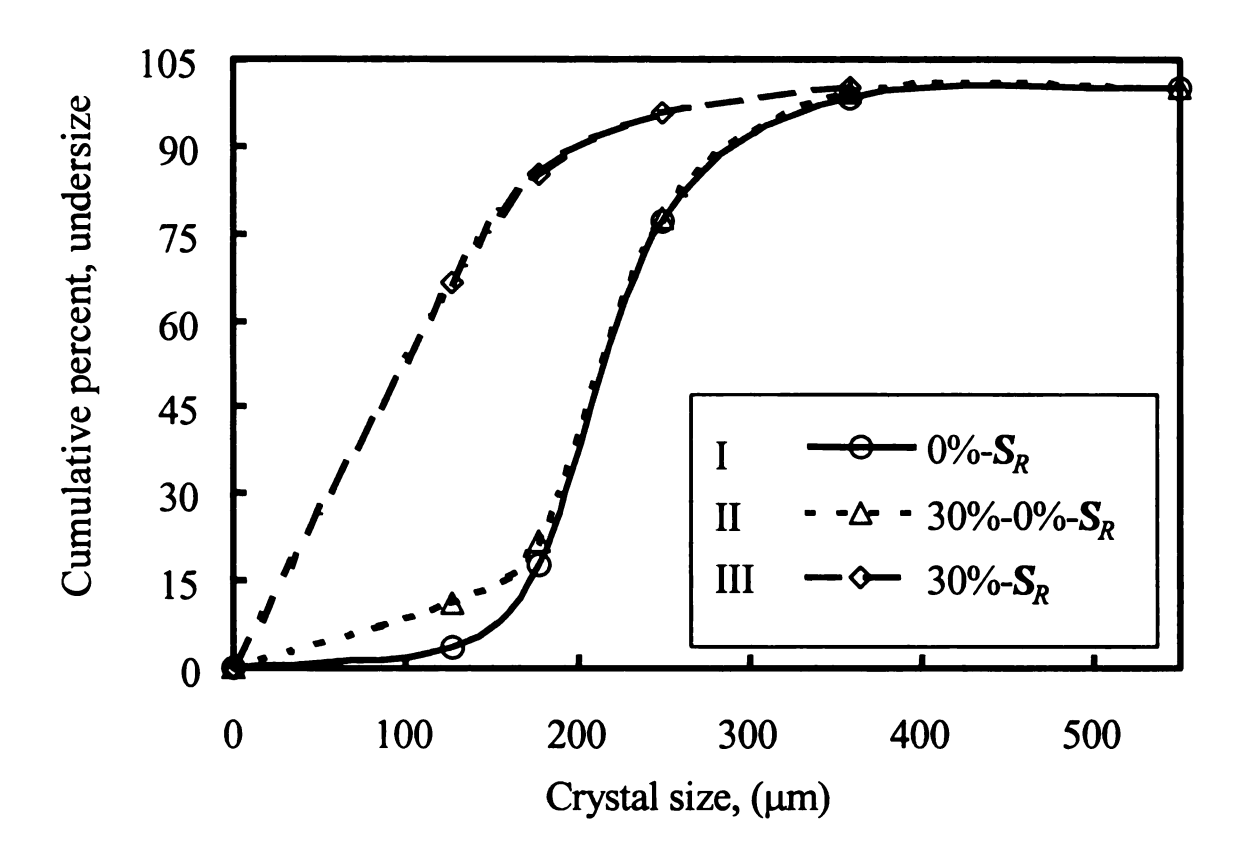


Figure 4.14. The crystal size distribution from three controlled supersaturation experiments. The three cases are: I. Seeding at 0% relative supersaturation, and controlled about 0% relative supersaturation during post acid addition; II. Seeding at 30% relative supersaturation, and controlled about 0% relative supersaturation during post seeding acid addition; III. Seeding at 30% relative supersaturation, and controlled at about 30% relative supersaturation during post acid addition.

contribute to more secondary nuclei in the 30%-0% relative supersaturation controlled case. From the crystal size distributions of the three controlled crystallization processes, we can conclude that 30% relative supersaturation control during the post-seeding acid addition is not favorable for crystal growth to occur; instead it promotes secondary nucleation and results in fine particles with an average size smaller than the seeds added. Zero percent relative supersaturation seeding and controlled crystallization results in significantly improved crystal size distribution. Thirty percent relative supersaturation seeding and 0% relative supersaturation control produce crystals with an acceptable mean crystal size, as shown in Table 4.3. However, it also causes a higher degree of secondary nucleation than the 0% relative supersaturation seeding case. The presence of smaller crystals as a result of secondary nucleation will further impede the rate of crystal growth due to the size-dependent growth rate.<sup>13</sup> Therefore, it is recommended that 0% relative supersaturation seeding and control is the most appropriate method to maximize the mean crystal size.

**Table 4.3.** The mean crystal size from three experiments which are controlled by different levels of supersaturation.

| Level of relative supersaturation controlled | Mean crystal size (μm) |  |
|--|------------------------|--|
| 30% seeding and then controlled at about 30% | 107                    |  |
| 30% seeding and then controlled at about 0%  | 212                    |  |
| 0% seeding and then controlled at about 0%   | 223                    |  |

#### 4.4 Conclusions

The ability to monitor the relative supersaturation in situ with ReactIR and the interface between the LabMax<sup>®</sup> and the ReactIR have allowed us to control the pH swing crystallization of HNic. The level of relative supersaturation at which seeding is performed significantly influences the final crystal size distribution. It was found that the lower relative supersaturation seeding yields a much more improved mean crystal size than high level relative supersaturation seeding. It is also demonstrated that feedback control of relative supersaturation has enabled us to maintain the relative supersaturation at a constant level during the post seeding acid addition process. It can be concluded that seeding at just above saturation and then maintaining the solution about saturation produces crystals with the maximum mean size.

#### References

- 1. Mullin, J. W. Crystallization, 3rd Edition, Butterworth-Heinemann Ltd: Oxford, 1993.
- 2. Randolph, A. D. K.; Larson, M. A. *Theory of Particulate Processes*, Academic Press, New York, USA., 1988.
- 3. Zimmerman, H. K. Chemical Reviews, 1952, 51, 25-65.
- 4. Dunuwila, D. D.; Berglund, K. A. J. Cryst. Growth, 1997, 179(1-2), 185-193.
- 5. Wang, F.; Berglund, K. A.. Ind. Eng. Chem. Res. 2000, 39, 2101-2104.
- 6. Jones, A. G. K. Mullin, J. W. Chem. Eng. Sci., 1974, 29, 105-118.
- 7. Jones, A. G.; Teodossiev, N. M. Cryst. Res. Technol, 1988, 23, 957-966.
- 8. Wang, F; Berglund, K. A. Chapter 3
- 9. Myerson, A. S. In *Handbook of Industrial Crystallization*; Myerson, A. S. Eds.; Butterworth-Heinemann Ltd: Oxford, 1992; Chapter2, pp 41.
- 10. http://www.jtbaker.com/msds/n3360.htm
- 11. Larson, M. A.; Garside, J. The Chemical Engineer, 1973, June, 318-328.
- 12. Tavare, N. S.; Garside, J.; Chivate, M. R. Ind. Eng. Chem. Process Des. Dev, 1980, 19, 653-665.
- 13. Garside, J.; Davey, R. J. Chem Eng Comm, 1980, 4, 393-424.

# Chapter 5

# AN INVESTIGATION OF SOLVENT-MEDIATED POLYMORPHIC TRANSFORMATION OF PROGESTERONE USING IN SITU RAMAN SPECTROSCOPY\*

\*Accepted by Organic Process Research & Development, May, 2000.

Many analytical techniques, such as Differential Scanning Calorimetry (DSC), X-Ray Diffraction (XRD), Infrared Spectroscopy (IR) and Raman spectroscopy can be used to differentiate between crystalline polymorphs of the same chemical entity. While all of these techniques are routinely applied to off-line analysis of materials, Raman spectroscopy has the advantage over these other techniques in that Raman technology currently exists for in situ monitoring of the solid phase behavior within a mixed suspension of liquid and solid. In this paper, we present our results from an in situ Raman study demonstrating the solvent-mediated polymorphic phase transformation of progesterone. In situ Raman analysis has shown that the appearance of Form I progesterone is always preceded by the formation of Form II progesterone. Phase transformation rates were found to increase monotonically as the temperature increases, which indicates that the polymorphic system is monotropic. Form I was found to be thermodynamically more stable than Form II, while Form II was found to be kinetically favored over Form I. The results from this study are consistent with Ostwald's law of stages and lead to an in-depth understanding of the polymorphic transformation process of progesterone. The in situ monitoring capabilities of Raman spectroscopy have allowed us to define the processing parameters required to control the morphology of crystalline progesterone.

#### 5.1 Introduction

The pharmaceutical industry is frequently confronted with the presence of multiple crystal polymorphs of the same chemical entity. The presence of multiple polymorphs of the active pharmaceutical ingredient is particularly challenging with solid, oral dosage drug products.<sup>1, 2</sup> The characteristics affected by the polymorphism include solubility, dissolution rate, stability, hygroscopicity and solid state reactivity. The effect of polymorphism on bioavailability is the most important consequence if the bioavailability is mediated via dissolution.<sup>2,3</sup> In situ monitoring of the solvent mediated polymorphic transformation is therefore of great significance in understanding the thermodynamics of the polymorphic systems and the mechanisms of polymorphic transformation. In situ monitoring offers tremendous potential for efficiently determining the crystallization parameters required to obtain a desired crystal form.

In polymorphic studies, Raman spectroscopy, coupled with an immersible fiber optic probe, has tremendous advantages over the traditional techniques, such as X-ray powder diffraction (XRD), differential scanning calorimetry (DSC), solid state NMR and infrared spectroscopy (IR). The fiber optic probe in Raman technique provides the capability of *in situ* or on-line monitoring of the formation of crystals and the transformation from one polymorph to another. DSC, XRD and NMR can perform off-line analysis, which can distinguish the polymorph of the end product,<sup>4</sup> but cannot reliably provide insight about transformation processes since a polymorphic transformation may continue to occur during sample filtration, drying and sampling preparation.

Infrared Spectroscopy (IR) can be used to monitor some processes in situ. However aqueous solutions may cause problems in IR measurements.<sup>5</sup> If water is used as a reagent, a byproduct or a solvent in a process, strong infrared absorption of water will mask some of the useful information from the species of interest. In contrast, water is a poor Raman scatterer, which often makes Raman preferable to IR when water is present in the processes.<sup>6</sup> This phenomenon can be explained by the different mechanisms of interaction of electromagnetic radiation with matter in the two spectroscopic techniques. Dipole moment changes during molecular vibrations cause IR absorption while changes in polarizability associated with molecular vibrations result in Raman scattering. Usually, molecules with polar functional groups and asymmetric vibrational modes have stronger absorption in IR and weaker absorption in Raman.<sup>7</sup> Raman scatterring also favors solid phase in a slurry other than the solution phase as the ATR-FTIR technique. The higher density of the solid phase results in stronger Raman scattering than the solution phase does. This allows us to monitor the disappearance of one solid phase and the appearance of the other solid phase. In addition, Raman spectroscopy can be used to perform remote sensing because the fiber optic probe can be made as long as a couple of hundred meters.<sup>8</sup> By comparison, the probe in Attenuated Total Reflectance (ATR)-FTIR can reach no further than 2-3 meters. Remote sensing is especially useful in hazardous environments, where operators can work safely by staying far from the reactor. This study employed Raman spectroscopy coupled with a fiber optic probe to study the polymorphic transformation of progesterone at a laboratory scale of less than 1 liter. The results from this study will be applied to a production scale process of several thousand liters.

Progesterone has five known polymorphs.<sup>10</sup> For the range of conditions considered in this study, only Form I and Form II will be produced. Raman spectroscopy was empoyed to differentiate the two forms of progesterone. In order to verify our interpretation of the Raman spectra, several samples were also characterized by DSC and XRD and compared to the known reference standards of these two polymorphs. Raman Spectroscopy was also employed to monitor the solvent-mediated phase transformation of progesterone from Form II to Form I in situ.

## 5.2 Experimental Section

The crude progesterone for this study was prepared at Pharmacia Corporation. Recrystallizations of progesterone were carried out in a 1-liter automatically controlled LabMax® reactor at different temperatures ranging from 5-45°C. The process which we analyzed involved 2 grams of progesterone dissolved in 25 mL of an organic solvent. This solution was then added to 500 mL of distilled water, which was kept at a constant temperature in the LabMax® reactor. Due to the heat released by mixing water with the progesterone solution and crystallization, a jacket supplied with a cooling fluid and close temperature control provided by LabMax® were necessary to keep the temperature within 1°C of the set-point. Following the completion of the addition, the system was allowed to stir isothermally for several hours. During this post-addition stir period, the polymorphic transformation from Form II (kinetically favored) to Form I (thermodynamically favored) was observed semi-continuously through *in situ* monitoring

with a HoloLab Series 5000 Raman spectrometer coupled to a remote fiber-optic probe equipped with an immersion optic.

Details of the HoloLab 5000 have been described previously<sup>11,12</sup>. Briefly, the 250 mW output from a 785 nm stabilized diode laser is transmitted through a fiber-optic cable to the remote probe. The laser light is focused into slurry using the immersion optic. Backscattered Raman light is collected by the same optics and transmitted back to the spectrometer for analysis. This spectrometer is equipped with a "HoloPlex" holographic transmission grating and a thermal-electrically-cooled charge coupled device (CCD) for detection. The HoloPlex grating allows simultaneous full spectral coverage (100 cm<sup>-1</sup> to 3450 cm<sup>-1</sup>) at high spectral resolution (4 cm<sup>-1</sup>) with no moving parts.

Solid state Raman analysis of pure Form I and Form II was carried out in aluminum trays. It is important to note that sample preparation for this Raman analysis was minimal. Unlike grinding and compression required for IR and XRD analysis (which may alter the polymorph of the material being analyzed), the sample preparation for Raman analysis consists simply of illuminating the crystalline sample in the vicinity of the focal point of the incident laser from the fiber optic probe. For analysis of prepared mixtures of these two polymorphs, the sample preparation was only slightly more complex. Varying relative amounts of Form I and Form II were stirred in water and Raman spectra was collected of the aqueous slurry. This slurry technique was used in order to distribute the Form I and Form II materials homogeneously. Because of the very limited solubility of progesterone in water, there was no concern of polymorphic

transformation during the 3-5 minutes required to collect any individual Raman spectrum.

Spectra were collected for a total of 11 samples of varying relative compositions of Form I and Form II.

The thermal properties of the polymorphs were characterized on a differential scanning calorimeter (TA instrument Model DSC 2920 modulated DSC) and a thermogravimetric analyzer (TA instrument Model HiRes TGA 2950).

X-Ray powder diffraction patterns of progesterone polymorphs were recorded with a Rigaku Miniflex X-ray diffractometer. The instrument operates using the Cu kai emission with a nickel filter at 1.50451. For each sample, fine powders were packed in an aluminum sample plate with a 2 mm indent or placed on a zero-background sample holder.

## 5.3 Results and Discussion

Crystallization of progesterone at various temperatures or various time length of mixing may yield different polymorphs. The XRD spectra (Figure 5.1(A) and (B)) show significant differences between the diffraction patterns of the two polymorphs. At a heating rate of 5 °C/min, the DSC thermodiagrams of Form I and Form II (Figure 5.2 (A) and (B)) present sharp endotherms with melting points at 129.1°C and 121.2°C, respectively. TGA of both forms indicated no weight loss. The melting points of Form I and Form II are comparable with their literature values.<sup>13</sup>

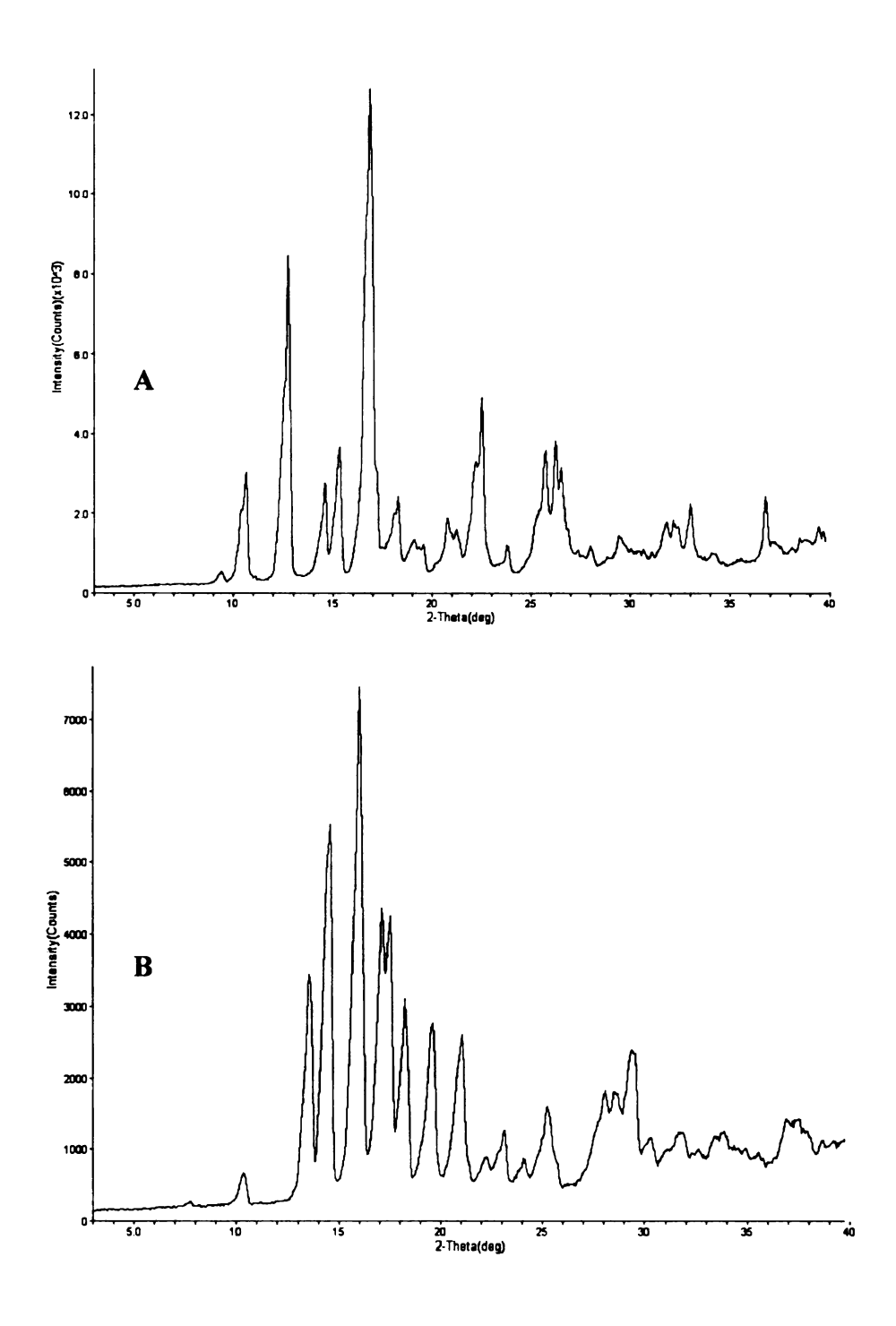


**Figure 5.1.** The X-ray diffraction patterns of progesterone polymorphs: (A) Form I and (B) Form II.

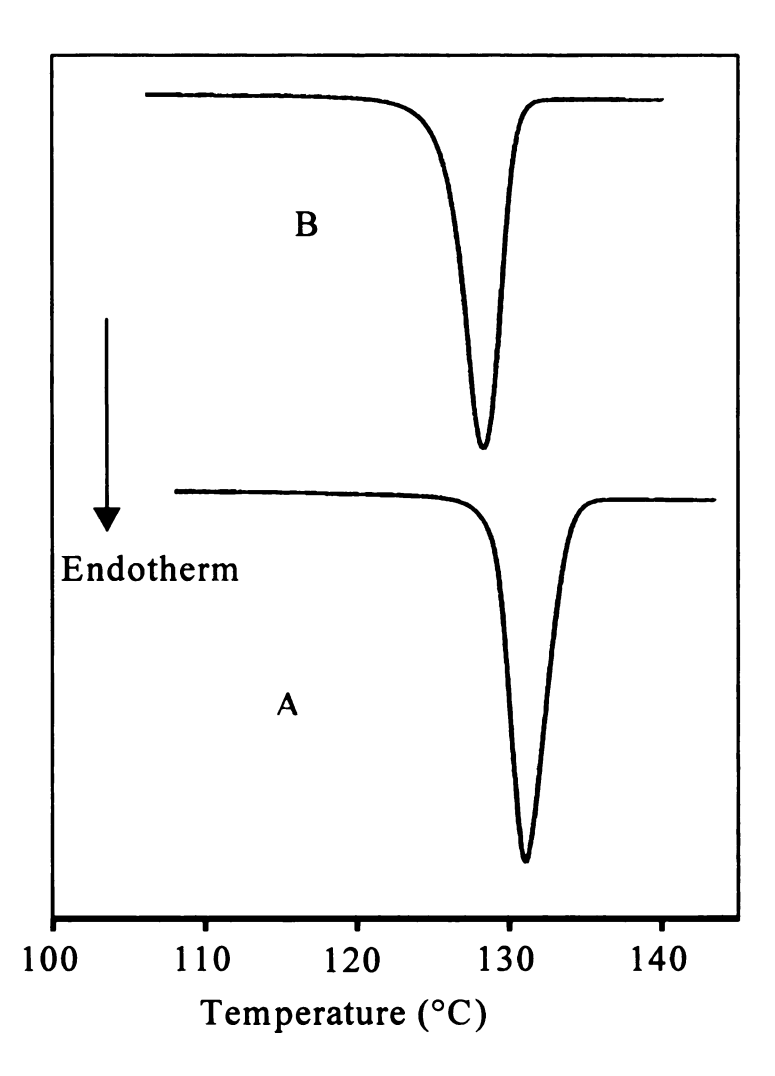


Figure 5.2. The DSC thermodiagrams of progesterone: (A) Form I and (B) Form II. The heating rate was 5 °C/min.

The Raman spectra of the solid state Form I and Form II are presented in Figure 5.3. Both XRD and DSC analysis had previously established the solid phase identity of these There are several spectral regions where peak shifts are present which samples. differentiate between Form I and Form II of progesterone. No attempts were made to assign all the peaks over the entire spectral region. The region where the most significant difference exists between the Raman spectra of the Form I and the Form II material can be explained by conjugation theory. <sup>14</sup> As shown in the structure of progesterone (Figure 5.4), the conjugation between the C=O at position 3 and C=C at position 4 results in the delocalization of the  $\pi$  electrons and reduces the double-bond character of both bonds. This causes the absorption at lower wavenumbers than those of the unconjugated systems. As a result of this interpretation, 1617 cm<sup>-1</sup> is assigned to C=C stretching and 1662 cm<sup>-1</sup> to C=O stretching for Form I while 1616 cm<sup>-1</sup> is from C=C stretching and 1667 cm<sup>-1</sup> from C=O stretching for Form II. The unconjugated C=O bond at position 20 contributes to the absorption at 1698 cm<sup>-1</sup> for Form I and 1706 cm<sup>-1</sup> for Form II. These Raman peak shifts indicate that the two crystalline polymorphs may have different modes of packing. Two ends of the molecule, functional groups around positions 3 and 20, which are less rigid than the rings, are likely affected the most by the different packing environments.

The peak with the largest observable shift during the transformation between the two polymorphs (1662 cm<sup>-1</sup> for Form I and 1667 cm<sup>-1</sup> for Form II) was used to set up a calibration (Figure 5.5) to correlate the concentration of Form I with the peak position. Eight wavenumber shift between 1698 cm<sup>-1</sup> and 1706 cm<sup>-1</sup> cannot be seen in the spectra

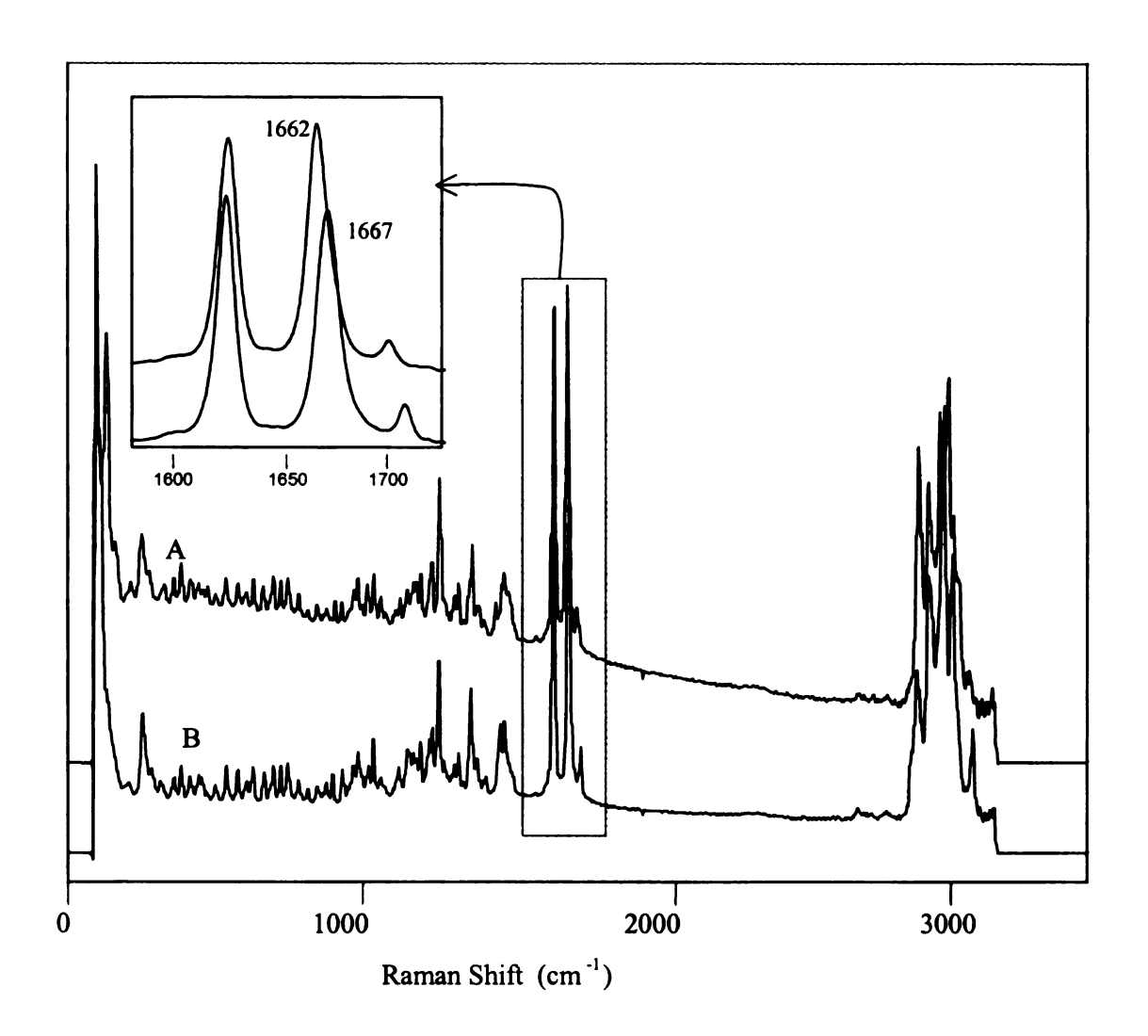


Figure 5.3. Raman spectra of solid state progesterone: (A) Form I and (B) Form II.

Figure 5.4. Molecular structure of progesterone.

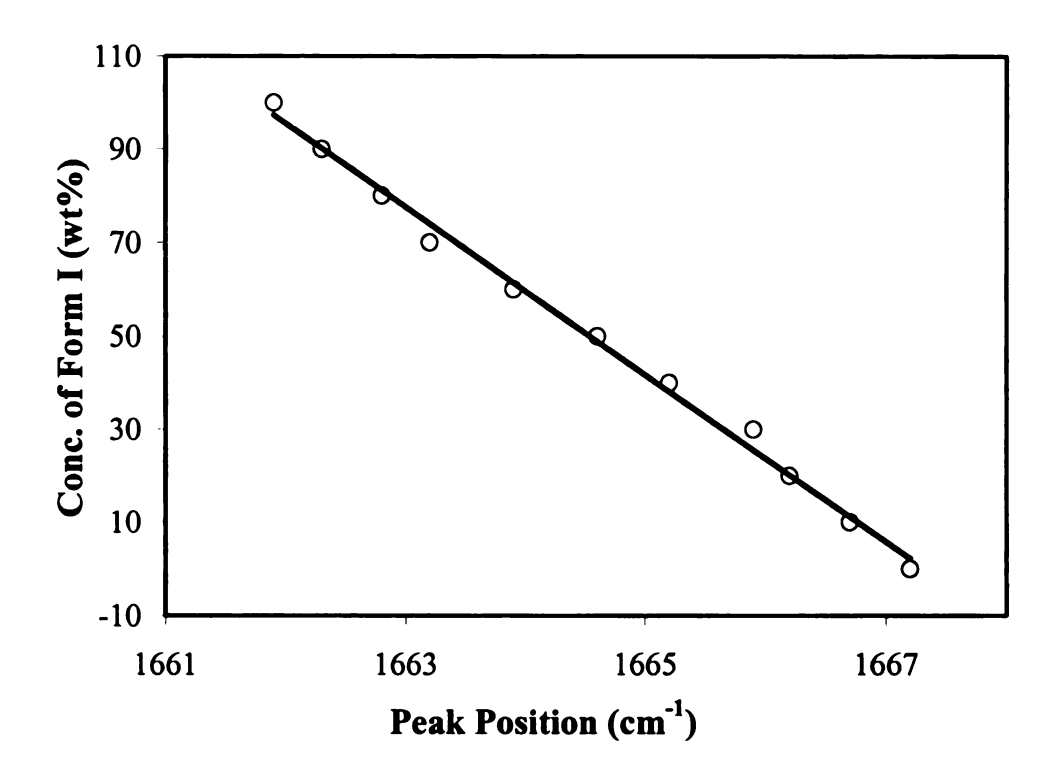


Figure 5.5. Calibration curve for the relative concentration of Form I in the mixture of Form I and Form II of progesterone slurried in water.

of slurries during the phase transformation because the organic solvent has strong scattering around 1700 cm<sup>-1</sup> region, which obscured the peak shift. The spectra of eleven mixtures of varying relative amounts of Form I and Form II show significant peak shift from pure Form I to pure Form II. The calibration curve in Figure 5.5 clearly indicates that we can adequately predict the relative amount of Form I to Form II simply by the position of the peak in the region from 1662 to 1667 cm<sup>-1</sup>. While more sophisticated peak deconvolution techniques exist, this straightforward relationship between peak position and solid phase composition was adequate for the purposes of this study.

Crystallizations were monitored using Raman spectroscopy over a range of temperatures from 5 to 45°C. Each crystallization was carried out isothermally and allowed to stir for several hours after the onset of the crystallization. During this process, the solid phase of the system was monitored semi-continously with *in situ* Raman spectroscopy. The data collected from one of these crystallizations, carried out at 45°C, are shown in Figures 5.6 and 5.7. As shown in Figure 5.6, the two bold spectra at 1667 cm<sup>-1</sup> and 1662 cm<sup>-1</sup>, which bracket all of the other spectra, were collected at the beginning and the end of the crystallization, respectively. The initial peak position at 1667 cm<sup>-1</sup> indicates that Form II formed at the beginning of the crystallization. With additional post crystallization stir time, the peak shifted gradually to 1662 cm<sup>-1</sup>, which indicates that Form II was gradually transforming to Form I. This process of polymorphic transformation is depicted in Figure 5.7 in which the concentration profiles, calculated from the calibration curve in Figure 5.5, are plotted against time. The polymorphic transformation from Form II to Form I

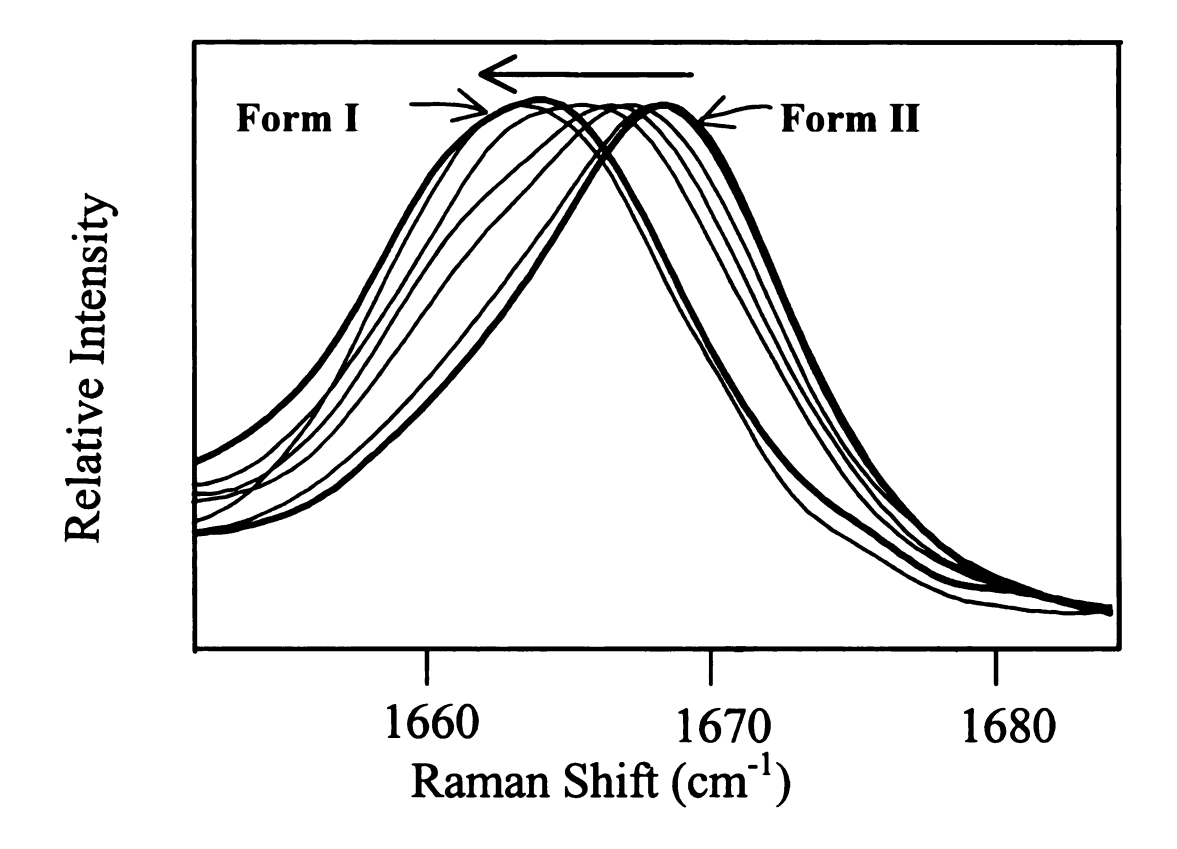
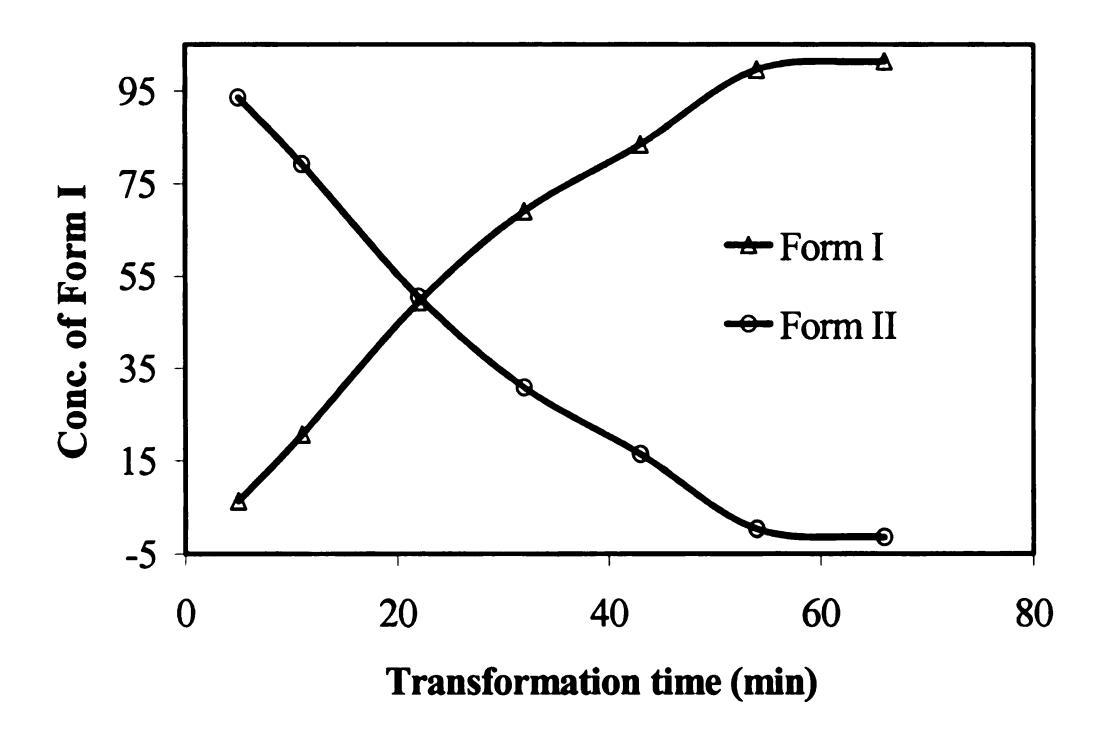


Figure 5.6. Raman spectra showing peak shift during the phase transformation process at 45°C.



**Figure 5.7.** Concentration profiles of Form I and Form II of progesterone throughout the phase transformation process at 45°C. The lines are drawn through the data as a guide to the eye.

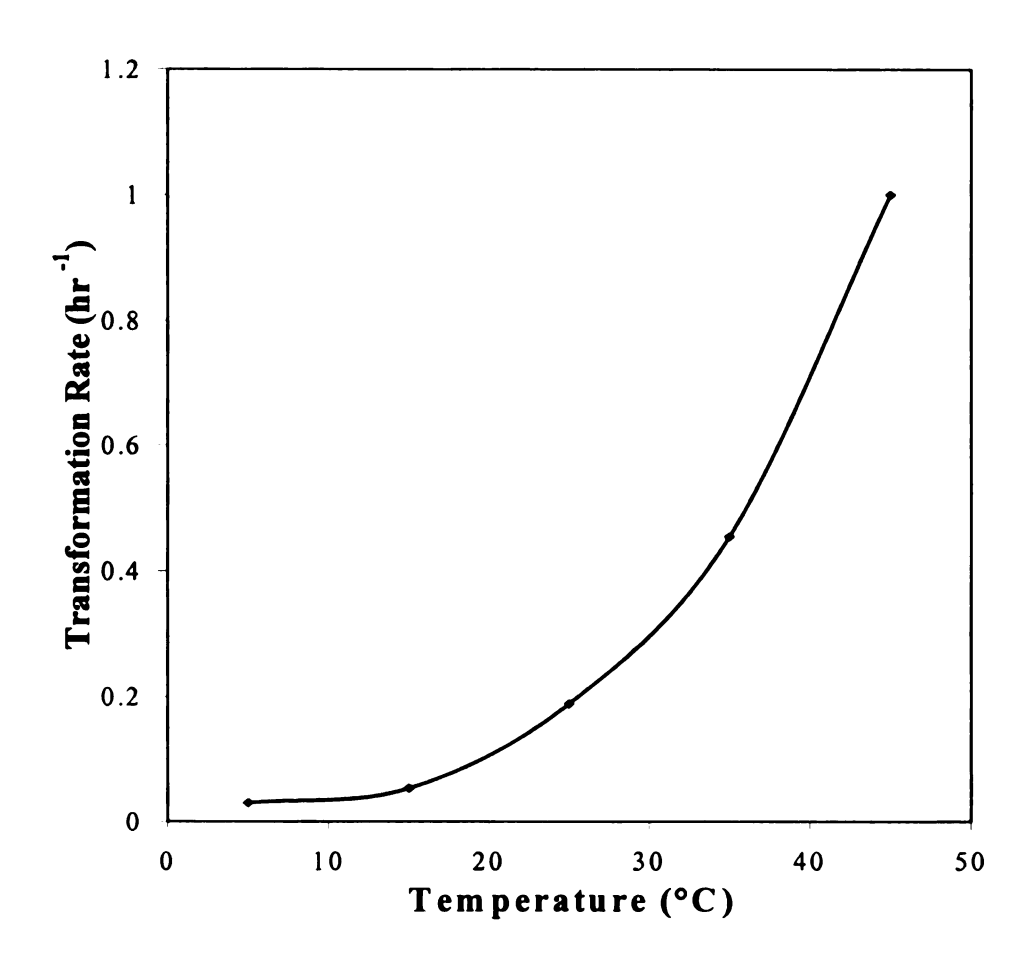


Figure 5.8. The temperature dependence of phase transformation rate of progesterone. The line is drawn through the data as a guide to the eye.

was monitored *in situ* at different temperatures ranging from 5 to 45°C. The transformation rates were found to increase as the temperature increases, as shown in Figure 5.8. This trend suggests that this polymorphic system is monotropic and Form I is the thermodynamically stable form while Form II is the metastable form.<sup>2</sup> This was confirmed by the thermal analysis result that showed the melting enthalpy of Form I is greater than that of Form II.<sup>11</sup> The melting enthalpy rule of Burger states that if the high melting form has the higher melting enthalpy, they are monotrophs. If the high melting form has the lower melting enthalpy, the two forms are enantiotrophs.<sup>16</sup> Therefore, *in situ* Raman techniques and thermal analysis are consistent in predicting that Form I and Form II are monotrophs. The phase transformation phenomenon observed by Raman spectroscopy is consistent with Ostwald's law of stages, which states that the formation of a metastable phase will precede the appearance of a thermodynamically stable phase once the supersaturation has spontaneously decreased.<sup>17</sup>

According to Burger, <sup>16</sup> if Form I and Form II are monotrophs and Form I is the stable form, the solubility of Form I will be lower than that of Form II. This is also confirmed by classical nucleation theory, which states that the solid phase modification that is first formed under given conditions has a higher equilibrium solubility. <sup>18</sup> This is because the nucleation rate is the maximum for those modifications having the lowest surface energy, which is inversely proportional to the equilibrium solubility. <sup>18</sup> The solubility difference between Form I and Form II provides additional insight about the phase transformation process. During the crystallization process, supersaturation is removed with respect to Form II as Form II crystallizes out from the solution as the initial solid phase. At a

certain point, the concentration decreases to the solubility of Form II. As the solubility of Form II is higher than that of Form I, the solution is supersaturated with respect to Form I. The solubility difference can be so large that the solubility of Form II lies in the unstable or labile region with respect to Form I, where spontaneous nucleation of Form I occurs. Even if this solubility difference is not so large, it can be reasonably assumed that, although Form II is the major solid phase in the mixture, some nuclei of Form I may also be formed.<sup>19</sup> These initial nuclei set the starting point for the transformation process. As the growth of the nuclei consumes the supersaturation of Form I, the solution goes into undersaturated zone with respect to Form II, which makes it possible for Form II to dissolve and produce continuous supersaturation for Form I to grow. The transformation will be complete when all of Form II dissolves and the solution is saturated with respect to Form I.

The advantage of Raman over off-line techniques lies in its ability of *in situ* monitoring the progress of the phase transformation between polymorphs. By contrast, an off-line analytical technique measures the system several steps removed from the crystallizer. These steps include drying, storage and sampling that have all been carried out on the material. During these extraneous steps, samples may undergo phase transformation, leading to conclusions from the off-line analysis that might be inaccurate and misleading. Based on the powerful insight provided by Raman spectroscopy coupled with an *in situ* immersion probe, instead of using off-line analytical techniques, we are able to efficiently measure the transformation rate of progesterone from Form II to Form I over a wide range of temperatures in this solvent system. As such, we now fully understand the

kinetics of polymorphic transformation of progesterone over a wide range of process temperatures. Consequently, we are now able to specify a process for consistently and reliably producing either of the two known polymorphs.

## 5.4 Conclusions

It is demonstrated that Raman spectroscopy can distinguish between Form I and Form II progesterone crystals. The principal advantage of the Raman technique over other methods is being able to analyze samples in their native state or without the need for sample preparation. More significantly, Raman spectroscopy is proved to be able to monitor the solvent-mediated phase transformation process in situ. Transformation rates were found to increase as temperature increases, which indicated that Form I and Form II of progesterone are monotrophs. The observations obtained through in situ monitoring with Raman spectroscopy are consistent with Ostwald's rule of stages. Because this system is monotropic, it is expected thermodynamically that Form I has a lower solubility than Form II. The solubility difference and crystallization theory were utilized to explain the mechanism of the phase transformation process. The data collected from in situ monitoring of this system has allowed us to estimate the rate of polymorphic transformation for this monotropic conversion over a wide range of process temperatures.

## 5.5 Acknowledgments

The authors would like to express appreciation to Kaiser Optical Systems for providing the Raman instrument, HoloLab series 5000 and to ASI Applied Systems for providing

the automatically controlled LabMax® reactor. We also wish to thank Pharmacia Corporation for permission to publish this work.

#### References

- (1) Yu, L.; Reutzel, S. M.; Stephenson, G. Pharm. Sci. Technol. To. 1998, 1(3), 118.
- (2) Giron, D. Thermochim. Acta, 1995, 248, 1.
- (3) Byrn, S. R. Solid-State Chemistry of Drugs, Academic Press: New York. 1982.
- (4) Raghavan, K.; Dwivedi, A.; Campbell, G. C.; Nemeth, G.; Hussain, M. A. J. Pharm. Biomed. Anal. 1994, 12(6), 777.
- (5) Colthup, N. B.; Daly, L. H.; Wiberley, S. E. Introduction to Infrared and Raman Spectroscopy; 3rd Edition, Academic press: Boston, 1990.
- (6) Pelletier, M. J. Analytical Applications of Raman Spectroscopy, Blackwell Science Ltd: Oxford, 1999.
- (7) Ingle, J. D. and Crouch, S. R. Spectrochemical Analysis, Prentice Hall: Englewood Cliffs, New Jersey, 1988.
- (8) Kaiser Optical Systems, Inc. HoloLab Series 5000 Operations Manual, Kaiser Optical Systems, Inc.: Ann Arbor, Michigan, 1997.
- (9) ASI Applied Systems, *ReactIR 1000 User's Guide*; 3rd Edition, ASI Applied Systems: Millersville, Maryland, 1997.
- (10) Brandstätter-Kuhnert, M.; Kofler, A. Oesterr. Apoth.-Ztg. 1959, 13, 297.
- (11) Battey, D.E.: Slater, J.B.: Wludyka, R. S.; Owen, H.: Pallister, D.M.; Morris, M.D.; Appl. Spectrosc., 1993, 47, 1913.
- (12) Owen, H.; Battey, D.E.; Pelletier, M.J.; Slater, J.B.; Proc. SPIE, 1995, 24(6), 260.
- (13) Muramatsu, M.; Iwahashi, M.; Ushio, T. J. Pharm. Sci. 1979, 68(2), 175.
- (14) Silverstein, R. M.; Bassler, C. G.; Morrill, T. C. Spectrometric Identification of Organic Compounds, 5th Edition, John Wiley & Sons: New York, 1991.
- (15) Mullin, J. W. Crystallization, 3rd Edition, Butterworth-Heinemann Ltd: Oxford, 1993.
- (16) Burger, A.; Ramberger R. Mikrochim. Acta II. 1979, 2(3-4), 259.
- (17) Ostwald, W. Z. Physik, Chem. (Leipzig), 1897, 22, 289.

- (18) Söhnel, O.; Garside, J. *Precipitation: Basic Principles and Industrial Applications*, Butterworth-Heinemann Ltd: Oxford, 1992.
- (19) Cardew, P. T.; Davey, R. J. Proc. R. Soc. Lond. A, 1985, 198, 415.

## Chapter 6

## CONCLUSIONS

This dissertation focuses on two studies including *in situ* monitoring and control of pH swing crystallization and *in situ* monitoring of polymorphic transformation. pH swing crystallization is more energy efficient than cooling crystallization in that heating and cooling are not necessary. It is also advantageous over antisolvent crystallization in that separation of solvents is not involved in the post-crystallization processes. The objective of the pH swing crystallization study was to develop a control strategy that enables the production of a crystalline product with the desired crystal size distribution. The study of polymorphic transformation aimed at obtaining the desired polymorph by *in situ* monitoring of the polymorphic transformation process.

The basic structural properties of the crystallizing species, HNic, were studied in Chapter 2. It was found that the transformation of the molecular structure upon dissolution in water results in significant peak shifts in its infrared spectrum. The calibrations for the solution concentrations of both NaNic and HNic were built accordingly on their corresponding IR absorbance regions. PLS calibration models were employed to extract accurate information on both species from the aqueous mixture. The solubility of HNic was found varying with the pH and with a change in C(NaNic). Attenuated Total Reflection Fourier Transform Infrared Spectroscopy (ATR-FTIR) was used for monitoring of pH swing crystallization of HNic in situ.

Using the method developed in Chapter 2, the metastable zone was measured *in situ* with ATR-FTIR in Chapter 3. The width of the metastable zone was found to be dependent on the acid concentration, acid addition rate and the agitation speed. Nucleation kinetics were determined by the relationship between the metastable zone width and the acid addition rate. In addition, the effect of micromixing was correlated with the metastable zone width. Crystalline products with the improved crystal size distribution were obtained under the optimized process conditions for spontaneous(primary) crystallization.

Due to the time-consuming nucleation in spontaneous(primary) crystallization, seeding was adopted to reduce the length of time to induce crystallization in Chapter 4. Seeding at different levels of relative supersaturation demonstrated that increased relative supersaturation increases secondary nucleation. With the communication between the LabMax and the ReactIR 1000, the feedback control of the relative supersaturation was realized to keep the solution constantly at low relative supersaturation in the post-seeding process, which promoted crystal growth and suppressed secondary nucleation. Consequently products with a large mean size and improved crystal size distribution were obtained using far less amount of time as compared to spontaneous(primary) crystallization.

The solvent-mediated polymorphic transformation of progesterone was monitored *in situ* using Raman spectroscopy in Chapter 5. The Raman analysis showed that the appearance of Form I progesterone is always preceded by the formation of Form II progesterone. Phase transformation rates were found to increase monotonically as the

temperature increases. Form I was found to be thermodynamically more stable than Form II, while Form II was kinetically favored over Form I. It was concluded that Form I and Form II of progesterone are monotropic. The solubility difference between Form I and Form II was used to explain the polymorphic transformation process. The *in situ* monitoring capability of Raman spectroscopy allowed us to define an operating procedure that produces the desired polymorph.

# **APPENDIX**

**Table A.1.** Data for Figure 3.2. The metastable zone of the crystallization of nicotinic acid measured under the conditions that the solution is agitated at 1.1 m/s and 2 M HCl is added at the rate of 60 g/hr at 30°C.

| Metastable Limit        |                       | Solu                  | bility                |
|-------------------------|-----------------------|-----------------------|-----------------------|
| C(NaNic)                | C(HNic)               | C(NaNic)              | C(HNic)               |
| $(m. f.^* \times 10^3)$ | $(m. f. \times 10^3)$ | $(m. f. \times 10^3)$ | $(m. f. \times 10^3)$ |
| 9.28                    | 5.23                  | 9.51                  | 4.06                  |
| 8.28                    | 4.81                  | 8.35                  | 3.86                  |
| 7.43                    | 4.51                  | 7.41                  | 3.73                  |
| 6.42                    | 4.43                  | 6.39                  | 3.46                  |
| 5.44                    | 4.16                  | 5.55                  | 3.31                  |
| 4.60                    | 3.89                  | 4.67                  | 3.07                  |
| 3.89                    | 3.68                  | 3.80                  | 3.04                  |
| 3.16                    | 3.57                  | 3.26                  | 2.92                  |

<sup>\*</sup>m. f.: mole fraction.

**Table A.2.** Data for Figure 3.3. Comparison of the first metastable limit measurement with different acid addition rates, 1 g/hr and 60 g/hr. The acid concentration is 2 M HCl and the agitation speed is 1.1 m/s. The temperature is 30°C.

| C(HNic) Profile with the acid addition rate of 1 g/hr |                       | •                     | ile with the acid     |
|---|-----------------------|-----------------------|-----------------------|
|   |                       |                       | te of 60 g/hr         |
| C(NaNic)  | C(HNic)               | C(NaNic)              | C(HNic)               |
| $(m. f. \times 10^3)$                                 | $(m. f. \times 10^3)$ | $(m. f. \times 10^3)$ | $(m. f. \times 10^3)$ |
| 16.67   | -0.01                 | 16.62                 | 0.00                  |
| 16.63   | 0.04                  | 16.59                 | 0.00                  |
| 15.83   | 0.80                  | 16.54                 | 0.00                  |
| 15.18   | 1.32                  | 16.11                 | 0.40                  |
| 14.51   | 1.72                  | 15.60                 | 0.83                  |
| 14.31   | 1.88                  | 15.18                 | 1.18                  |
| 13.77   | 2.24                  | 14.73                 | 1.55                  |
| 13.37   | 2.53                  | 14.35                 | 1.83                  |
| 12.92   | 2.81                  | 13.91                 | 2.14                  |
| 12.57   | 3.05                  | 13.44                 | 2.51                  |
| 12.29   | 3.24                  | 13.03                 | 2.79                  |
| 11.96   | 3.43                  | 12.69                 | 3.01                  |
| 11.62   | 3.65                  | 12.28                 | 3.32                  |
| 11.08   | 4.08                  | 11.89                 | 3.57                  |
| 10.95   | 4.13                  | 11.56                 | 3.81                  |
| 10.62   | 4.34                  | 11.18                 | 4.08                  |
| 10.24   | 4.59                  | 11.20                 | 4.05                  |
| 10.07   | 4.68                  | 11.15                 | 4.10                  |
| 9.67  | 4.97                  | 11.11                 | 4.13                  |
| 9.52  | 5.06                  | 11.00                 | 4.21                  |
| 9.28  | 5.21                  | 11.01                 | 4.25                  |
| 9.36  | 5.13                  | 10.75                 | 4.48                  |
| 9.30  | 5.11                  | 10.77                 | 4.44                  |
| 9.35  | 4.98                  | 10.73                 | 4.46                  |
| 9.30  | 4.95                  | 10.64                 | 4.54                  |
| 9.33  | 4.68                  | 10.58                 | 4.57                  |
| 9.38  | 4.40                  | 10.55                 | 4.63                  |
| 9.44  | 4.17                  | 10.55                 | 4.57                  |
| 9.51  | 4.08                  | 10.50                 | 4.46                  |
| 9.49  | 4.09                  | 10.50                 | 4.36                  |
| 9.44  | 4.12                  | 10.49                 | 4.26                  |

**Table A.3.** Data for Figure 3.5. The crystal size distribution of the product from the experiment with the addition of 0.5 M HCl at the rate of 1 g/hr and agitation speed of 1.1 m/s.

| Size of the Sieve Aperture (µm) | Cumulative Percent Undersize (wt%) |
|---------------------------------|------------------------------------|
| 0                               | 0                                  |
| 127                             | 34.9                               |
| 177                             | 54.0                               |
| 250                             | 96.7                               |
| 359                             | 100                                |

**Table A.4.** Data for Figure 4.1. Concentration profile of the seeded crystallization of nicotinic acid at 60% relative supersaturation seeding.

| Time Since the Start of Acid | Solubility of HNic             | Metastable limit of HNic                | C(NaNic)<br>(m. f. $\times 10^3$ ) | C(HNic)<br>(m. f. × 10 <sup>3</sup> ) |
|------------------------------|--------------------------------|---|------------------------------------|---------------------------------------|
| Addition (hr)                | $(\mathbf{m. f.} \times 10^3)$ | $(\mathbf{m}.\ \mathbf{f}.\times 10^3)$ |                                    |                                       |
| 0.00                         | 5.30                           | 6.43                                    | 16.56                              | -0.04                                 |
| 0.02                         | 5.28                           | 6.42                                    | 16.49                              | 0.03                                  |
| 0.03                         | 5.21                           | 6.33                                    | 16.08                              | 0.46                                  |
| 0.05                         | 5.09                           | 6.19                                    | 15.43                              | 1.00                                  |
| 0.07                         | 4.98                           | 6.05                                    | 14.80                              | 1.47                                  |
| 0.10                         | 4.78                           | 5.81                                    | 13.68                              | 2.29                                  |
| 0.12                         | 4.68                           | 5.69                                    | 13.13                              | 2.68                                  |
| 0.15                         | 4.51                           | 5.49                                    | 12.16                              | 3.34                                  |
| 0.18                         | 4.33                           | 5.27                                    | 11.14                              | 4.05                                  |
| 0.22                         | 4.31                           | 5.25                                    | 11.05                              | 4.10                                  |
| 0.25                         | 4.27                           | 5.20                                    | 10.83                              | 4.27                                  |
| 0.28                         | 4.25                           | 5.18                                    | 10.71                              | 4.33                                  |
| 0.32                         | 4.22                           | 5.14                                    | 10.54                              | 4.46                                  |
| 0.37                         | 4.19                           | 5.10                                    | 10.38                              | 4.55                                  |
| 0.43                         | 4.17                           | 5.09                                    | 10.29                              | 4.61                                  |
| 0.50                         | 4.15                           | 5.05                                    | 10.13                              | 4.73                                  |
| 0.57                         | 4.14                           | 5.05                                    | 10.13                              | 4.73                                  |
| 0.62                         | 4.14                           | 5.04                                    | 10.10                              | 4.75                                  |
| 0.67                         | 4.14                           | 5.04                                    | 10.08                              | 4.71                                  |
| 0.73                         | 4.15                           | 5.05                                    | 10.13                              | 4.60                                  |
| 0.80                         | 4.15                           | 5.05                                    | 10.14                              | 4.55                                  |
| 0.83                         | 4.14                           | 5.05                                    | 10.11                              | 4.55                                  |
| 0.90                         | 4.15                           | 5.05                                    | 10.14                              | 4.48                                  |
| 0.97                         | 4.14                           | 5.05                                    | 10.11                              | 4.46                                  |
| 1.00                         | 4.14                           | 5.05                                    | 10.13                              | 4.43                                  |
| 1.08                         | 4.14                           | 5.05                                    | 10.13                              | 4.38                                  |
| 1.25                         | 4.14                           | 5.05                                    | 10.10                              | 4.37                                  |
| 1.42                         | 4.15                           | 5.06                                    | 10.17                              | 4.29                                  |
| 1.58                         | 4.17                           | 5.08                                    | 10.26                              | 4.18                                  |
| 1.75                         | 4.16                           | 5.07                                    | 10.20                              | 4.23                                  |
| 1.92                         | 4.16                           | 5.07                                    | 10.20                              | 4.24                                  |
| 2.08                         | 4.16                           | 5.07                                    | 10.20                              | 4.23                                  |
| 2.25                         | 4.16                           | 5.07                                    | 10.22                              | 4.20                                  |
| 2.58                         | 4.16                           | 5.07                                    | 10.21                              | 4.22                                  |
| 2.92                         | 4.16                           | 5.07                                    | 10.23                              | 4.19                                  |

**Table A.5.** Data for Figure 4.3. Turbidity profile for 60% relative supersaturation seeding crysallization.

| Time since the Start of Acid Addition | Turbidity            |
|---------------------------------------|----------------------|
| (hr)                                  | (Relative Intensity) |
| 0.00                                  | 0.02                 |
| 0.10                                  | 0.02                 |
| 0.20                                  | 0.02                 |
| 0.30                                  | 0.02                 |
| 0.40                                  | 0.02                 |
| 0.50                                  | 0.02                 |
| 0.60                                  | 0.02                 |
| 0.62                                  | 0.02                 |
| 0.63                                  | 0.02                 |
| 0.65                                  | 0.13                 |
| 0.67                                  | 0.16                 |
| 0.70                                  | 0.21                 |
| 0.73                                  | 0.26                 |
| 0.77                                  | 0.28                 |
| 0.80                                  | 0.31                 |
| 0.83                                  | 0.33                 |
| 0.87                                  | 0.34                 |
| 0.90                                  | 0.39                 |
| 0.93                                  | 0.41                 |
| 0.97                                  | 0.43                 |
| 1.00                                  | 0.42                 |
| 1.08                                  | 0.44                 |
| 1.25                                  | 0.55                 |
| 1.42                                  | 0.55                 |
| 1.58                                  | 0.55                 |
| 1.75                                  | 0.58                 |
| 1.92                                  | 0.50                 |
| 2.08                                  | 0.54                 |
| 2.25                                  | 0.53                 |
| 2.42                                  | 0.53                 |
| 2.58                                  | 0.53                 |
| 2.75                                  | 0.50                 |
| 2.92                                  | 0.50                 |

**Table A.6.** Data for Figures 4.6 and 4.7. The comparison of the crystal mean size and the crystal size distribution resultant from seeding at three levels of relative supersaturation, 30%, 45% and 60%.

| Size of the Sieve Aperture (µm) | Cumulative Percent Undersize (wt%) |                     |                     |
|---------------------------------|------------------------------------|---------------------|---------------------|
| ***                             | $30\%$ - $S_R$                     | 45%- S <sub>R</sub> | 60%- S <sub>R</sub> |
| 0                               | 0                                  | 0                   | 0                   |
| 127                             | 4                                  | 18                  | 20                  |
| 177                             | 34                                 | 41                  | 73                  |
| 250                             | 86                                 | 89                  | 94                  |
| 359                             | 98                                 | 100                 | 100                 |
| 550                             | 100                                |                     |                     |
| Crystal Mean Size (µm)          | 204                                | 185                 | 156                 |

**Table A.7.** Data for Figure 4.14. The comparison of the mean crystal size and the crystal size distribution resultant from three controlled relative supersaturation experiments. I. Seeding at 0%-  $S_R$  and control about 0%-  $S_R$ ; II. Seeding at 30%-  $S_R$  and control about 0%-  $S_R$ ; III. Seeding at 30%-  $S_R$  and control about 30%-  $S_R$ .

| Size of the Sieve Aperture (µm) | Cumulative Percent Undersize (wt%) |                        |                     |
|---------------------------------|------------------------------------|------------------------|---------------------|
|                                 | 0%- S <sub>R</sub>                 | 30%-0%- S <sub>R</sub> | 30%- S <sub>R</sub> |
| 0                               | 0                                  | 0                      | 0                   |
| 127                             | 3                                  | 11                     | 67                  |
| 177                             | 18                                 | 22                     | 85                  |
| 250                             | 77                                 | 78                     | 96                  |
| 359                             | 98                                 | 99                     | 100                 |
| 550                             | 100                                | 100                    |                     |

**Table A.8.** Data for Figure 5.5. The concentration of Form I progesterone vs. the peak position around 1660-1667 cm<sup>-1</sup>.

| wt% of Form I | Peak Position (cm <sup>-1</sup> ) |
|---------------|-----------------------------------|
| 0             | 1667.2                            |
| 10            | 1666.7                            |
| 20            | 1666.2                            |
| 30            | 1665.9                            |
| 40            | 1665.2                            |
| 50            | 1664.6                            |
| 60            | 1663.9                            |
| 70            | 1663.2                            |
| 80            | 1662.8                            |
| 90            | 1662.3                            |
| 100           | 1661.9                            |

**Table A.9.** Data for Figure 5.7. Concentration profiles of Form I and Form II of progesterone throughout the phase transformation at 45°C.

| Transformation time (min) | C(Form I)<br>(wt%) | C(Form II)<br>(wt%) |
|---------------------------|--------------------|---------------------|
| 5                         | 6                  | 94                  |
| 11                        | 21                 | 79                  |
| 22                        | 49                 | 51                  |
| 32                        | 69                 | 31                  |
| 43                        | 83                 | 17                  |
| 54                        | 100                | 0                   |
| 66                        | 100                | 0                   |

Table A.10. Temperature dependence of phase transformation rate of progesterone.

| Temperature (°C) | Transformation Rate (hr <sup>-1</sup> ) |
|------------------|---|
| 5                | 0.03                                    |
| 15               | 0.05                                    |
| 25               | 0.19                                    |
| 35               | 0.45                                    |
| 45               | 1.00                                    |

